

Aus dem Bereich Physiologie

Theoretische Medizin und Biowissenschaften

der Medizinischen Fakultät

der Universität des Saarlandes, Homburg/Saar

Different domains of Complexin II regulate tonic secretion and Synaptotagmin-mediated synchronous transmitter release

Dissertation

zur Erlangung des Grades eines Doktors der Naturwissenschaften

der Medizinischen Fakultät

der UNIVERSITÄT DES SAARLANDES

2020

vorgelegt von: Mazen Makke

geb. am. 08.03.1988 in Habbouch, Libanon

Doctoral supervisor: Prof. Dr. Dieter Bruns

I dedicate this work to my family, and to my late grandfather Akil Chraim and my late grandmother Nemri Toufaily may their souls rest in peace.

Table of Contents

1	Summary	8
	Zusammenfassung	10
	Abbreviations	12
2	Introduction	16
2.1	Lipid membranes and membrane fusion	16
2.1.1	<i>SNARE proteins drive membrane fusion and exocytosis</i>	<i>18</i>
2.2	Docking and priming of synaptic vesicles	20
2.3	Complexin, a regulator of the late steps in exocytosis	22
2.3.1	<i>Functional domains of CpxII</i>	<i>23</i>
2.4	Synaptotagmin, the calcium sensor for molecular exocytosis	25
3	Aims of the thesis	29
4	Materials and methods.....	30
4.1	Materials and reagents	30
4.2	Transgenic mice and genotyping.....	30
	Genotyping	30
	DNA extraction.....	31
	PCR programs.....	32
4.3	Mouse chromaffin cell preparation.....	33
4.4	Electrophysiology	35
4.4.1	<i>Primer on the patch clamp technique</i>	<i>37</i>
4.4.2	<i>Principle of whole cell voltage clamp for membrane capacitance measurements</i>	<i>38</i>
4.5	Measuring exocytosis and determination of vesicle pools in chromaffin cells	44
4.1	Flash photolysis of caged Ca ²⁺ and the calibration curve for intracellular calcium estimation.....	45
4.1.1	<i>Calcium calibration curve for intracellular calcium imaging.....</i>	<i>46</i>
4.1	Kinetic model of priming and fusion in chromaffin cells.....	50
4.1.1	<i>Calcium imaging and calcium uncaging procedure</i>	<i>52</i>
4.1.2	<i>Tonic exocytosis</i>	<i>53</i>
4.2	Data acquisition and analysis	54
4.3	Peptide dissolution and infusion	54
4.4	BIOCHEMISTRY	55
	<i>Protein assays</i>	<i>56</i>
4.4.1	<i>Recombinant protein production and purification.....</i>	<i>56</i>
4.4.2	<i>Gel electrophoresis</i>	<i>58</i>
4.4.3	<i>Native protein extraction</i>	<i>60</i>
4.4.4	<i>Western Blot</i>	<i>60</i>

4.5	Immunocytochemistry	61
4.6	Chemical fixation of chromaffin cells for Electron Microscopy imaging	62
5	Results.....	65
5.1	Complexin II inhibits premature exocytosis in chromaffin cells via its carboxyl-terminal domain	65
5.1.1	<i>Complexin II regulates exocytosis in chromaffin cells.....</i>	<i>65</i>
5.1.2	<i>CpxII clamps premature release via its C-terminal domain (CTD).....</i>	<i>67</i>
5.1.3	<i>CpxII 1-100 competes with endogenous CpxII for binding to SNARE proteins</i>	<i>67</i>
5.1.4	<i>The CpxII-CTD reduces tonic release in wt cells.....</i>	<i>68</i>
5.1.5	<i>CpxII-CTD reduces the asynchronous release and increases exocytotic burst in wt cells.....</i>	<i>70</i>
5.1.6	<i>The CpxII CTD peptide requires other domains of CpxII to clamp premature vesicle fusion</i>	<i>72</i>
5.1.7	<i>The CpxII CTD peptide rescues the clamp loss by the dominant negative Cpx1-100 in wt cells.....</i>	<i>74</i>
5.1.8	<i>Anchoring CpxII to the vesicle membrane aggravates Cpx's functions.....</i>	<i>75</i>
5.2	CpxII CTD interacts with t-SNAREs and Syt1 and is structurally similar to SNAP25-SN1.....	77
5.2.1	<i>CpxII CTD interacts with the calcium sensor for fast exocytosis Syt1.....</i>	<i>77</i>
5.2.2	<i>The CpxII CTD preferentially interacts with Syt1 and the t-SNAREs</i>	<i>78</i>
5.2.3	<i>CpxII CTD slows down the kinetics of SNARE complex formation</i>	<i>79</i>
5.2.4	<i>The sequence of CpxII CTD is highly similar to that of the SNAP25 SN1 motif.....</i>	<i>80</i>
5.3	CpxII-SNAP25 SN1 chimeras support full regulation of exocytosis	82
5.3.1	<i>Complexin-SNAP 25 chimeras functionally resemble the wt complexin</i>	<i>82</i>
5.3.2	<i>A shorter CpxII CTD exchange with SNAP25-SN1 fully restores CpxII's function.....</i>	<i>84</i>
5.4	Two functionally distinct regions reside within the CpxII CTD	86
5.4.1	<i>The amphipathic character of the last 19 amino acids in CpxII CTD is key for its clamp function</i>	<i>86</i>
5.4.2	<i>The cluster of Glutamate residues E¹⁰⁸-E¹¹⁴ in CpxII CTD facilitates vesicle fusion.....</i>	<i>89</i>
5.5	The CpxII N terminal domain accelerates exocytosis in cooperation with the calcium sensor Syt1.....	91
5.5.1	<i>N-terminal domain of Complexin adapts the calcium sensitivity for exocytosis</i>	<i>91</i>
5.5.2	<i>CpxII NTD tunes the speed of Syt1 mediated synchronized exocytosis</i>	<i>91</i>
5.5.3	<i>CpxII modulates Syt1 triggered exocytosis via its NTD</i>	<i>94</i>
5.5.4	<i>Complexin mutants are expressed to similar levels in chromaffin cells</i>	<i>97</i>
5.6	Synaptobrevin 2 TMD.....	99
5.6.1	<i>The flexibility of the SybII TMD is essential for efficient membrane fusion</i>	<i>99</i>
5.6.2	<i>The highly conserved G100 amino acid in the SybII TMD is not critical for fusion catalysis</i>	<i>101</i>
5.6.3	<i>The rigid SybII PolyL traps secretory vesicles in a non-fusogenic state.....</i>	<i>102</i>
6	Discussion.....	104
6.1	Complexin clamps fusion with its CTD	104
6.1.1	<i>CpxII CTD hinders zipping by competing with SybII for the interaction with the t-SNAREs to clamp asynchronous exocytosis.....</i>	<i>106</i>
6.2	CpxII NTD cooperates with Syt1 to facilitate synchronized vesicle fusion	109
6.3	SybII TMD catalyzes membrane fusion	112
7	Conclusions.....	115

References.....	116
List of Publications.....	128
Conferences.....	128
Acknowledgements	129
Curriculum vitae	130

Table of figures

Figure 1. The cytoplasmic membrane of the animal cell.....	16
Figure 2. Membrane transition states en route to fusion.	17
Figure 3. Zippering of SNARE machinery drives membrane fusion.	19
Figure 4. Molecular steps for vesicle maturation on route to fusion.	21
Figure 5. The secondary structure of CpxII.	23
Figure 6. The structure of Synaptotagmin1.	26
Figure 7. Calcium coordination by Syt1 C2AB domains.	27
Figure 8. The five configurations of the patch clamp recording.	37
Figure 9. The RC circuit representation of the cell membrane and the corresponding electric signals in whole cell recording.	40
Figure 10. Compensation of membrane capacitance and series resistance R_s in voltage clamp recordings.....	41
Figure 11. Electrical circuit representation of a voltage clamp in a whole cell configuration.	43
Figure 12. Florescence profile of Fura2 and the reversible Ca^{2+} buffering by NP-EGTA.	46
Figure 13. Calcium calibration curve for calcium imaging.	49
Figure 14. Schematic representation of vesicle pools.	50
Figure 15. Synchronized exocytosis in chromaffin cells is composed of three kinetically distinct phases.	51
Figure 16. The C-terminal domain of CpxII controls the magnitude of the synchronous secretion.	66
Figure 17. Cpx 1-100 over expression has a dominant negative phenotype in CpxII in wt cells.	68
Figure 18. CpxII-CTD inhibits tonic release in wt cells.	69
Figure 19. CpxII-CTD in isolation inhibits tonic release and enhances the synchronous release in wt cells.	71
Figure 20. CpxII-CTD does not inhibit premature vesicle fusion in the absence of wt CpxII.	71
Figure 21. CpxII CTD cooperates with Cpx1-100 to suppress asynchronous vesicle fusion.	73
Figure 22. CpxII-CTD rescues the dominant-negative phenotype of Cpx 1-100 in wt cells.	74
Figure 23. A membrane anchored CpxII 1-100 fails to regulate secretion.	76
Figure 24. Truncation of CpxII CTD reduces CpxII's interaction with the calcium sensor Syt1.	77
Figure 25. CpxII CTD specifically interacts with the t-SNARES and Syt1.	78
Figure 26. CpxII-CTD slows down the SNARE complex formation <i>in vitro</i>	80
Figure 27. CpxII-CTD shows high sequence similarities with the SN1motif of SNAP-25.....	81
Figure 28. Cpx1-100 - SNAP25 SN1 chimera largely restores the synchronous release.	84

Figure 29. Cpx 1-115 - SNAP25 SN1 fully recovers the synchronous release like wt complexin.	85
Figure 30. Predicted structure of the CpxII-CTD.	86
Figure 31. Replacing the CpxII CTD with an amphipathic helix compromises CpxII's functions.....	87
Figure 32. A synthetic amphipathic helix can functionally replace the last 19 amino acids of CpxII CTD in clamping asynchronous fusion.....	89
Figure 33. The Glutamate cluster aids in lifting the clamp imposed by the CpxII-CTD.....	90
Figure 34. CpxII-NTD supports Syt1 in facilitating synchronized vesicle fusion.....	92
Figure 35. CpxII cooperates with Syt1 to accelerate the synchronized exocytosis.	94
Figure 36. CpxII wt rescues the slow release kinetics of Syt1 R233Q while the CpxII Δ N mutant further aggravates it.	95
Figure 37. CpxII Δ N decelerates the release kinetics of Syt1 D232N triggered secretion.	96
Figure 38. Expression levels of CpxII and its mutants in chromaffin cells.	98
Figure 39. A flexible helix SybII TMD supports undiminished secretion.....	100
Figure 40. The amino acid G100 is not a crucial amino acid for the function of SybII-TMD in membrane fusion.	101
Figure 41. Ultrastructural analysis of stimulated dko chromaffin cells expressing SybII wt vs SybII polyL.	103
Figure 42. Proposed mechanism for complexin clamping by hindering SNARE complex zippering.....	106
Figure 43. Proposed mechanism for membrane fusion catalysis by SybII TMD.	113

1 Summary

Exocytosis of transmitter-storing vesicles requires specialized proteins known as SNARE proteins (Soluble N-ethylmaleimide sensitive fusion protein Attachment Receptor), which comprise the vesicular membrane-associated (v-SNARE) Synaptobrevin and the two cytoplasmic membrane-associated target SNARE proteins (t-SNAREs), Syntaxin and SNAP25. The assembly of membrane-bridging SNAREs provides the force for overcoming the energy barriers of vesicle fusion. To avoid unregulated fusion, SNARE complex activity requires tight control by the auxiliary proteins, like complexin (Cpx) and synaptotagmin (Syt), but their precise mode of action remained enigmatic.

The experimental work in this doctoral thesis was designed to provide new insight into the mode of Cpx action in Ca^{2+} -triggered exocytosis. For this, chromaffin cells were used as a model system and defined mutants of CpxII were expressed in CpxII ko cells to study its impact in a gain-of-function approach. The results show that the carboxyl-terminal domain (CTD) of CpxII hinders premature fusion of vesicles, thereby augmenting the pool of primed vesicles. Biochemical experiments indicate that the CpxII CTD interacts with t-SNARE proteins and slows SNARE complex formation. Sequence alignments pinpoint a high degree of similarity between amphipathic region of the CpxII CTD and the SNARE motif SNAP25 SN1. Indeed, chimera proteins between CpxII and SNAP25 show that the corresponding SNAP25 SN1 domain fully restores the inhibitory function of CpxII. These results support a model wherein the amphipathic region of CpxII CTD competes with the SNAP25-SN1 domain for binding to the SNARE complex. Collectively, they provide new insight into the postulated molecular 'clamp', which arrests prefusion intermediates awaiting the Ca^{2+} -trigger. The N-terminal domain (NTD) of CpxII, instead, was found to increase the rate of Ca^{2+} -triggered synchronized fusion, indicating that CpxII provides two independent functions that synergize in increasing synchronous fusion. Truncation of the CpxII NTD (CpxII Δ N) decelerated synchronous fusion in wild type and Syt7-deficient chromaffin cells, but not Syt1 knock out cells, suggesting that CpxII cooperates with Syt1. In knock-ins of Syt1 with reduced Ca^{2+} affinity (R233Q), CpxII expression accelerated whereas CpxII Δ N expression decelerated the stimulus-secretion coupling, indicating that CpxII modulates Syt1 function in an NTD-dependent fashion.

The second part of the thesis addresses the important question of whether the SybII TMD serves simply as passive membrane anchor or plays an active role in catalyzing membrane fusion. The latter hypothesis bases on the observation that v-SNARE TMDs are characterized by their high content of β -branched amino acids, like valine and isoleucine residues, which promote structural

flexibility to the TMD helix. The results show that substituting the core residues of the SybII TMD with a stretch of rigidifying leucine hinders the fusion process leading to an accumulation of fusion-incompetent vesicles underneath the plasma membrane. Conversely, reintroducing flexibility to the SybII TMD with isoleucine residues reinstates the fusogenicity of the secretory vesicles. Thus, flexibility of SybII's TMD is required for facilitating the fusion process, suggesting that SNARE TMDs do not simply serve as passive membrane anchors, but play an active role in Ca^{2+} -triggered secretion, most likely by reducing the energy barrier for fusion between opposing membranes.

Overall, the results provide new insight into the well-orchestrated secretion machinery by elucidating CpxII's action in regulating fusion, its interplay with the main Ca^{2+} -sensor Syt1, and the contribution of SybII TMD in Ca^{2+} -triggered exocytosis.

Zusammenfassung

Die Exozytose transmitterspeichernder Vesikel erfordert spezialisierte Proteine, die als SNARE-Proteine (Soluble N-ethylmaleimide sensitive fusion protein Attachment Receptor) bekannt sind. Letztere umfassen das vesikulär-membranassoziierte (v-SNARE) Synaptobrevin und die beiden zytoplasmatischen-membranassoziierten SNARE-Zielproteine (t-SNAREs), Syntaxin und SNAP25. Die Assemblierung membranüberbrückender SNAREs liefert die Kraft zur Überwindung der Energiebarrieren während. Um eine unregulierte Fusion zu vermeiden, erfordert die SNARE-Komplexbildung eine strenge Kontrolle durch Hilfsproteine, wie z. B. Complexin (Cpx) und Synaptotagmin (Syt), deren genaue Wirkmechanismen jedoch unklar sind.

Die experimentellen Arbeiten in dieser Doktorarbeit sollen neue Einsichten in die Wirkungsweise von Cpx bei der Ca^{2+} -getriggelter Exozytose liefern. Dazu wurden Chromaffinzellen als Modellsystem verwendet und definierte Mutanten von CpxII in CpxII ko-Zellen exprimiert, um die Wirkung von CpxII in einem ‚gain-of-function‘-Ansatz zu untersuchen. Die Ergebnisse zeigen, dass die carboxyterminale Domäne (CTD) von CpxII eine vorzeitige Fusion der Vesikel verhindert und dadurch den Pool der fusionsbereiten Vesikel vergrößert. Biochemische Experimente weisen darauf hin, dass die CpxII-CTD mit t-SNARE-Proteinen interagiert und die Bildung von SNARE-Komplexen verlangsamt. Sequenzvergleiche offenbaren eine starke Ähnlichkeit zwischen der amphipathischen Region des CpxII CTD und dem SNARE-Motiv SNAP25 SN1. Praktisch zeigen Chimärenproteine zwischen CpxII und SNAP25, dass die entsprechende SNAP25 SN1-Domäne die inhibitorische Funktion von CpxII wieder vollständig herstellt. Diese Ergebnisse unterstützen ein Modell, in dem die amphipathische Region von CpxII CTD mit der SNAP25-SN1-Domäne um die Bindung an SNARE-Komplexe konkurriert. Zusammengefasst liefern sie neue Erkenntnisse zur postulierten molekularen "Klammer", die Präfusionszwischenprodukte vor dem eigentlichen Ca^{2+} -Stimulus arretiert. Die N-terminale Domäne (NTD) von CpxII hingegen erhöht die Rate der Ca^{2+} -getriggerten synchronen Fusion, was zeigt, dass CpxII zwei unabhängige Funktionen ausübt, die bei der Erhöhung der synchronen Fusion synergistisch zusammenwirken. Die Verlust der CpxII NTD (CpxII Δ N) verzögert die synchrone Fusion in Wildtyp- und Syt7-defizienten Chromaffinzellen, nicht aber in Syt1 knock-out-Zellen, was darauf hindeutet, dass CpxII mit Syt1 kooperiert. In Knock-in Varianten von Syt1 mit reduzierter Ca^{2+} -Affinität (R233Q) wird die Reiz-Sekretions-Kopplung durch Expression von CpxII beschleunigt und durch Expression von CpxII Δ N verlangsamt. Diese Befunde zeigen, dass CpxII die Funktion von Syt1 in einer NTD-abhängigen Weise moduliert.

Der zweite Teil der Arbeit befasst sich mit der wesentlichen Frage, ob die SybII TMD lediglich als passiver Membrananker dient oder eine aktive Rolle bei der Katalyse der Membranfusion spielt. Letztere Hypothese basiert auf der Beobachtung, dass v-SNARE TMDs durch eine Überrepräsentation von β -verzweigten Aminosäuren, wie Valin- und Isoleucin, charakterisiert werden. Diese Eigenschaft, die strukturelle Flexibilität der TMD-Helix fördert, ist die Ursache für die beobachtete Funktion. Die Ergebnisse zeigen, dass eine Substitution der Kernreste der SybII-TMD durch eine gleichlange Poly-Leucin Region den Fusionsprozess behindert, was zu einer Anhäufung von fusionskompetenten Vesikeln an der Plasmamembran führt. Umgekehrt kann durch Wiedereinführung flexibler Poly-Isoleucin-Reste in die SybII TMD die Fusogenität der sekretorischen Vesikel wiederhergestellt werden. Somit lässt sich schlussfolgern, dass die Flexibilität der SybII-TMD den Fusionsprozess erleichtert. Offensichtlich dienen SNARE-TMDs nicht nur als passiver Membrananker, sondern spielen darüber hinaus eine aktive Rolle bei der Ca^{2+} -getriggerten Sekretion. Möglicherweise erzeugt die strukturelle Flexibilität der SybII TMD lokale Membranperturbationen und verringert somit die Energiebarriere für die Fusion gegenüberliegender Membranen. Insgesamt liefern die Ergebnisse neue Einblicke in die erstaunlich organisierte Sekretionsmaschinerie, indem sie die Wirkung von CpxII bei der Regulierung der Fusion, sein Zusammenspiel mit dem Ca^{2+} -Hauptsensor Syt1 und den Beitrag von SybII TMD bei der Ca^{2+} -getriggerten Exozytose veranschaulichen.

Abbreviations

aa:	amino acid
ATP:	Adenosine triphosphate
BAPTA:	1,2-bis(<i>o</i> -aminophenoxy)ethane- N,N,N',N'-tetraacetic acid
°C:	Degrees Celsius
Ca ²⁺ :	Calcium
CaCl ₂ :	Calcium chloride
[Ca ²⁺] _i :	Intracellular free calcium ion concentration
cDNA:	complementary DNA
cm:	Centimeter
CM:	Membrane capacitance
CO ₂ :	Carbon dioxide
Cpx:	Complexin
CpxII ko:	Complexin II knock out
Cpx ΔN	Complexin Delta amino terminal
CpxII CTD	Complexin II Carboxy terminal domain
CpxII NTD	Complexin II Amino terminal domain
Cs:	Cesium
CsOH:	Cesium hydroxide
CTD:	Carboxyl Terminal Domain
ΔCM:	Delta (change) in membrane capacitance
DDW:	Double distilled water
Dko:	Double knockout
DMEM:	Dulbecco's Modified Eagle's Medium
DMSO:	Dimethylsulfoxide
DNA:	Deoxyribonucleic acid
DPTA:	1,3-diaminopropane-N,N,N',N'-tetraacetic acid

EB:	Exocytotic burst
EDTA:	Ethylenediaminetetraacetic acid
EGFP:	Enhanced Green Fluorescent Protein
EGTA:	Ethyleneglycoltetraacetic acid
fF:	Femtofarad
fF/s:	Femtofarad per second
Fw-Primer:	Forward Primer
g:	gram
Gm:	Membrane conductance
Gs:	Series conductance
GTP:	Guanosine triphosphate
h:	Hour
H ₂ O:	Water
HEPES:	4-(2-Hydroxyethyl) piperazine-1-ethanesulfonic acid
HCl:	Hydrochloric acid
Hz:	Hertz
kb:	Kilobase pair
KCl:	Potassium chloride
kDa:	Kilodalton
KHz:	Kilohertz
ko:	Knockout
LDCV:	Large dense-core vesicles
μL:	Microliter
mg:	Milligram
Mg ²⁺ :	Magnesium
min:	Minutes
mL:	Milliliter
mM:	Millimolar

mOsm:	Milliosmol
ms:	Milliseconds
Munc-18:	Mammalian uncoordinated-18
mV:	Milli volt
MΩ:	Mega ohm
n:	Number of the elements (e.g., cells)
Na ₂ EDTA:	Sodium EDTA
Na ₂ GTP:	Sodium GTP
NaHCO ₃ :	Sodium bicarbonate
NaCl:	Sodium chloride
(NH ₄) ₂ SO ₄ :	Ammonium sulfate
nm:	Nanometer
nM:	Nanomolar
NMJ:	Neuromuscular junction
NP-EGTA:	Nitrophenyl-EGTA
nS:	Nanosiemens
NSF:	N-ethylmaleimide sensitive factor
p:	p-value, probability value
PCR:	Polymerase chain reaction
R:	Ratio
Rev-Primer:	Reverse Primer
RNA:	Ribonucleic acid
rpm:	Revolutions per minute
RRP:	Readily releasable pool
s:	Seconds
SB-buffer:	Soriano buffer
SDS:	Sodium dodecyl sulfate (detergent)
SFV:	Semiliki Forest Virus

SNAP:	Soluble NSF attachment protein
SNAP-25:	Synaptosomal-associated protein of 25 kDa
SNARE:	The SNAP receptor
SR:	Sustained rate
SRP:	Slowly releasable pool
Syb:	Synaptobrevin
Syt:	Synaptotagmin
Syx:	Syntaxin
τ :	Time constant
TAE:	Tris-acetate-EDTA
TMD:	Transmembrane domain
TRIS:	Tris(hydroxymethyl)aminomethane
t-SNARE:	Target SNARE
UV:	Ultraviolet
V:	Volt
VAMP:	Vesicle-associated membrane protein
v-SNARE:	Vesicular SNARE
wt:	Wildtype

2 Introduction

2.1 Lipid membranes and membrane fusion

The plasma membrane utilizes phospholipids as elementary building blocks to establish a continuous lipid bilayer separating the cytosol from the extracellular surrounding (Figure 1 A). Integral transport channels that render the membrane permeable to specific ions, allow for cellular signaling and communication (Figure 1 B). Such membrane organization preserves the functional integrity of a cell while allowing it to be a part of a fully organized system relying on cell-cell communication (Alberts 2008).

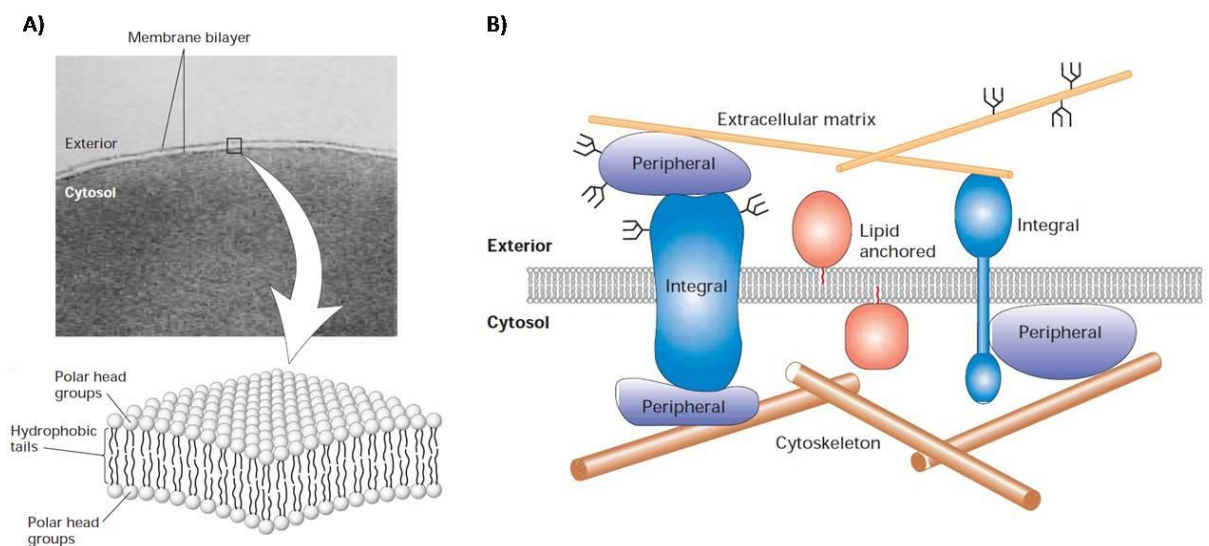


Figure 1. The cytoplasmic membrane of the animal cell. (A) Electron micrograph showing the plasma membrane of an erythrocyte, demonstrating the typical railroad track like structure surrounding the cell, which are the polar layers of the phospholipid membranes. As interpreted in the lower schematic, the polar head groups face the aqueous environment, thus shielding inside their hydrophobic fatty acyl chains. **(B)** Proteins may interact or span biological membranes; these can be integral proteins that span the entire lipid bilayer, or lipid-anchored proteins, which are attached by post-translational modifications such as palmitoylation. (Adapted from (Lodish et al., 2003).

Small sized lipid bilayer structures known as vesicles shuttle macromolecule, such as neurotransmitters and hormones that serve as messengers between cells. Vesicles have to fuse with the plasma to discharge their cargo to the extracellular space through a fusion pore formed after the merger of the vesicular membrane with the plasma membrane (Sudhof 2013b).

For exocytosis, the widely accepted mechanism for membrane fusion from the biophysical point of view consists of three stages: contact, hemi-fusion, and the opening of a fusion pore that expands wide enough for neurotransmitters to diffuse through (Jahn et al., 2003; Chernomordik et al., 2006) (Figure 2).

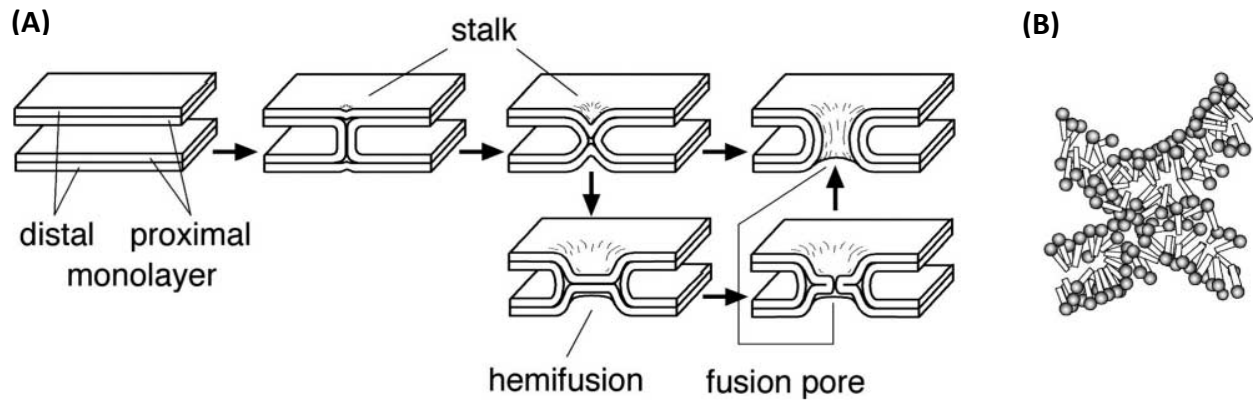


Figure 2. Membrane transition states en route to fusion. (A) Proximal monolayers of the opposing membranes are represented as smooth and bendable sheets. According to the stalk hypothesis, the first step in the fusion process includes a non-bilayer intermediate believed to be initiated by the splay of lipid tails into the hydrophilic medium depicted in the illustration to the right. This is followed by the stalk formation with a continuity between the proximal bilayers is achieved. Either this state can directly develop to an open fusion pore, or it passes to a hemi-fused intermediate where the distal membranes meet, and that can later transit into a fusion pore. (B) An illustration showing lipid molecules exposing their hydrophobic tails to the hydrophilic surrounding in a process known as lipid splay. (adapted from (Jahn et al., 2003).

Membrane fusion is described as a multistep, high energy demanding process that requires the opposing membranes to fuse and become one continuous structure. Several intrinsic forces prevent membranes from random fusion, such as electrostatic repulsion between the head groups of the opposing lipid bilayers, as well as the hydration repulsion force imposed by the aqueous environment separating the proximal and the distal monolayers (Bentz et al., 1988) (Figure 2 A). To fuse, it is a prerequisite for membranes to overcome the intrinsic repulsive forces, which makes unassisted membrane fusion nearly impossible (Parsegian 1989). Membrane fusion starts by bringing the opposing membranes into close proximity, this reduces the distance between the proximal and the distal monolayers and aids in diminishing the hydration repulsion between the lipid layers (Figure 2). The second step in this process is the introduction of structural deformations in the lipid bilayers; allowing lipid molecules to expose their hydrophobic tails to the aqueous environment which is known as lipid splay (Figure 2 B). The resulting discontinuity of the membrane leaflets allow for the nucleation of a fusion stalk which is formed by the merger of the

proximal leaflets of the opposing lipid bilayers with little to no changes in the distal leaflets (Figure 2 A). The radial widening of the stalk structure allows the distal monolayers to come into contact forming the hemi fused diaphragm which evolves later into an aqueous duct known as a fusion pore, through which the cargo can pass from the vesicle lumen to the extracellular space in a process known as exocytosis (Figure 2 A) (Jahn et al., 2003). The stalk formation as well as fusion pore formation and expansion are the most energy demanding steps in the process of membrane fusion (Cohen et al., 2004). In secretory cells, a conserved family of proteins known as the SNARE proteins assist membranes to fuse (Weber et al., 1998). SNARE proteins play a fundamental role in all steps of membrane fusion; they pull the opposing membranes into contact, and reduce energy barriers for the fusion of the opposing membranes by promoting lipid splay (for review see Yoon et al., 2018).

2.1.1 SNARE proteins drive membrane fusion and exocytosis

The SNARE (soluble N-ethylmaleimide-sensitive fusion protein attachment protein receptor) is a 76 KD complex (Block et al., 1988) that was first found to mediate the intracellular trafficking and fusion of the Golgi transport vesicles (Weidman et al., 1989). Later, SNARE proteins were proven to be the core machinery for vesicle fusion at synaptic release sites in neurons (Sollner et al., 1993). SNAREs are categorized based on their membrane localization to a 16 KD vesicular membrane-associated protein (v-SNARE) Synaptobrevin (Syb) that is anchored to the membrane via its helical transmembrane domain (TMD) at its carboxyl terminal (Figure 3 B). The second group are the plasma membrane SNARE proteins (t-SNAREs) Syntaxin and SNAP-25. Syntaxin (Syx), which is a 35 kD protein that is anchored to the cytoplasmic membrane via its C terminal TMD (Figure 3 B), with an N terminal extension forming a three-helical bundle (Habc domain) that interacts with Munc 18-1 protein upstream to the SNARE forming domain. Munc 18-1 holds syntaxin in a closed conformation and prevents the formation of SNARE complexes (Fernandez et al., 1998; Dulubova et al., 1999). This inhibition is later removed by the action of Munc 13, yet another regulator for SNARE complex assembly which allows Syx to assemble with Syb and SNAP-25 (Wang et al., 2019). The second t-SNARE is SNAP-25 (25 kD) lacks a TMD but still able to associates to the inner leaflet of the plasma membrane via its palmitoylated linker sequence (Hess et al., 1992; Lane et al., 1997) (Figure 3 B). The process of exocytosis is orchestrated by the action of SNARE proteins on the opposing membranes that provide the activation energy for fusion (for review see Han et al., 2017).

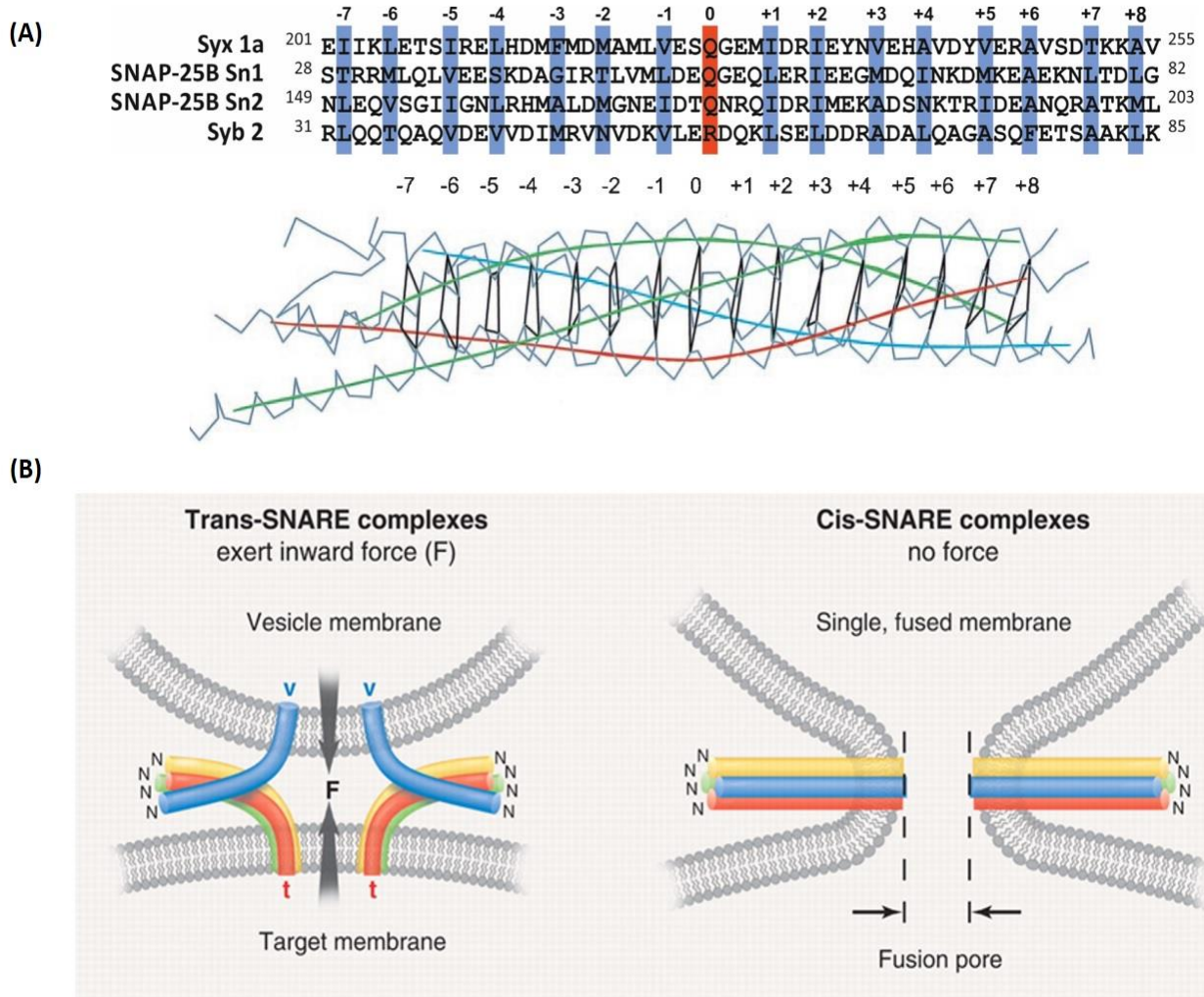


Figure 3. Zippering of SNARE machinery drives membrane fusion. (A) Sequence alignment of the cytosolic domains of the SNARE proteins showing the highly conserved periodic distribution of hydrophobic amino acids forming hydrophobic layers upon the assembly of the SNARE pin, which are labeled from -7 to +8 those are highlighted with blue and the central ionic zero layer is in red. Lower panel represents a ribbon illustration of the assembled SNARE pin's cytosolic domain backbone having a coiled coil cylindrical form, with Synaptobrevin in blue, Syntaxin in red, and SNAP-25 in green (adapted from Sutton et al., 1998). (B) The trans-SNARE complex (the t-SNAREs and the v-SNARE dwell at two independent membranes) showing the transmembrane domain of the v-SNARE Synaptobrevin (blue) integrated into the vesicular membrane, and the t-SNAREs Syntaxin (red) and SNAP25 (green and yellow) with Syntaxin's TMD integrated in the cytoplasmic membrane and SNAP 25 anchored via its palmitoylated stretch of cysteine amino acids in its linker domain. The zippering of the trans-SNARE complex from the N to the C terminal provides the force required to bring opposing membranes into close proximity and drives membrane fusion causing a fusion pore to form. After membrane fusion the SNARE force is used up, with the t-SNAREs and the v-SNARE now dwelling at the same membrane as fully zippered Cis-SNARE complexes (Sudhof et al., 2009).

To drive membrane fusion, the cytosolic region of the SNARE proteins zipper from the N to the C-terminus (Sorensen et al., 2006) into a thermally stable and SDS resistant tightly packed parallel four-helix bundle (Weber et al., 1998). The assembly of the SNARE pin is guided by highly

conserved periodic repeats of hydrophobic amino acids that are referred to as the SNARE hydrophobic layers (Figure 3 A) (Sollner et al., 1993; Hayashi et al., 1994; Fasshauer et al., 1997; Sutton et al., 1998). On the functional level, the integrity of the amino acids in the hydrophobic layers is essential for the proper zipping of SNARE proteins as well as for the exocytosis process to take place (Fasshauer et al., 1998). The zipping of the SNARE proteins into a pin generates the force required to bring the vesicular and the plasma membrane together (Figure 3 B left panel). The energy generated by the full zipping of the SNAREs' cytosolic domains is propagated to the membranes by the membrane anchors of the SNARE proteins that in turn, employs this energy to merge the two membranes and help expanding the fusion pore (for review see Fang et al., 2014).

2.2 Docking and priming of synaptic vesicles

Prior to fusion, secretory vesicles are believed to undergo several steps of molecular maturation allowing efficient and reliable exocytosis. Docking and priming are the last maturation stages for the vesicle before vesicle fusion commences. Both processes involve cooperation between the SNARE proteins and the synaptic accessory proteins that catalyze and regulate the activity of SNAREs that mediate these crucial molecular steps *en route* to fusion (Figure 4). "Docking" reflects a morphological positioning of the vesicle in close opposition to the presynaptic plasma membrane (Figure 4), yet different criteria have been used to define a vesicle in a docked state (Verhage et al., 2008; Imig et al., 2014). At the protein level, several factors were found to regulate the docking process, such as the calcium-independent interaction of the calcium sensor for fast release synaptotagmin 1 (Syt1) with the SNARE acceptor complex formed by Syx and SNAP 25 (Borisovska et al., 2005; de Wit et al., 2006; de Wit et al., 2009). In addition, Munc 18-1, a synaptic accessory protein plays an essential role in the docking process, it holds the vesicle near the plasma membrane through its association with Syx, and simultaneously bridging the opposing membranes (Ma et al., 2011; Dawidowski et al., 2016). Only a fraction of the docked vesicles undergo molecular maturation to become fusion competent "primed" (for review see Sudhof 2013b). The pool of primed vesicles is also known as the Readily Releasable Pool (RRP), which represents those vesicles with the highest release probability (von Ruden et al., 1993). Priming of a vesicle requires the initiation of the trans-SNARE complex (Becherer et al., 2006; Mohrmann et al., 2010) holding the vesicle in contact with the plasma membrane (Nofal et al., 2007; Li et al., 2014) (Figure 4). Beside SNARE proteins, SNARE regulating accessory proteins also play a pivotal role in the priming process. Munc-13, for instance, mediates the first step of the priming process by transforming the closed Syx in the Syntaxin/Munc-18 complex into its open confirmation, making the assembly of

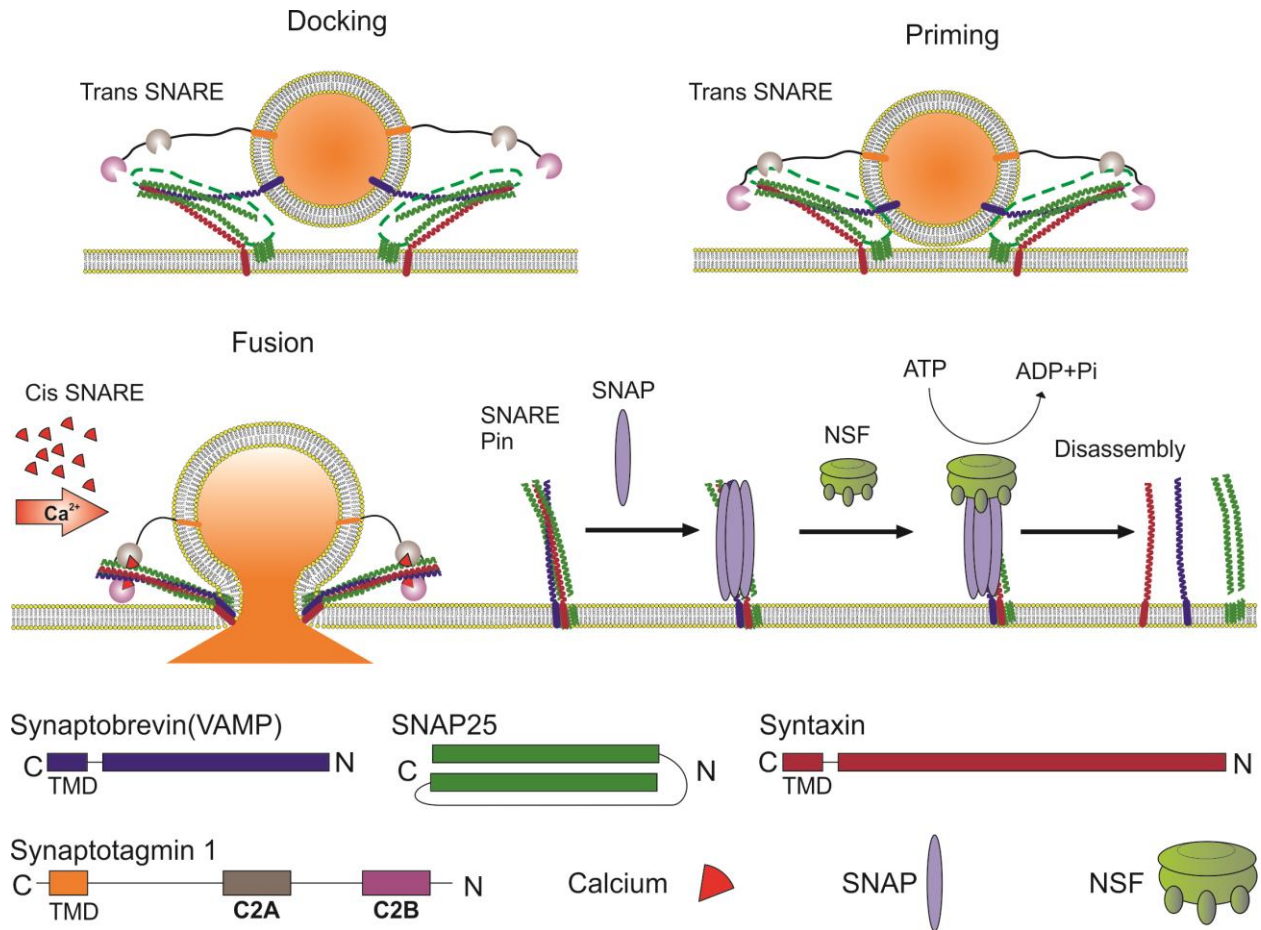


Figure 4. Molecular steps for vesicle maturation on route to fusion. The target SNARE proteins syntaxin and SNAP25 form the acceptor complex for the vesicle-associated membrane protein synaptobrevin. The interaction between synaptobrevin and the acceptor complex is a prerequisite for vesicle docking, where the N terminal cytosolic domains of the SNARE proteins are interacting while the transmembrane domains remain in two independent lipid bilayers. Molecular priming takes place in a calcium-dependent manner where the vesicle is brought closer to the plasma membrane and becomes fusion competent. Synaptotagmins bind the calcium ions fluxed into the cell upon stimulus, which triggers the full assembly of the SNARE proteins and drives vesicle fusion. The cargo is discharged through the opening of the fusion pore and the SNAREs are fully assembled into a pin at the same membrane (cis SNAREs). To keep up with the high frequency of exocytosis events, used SNARE pins must be restored to back into their individual protein constituents to be readily available to fuse newly coming vesicles. The SNAP protein cooperates with the NSF protein in an ATP demanding process to disassemble the SNARE pins into individual SNARE proteins.

the SNARE complex possible (Ma et al., 2011). Furthermore, we have previously shown that other SNARE regulatory proteins also contribute to the accumulation of primed vesicles, e.g. the inhibitor of asynchronous fusion “complexin” (Cpx) prevents the premature fusion of primed vesicles, allowing a significant enhancement in the pool size of the primed vesicles (Dhara et al., 2014). Moreover, the calcium sensor synaptotagmin 1 (Syt1) maintains the stability of the primed pool (Mohrmann et al., 2013) and relieves the inhibitory action of complexin on the fusion machinery upon calcium binding, enabling the fast calcium-triggered fusion. After exocytosis takes

place the α -SNAP (α -soluble N-ethylmaleimide-sensitive factor attachment protein) and NSF (N-ethylmaleimide-sensitive factor) use the energy from ATP to disassemble the Cis SNARE pins to make the SNARE proteins available for a second round of exocytosis (Huang et al., 2019).

2.3 Complexin, a regulator of the late steps in exocytosis

Zippering of SNARE protein is an energetically favored process, in order to avoid random fusion of vesicles they require a high degree of regulation (Nichols et al., 1998). Even though docked vesicles have a low release probability at the active zone (Allen et al., 1994), uncontrolled exocytosis at the synaptic terminals drives the process of neuronal communication off balance, resulting in neurological disorders and diseases, such as schizophrenia and depression (Eastwood et al., 2001), Parkinson's disease (Basso et al., 2004), Huntington's disease (Morton et al., 2001), bipolar disorder (Eastwood et al., 2001), and Alzheimer disease (Tannenberg et al., 2006). These neurological disorders were linked to the altered expression levels of the cytosolic protein complexin (Cpx), which is one of the main regulators that oversee SNARE activity during last steps in exocytosis.

Cpxs constitute a family of small (15-20 KD) highly charged cytosolic soluble proteins that function at the synapses to regulate exocytosis (Mohrmann et al., 2015). Cpx can bind to the SNARE complex as well as to the docking complex formed by the t-SNARES Syx and SNAP25 but not to individual SNARE proteins (Ishizuka et al., 1995; McMahon et al., 1995a; McMahon et al., 1995b). All four isoforms of complexin, Cpx I, II, III, and IV, are present in are expressed in the mammalian central nervous system, with complexins III and IV being predominantly expressed at the ribbon synapse of the retina (Takahashi et al., 1995; Reim et al., 2005). CpxII is the only isoform expressed in adrenal chromaffin cells. Based on sequence and structural similarities, Cpx isoforms are divided into two subfamilies; the first subfamily includes CpxI and CpxII orthologues that share high sequence identity (86%), whereas members of the second subfamily CpxIII and CpxIV share a 91% identity in between them. Structural differences between these two Cpx subfamilies mainly reside at their carboxyl termini. Cpx III/IV are equipped at their C terminal end with a prenylated CAAX-box motif that inserts to membranes (Wragg et al., 2013), conversely Cpx I and II lack such a domain. A high degree of sequence conservation has been observed among the mammalian complexin orthologues (humans and murines). Nevertheless, the invertebrate isoforms also share sequence similarities to their mammalian counterparts, in particular to CpxIII and IV by containing a CAAX-box farnesylation motif allowing membrane binding (Buhl et al., 2013). Functionally, the genetic loss of both ,Cpx I and II, in mice is lethal for newborn pups, emphasizing the important

role this regulatory protein plays in neuronal transmission (Reim et al., 2001). Ever since, the function of complexin in regulating exocytosis has been intensely studied, yet the mechanism of its action on the exocytotic machinery remains to be identified.

2.3.1 Functional domains of CpxII

The role and the mechanism by which complexin regulates exocytosis has been under investigation for the past two decades. Knock down of complexin I/II in cortical neurons

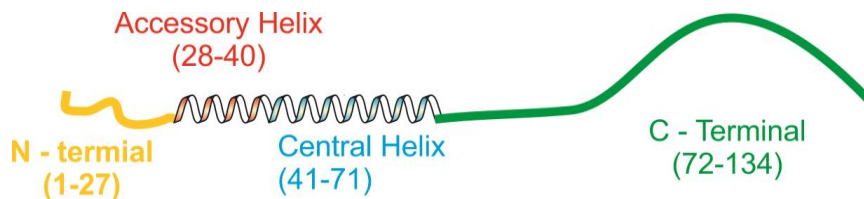


Figure 5. The secondary structure of CpxII. A representation of CpxII structure, a 134 aa long cytosolic protein with 4 functional domains. An unstructured N terminal domain (1-27) in yellow which facilitates vesicle fusion, followed by an accessory α helix (28-40) in red having a mild inhibitory function. The central helix (41-71) in blue is the domain responsible for CpxII-SNARE complex interaction and instrumental for all Cpx functions. An unstructured C-terminal domain holding the main inhibitory function on uncontrolled exocytosis shown in green.

significantly increased asynchronous release and reduced the primed vesicle pool (Maximov et al., 2009). A similar phenotype was also reported in mouse adrenal chromaffin cells (Dhara et al., 2014), as well as at the neuromuscular junctions in motor neurons of *C. elegans* (Martin et al., 2011). Moreover, the addition of complexin I into reduced vesicle fusion assays decreased spontaneous fusion and enhanced calcium driven synchronous fusion (Lai et al., 2017). Structure-function studies on of Cpx I and II have led to the identification of four functionally independent, yet cooperative domains in these proteins, i.e., an accessory α helix, and a central helical domain that are important for interacting with SNARE complexes, flanked by an unstructured N-terminal domain that enhances fusion kinetics, and a C-terminal domain that clamps asynchronous release (Figure 5).

2.3.1.1 The central α helix

Complexins have a central helical region (aa 41-72) (Figure 5 Blue) that is evolutionary highly conserved (Pabst et al., 2000; Chen et al., 2002), and essential for the 1:1 complexin interaction with the ternary SNARE complex (Pabst et al., 2000; Wragg et al., 2017). Crystallography studies

have shown that the central helix fits into the groove between the SNARE proteins Syb and Syx (Chen et al., 2002). Consequently, mutations in the central helix of complexin caused a reduction in Cpx binding to the SNARE complex, and resulted in defective regulation of neuronal transmission (Xue et al., 2007). Furthermore, FRET experiments showed that complexin could interact and stabilize the binary Syx/SNAP25 acceptor complex, increasing the chance of forming a functionally active, fusion initiating SNARE complex (Weninger et al., 2008; Zdanowicz et al., 2017). Moreover, a recent study explaining the crystal structure of the tripartite interface between SNAREs:Cpx:Syt1, has proposed that the complexin central helix is crucial for achieving the primed vesicle state (Zhou et al., 2017).

2.3.1.2 The accessory α helix

The accessory α helix of complexin (aa 27-40) (Figure 5 Red), is N-terminally adjacent to the central helix. Even though it has a stable secondary helical structure, its primary sequence is not conserved throughout the animal kingdom (Pabst et al., 2000; Chen et al., 2002). The function of the accessory helix is still controversial to this day, it was proposed to inhibit vesicular fusion by competing with Syb2 CTD to bind to the t-SNAREs thus preventing full SNARE zippering (Giraud et al., 2008; Lu et al., 2010). A second mechanism suggested that the accessory α helix electrostatically repels the vesicle and cytoplasmic membranes away from each other to prevent their fusion (Trimbuch et al., 2014). On the other hand, several lines of evidence emerged suggesting that the accessory helix provides structural stability to the central α helix. Biochemical experiments showed that the deletion of the accessory α helix compromises the binding of Cpx with the SNAREs (Xue et al., 2007). Along the same line, substitution of the accessory helix with unrelated helix having seven repeats of the motif "EAAK" (Glu-Ala-Ala-Lys) restored the clamp function of Cpx. Those results indicate that the helical structure of the accessory helix is important for the nucleation and the stability of the SNARE-interacting central helix (Radoff et al., 2014). Taken together, the contribution of the accessory helix to the clamping function remains a point of debate whether it clamps fusion by itself or if it only provides structural support for the central helix, and thus the integrity of complexin function.

2.3.1.3 C-terminal domain of complexin

Recent evidence with mutants of CpxII lacking the C terminal domain, but with a preserved accessory α helix showed a total loss of Cpx clamp function in cultured chromaffin cells (Dhara et al., 2014). The C-terminal stretch of Cpx (aa 73-134) (Figure 5 Green), not only inhibited premature

secretion in neuroendocrine chromaffin cells (Dhara et al., 2014), but also hindered spontaneous release in neurons (Cho et al., 2010; Martin et al., 2011; Kaeser-Woo et al., 2012). The C-terminal domain carries out protein-protein as well as protein-lipid interactions. The first of which is with the calcium sensor for fast exocytosis Syt1 (Tokumaru et al., 2008), and the latter being with the membrane of secretory vesicles to concentrate complexin at the fusion sites (Wragg et al., 2013; Snead et al., 2014; Gong et al., 2016). Based on interactions, a correlation between vesicle targeting by the CTD and the clamping function of complexin was proposed, whereby Cpx CTD tethers other inhibitory domains of CpxII such as the accessory α helix to the fusion site to clamp the SNAREs (Giraudo et al., 2006; Giraudo et al., 2008; Giraudo et al., 2009). This limited function of the CTD in clamping fusion was later challenged, where a complexin with a mutated CTD which preserved its membrane interaction properties, failed to inhibit asynchronous release (Snead et al., 2017; Wragg et al., 2017). Despite the intensive efforts, these controversial observations have left the molecular mechanism by which Cpx CTD hinders premature release still to be unveiled.

2.3.1.4 N-terminal domain of complexin

The N terminal domain of Cpx (aa 1-27) (Figure 5 Yellow) enhances vesicle fusogenicity in calcium-triggered exocytosis (Xue et al., 2007; Dhara et al., 2014). Several theories arose to explain the mechanism for the N terminal domain to facilitate fusion, since the NTD could be functionally replaced with the viral lipid interacting HA fusion peptide, it was proposed to facilitate fusion by interacting with the vesicle membrane (Lai et al., 2016). Alternatively, the NTD was proposed to interact and stabilize SNARE proteins, thus increasing the energy output of SNAREs (Xue et al., 2010), or by modulating the calcium sensitivity for exocytosis (Tadokoro et al., 2005; Dhara et al., 2014). These diverging explanations keep the mechanism by which CpxII NTD facilitates fusion, and whether it cooperates with calcium sensors for exocytosis for its facilitation role unclear.

2.4 Synaptotagmin, the calcium sensor for molecular exocytosis

The mammalian family of synaptotagmins includes 16 evolutionarily conserved members of which only 8 can bind calcium, those include synaptotagmins 1, 2, 3, 5, 6, 7, 9, and 10. (Sudhof 2012). Structurally, calcium-sensing synaptotagmins are anchored with their NTD to vesicle membranes, a central linker sequence, and two C2 domains that coordinate calcium (Figure 6) (Sudhof 2012). The loops at the C2 domains sense calcium with conserved aspartates (Davis et al., 1999) to initiate calcium-dependent membrane fusion. Nonetheless, synaptotagmins have different calcium

association and dissociation kinetics which arises from the different amino acid content in their C2 domains (Zhang et al., 2011; Moghadam et al., 2013; Rao et al., 2014). This diversity allows Syt to mediate vesicle trafficking and fusion at a wide dynamic range of Ca^{2+} (Seven et al., 2013; MacDougall et al., 2018; Volynski et al., 2018). Further, synaptotagmins have calcium dependent membrane and protein interactions to initiate fusion, founding the correlation between Ca^{2+} affinity and the differences fusion initiating potency of Syts (Hui et al., 2005). That being said, secretory cells are often equipped with a combination of calcium-sensing synaptotagmin isoforms to support versatile secretion patterns depending on the strength of the Ca^{2+} stimulus (Moghadam et al., 2013; Rao et al., 2017).

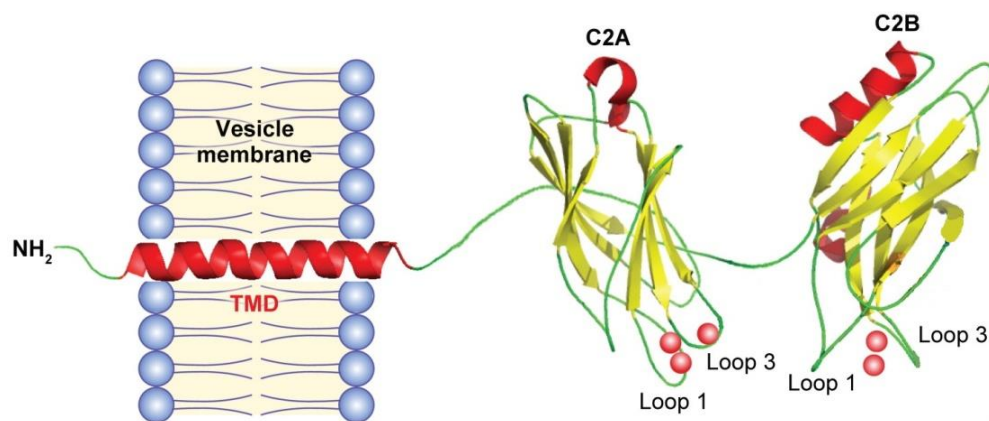


Figure 6. The structure of Synaptotagmin1. Synaptotagmin 1 anchored to the vesicle membrane with its transmembrane domain (TMD) at its N terminus. C2A and C2B containing the calcium binding sites are connected via a flexible linker. C2A coordinates 3 calcium ions and C2B 2 (red spheres) calcium ions by their flexible loops (loop 1 and loop 3). Adapted from (Chapman 2008).

Syt1 and Syt7 are the two main calcium sensors that mediate calcium-triggered exocytosis in neurons and neuroendocrine cells. Compared to Syt1, Syt7 has a high affinity to calcium ($\text{EC}_{50} \approx 1\text{--}2 \mu\text{M}$) (Sugita et al., 2002) and coordinates 6 calcium at its C2 domains. Functionally, Syt7 plays crucial roles in regulated exocytosis, it mediates the slow release phase in synchronous fusion (Luo et al., 2017), and the filling of the synchronous pool as well as the asynchronous release at low intracellular calcium concentrations (Neher et al., 1976; Chen et al., 2017; Rao et al., 2017). The second calcium sensor Syt1 has a lower affinity to calcium than Syt7 ($\text{EC}_{50} \approx 10\text{--}20 \mu\text{M}$) (Sugita et al., 2002). Syt1 mainly drives fast synchronous neurotransmitter release, and reduces the latency of the calcium-triggered exocytosis (Sorensen et al., 2003; Schonn et al., 2008; Bacaj et al., 2013; Lai et al., 2016; Chen et al., 2017), and helps maintaining the capacity of the primed vesicle pool (Bacaj et al., 2015). To fulfill their role in regulated exocytosis, Syts coordinate calcium with the

acidic amino acids in the C2A and C2B loops. Syt1 has been identified to cooperate five Ca^{2+} ions with its C2 domains (Figure 7). Three molecules of Ca^{2+} cooperate to the C2A (D172, D178, D230, D232, D238 for Syt1) and two Ca^{2+} ions in the C2B (D303, D309, D363, D365, D371) (for review see Chapman 2008).

The C2B domain of syt1 was reported to drive the synchronous release by its simultaneous interaction with SNAREs, and the lipid membranes in a calcium dependent manner (Bacaj et al., 2015; Wang et al., 2016; Chang et al., 2018; MacDougall et al., 2018). Nevertheless, the binding of calcium to C2A is critical for the proper function of Syt1. Mutational analysis identified crucial amino acids in the C2A domain R233Q reduced the Ca^{2+} affinity as well as the lipid interactions by Syt1 and slowed down synchronous fusion (Sorensen et al., 2003). On the other hand, a mutation in a calcium coordinating amino acid D232 mutation enhanced Syt1's interaction with the SNARE complex, and boosted the calcium triggered exocytosis in hippocampal neurons (Fernandez-Chacon et al., 2002; Pang et al., 2006).

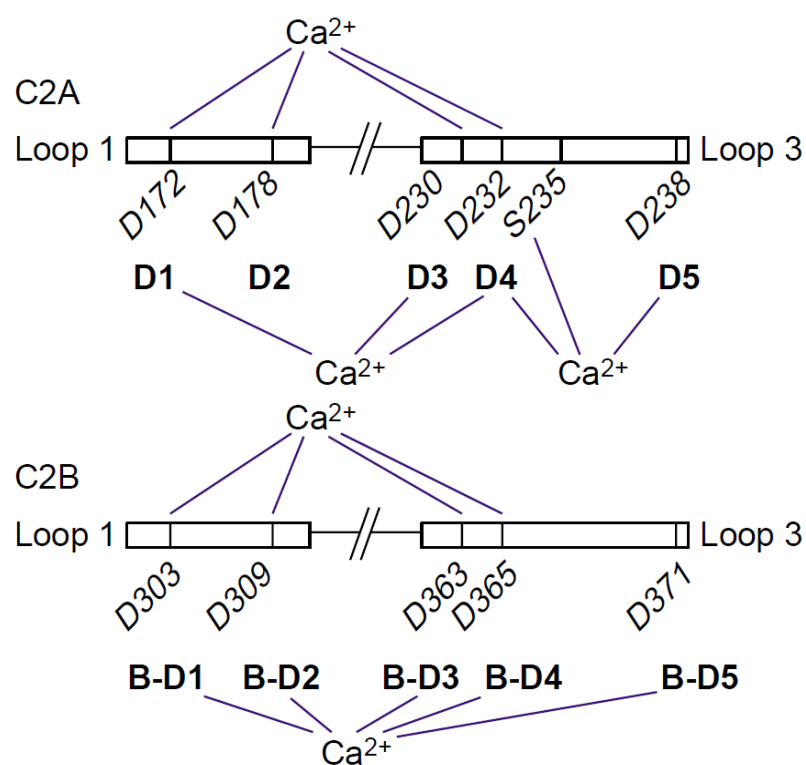


Figure 7. Calcium coordination by Syt1 C2AB domains. Calcium is coordinated by the acidic amino acids of the loops 1 and 3 of the C2AB, 3 Ca^{2+} ions by the C2A, and 2 Ca^{2+} ions by the C2B domain. The coordination of Ca^{2+} neutralizes the negatively charged amino acids in the C2AB domains which allows the loops to interact with lipid membranes (Chapman 2008).

As complexin arrests release via its inhibitory domains, the calcium sensor for exocytosis Syt1 antagonizes the inhibitory action of complexin, allowing the calcium-triggered fusion of vesicles to proceed upon calcium elevation in the cell. The functional interplay between the accessory regulators for vesicular fusion in excitable cells Syt and Cpx ensure a tightly controlled, and efficient synchronized vesicle release upon cell excitation (Tang et al., 2006; Roggero et al., 2007). Nevertheless, their mechanism in determining the timing and the speed of fusion remains unknown.

3 Aims of the thesis

SNARE proteins are the core machinery that mediates exocytosis for cellular maturation and communication. The activity of SNARE proteins is under tight regulation by accessory proteins such as complexin (Cpx) and synaptotagmin (Syt) that govern the timing and magnitude of synchronized vesicle fusion in secretory cells. The two proteins play antagonizing roles in regulation of exocytosis, where Cpx inhibits premature exocytosis allowing for the buildup of a pool of primed vesicles, on the other hand, binding of Ca^{2+} to Syt triggers vesicle fusion.

Yet, extensive work over the last years in neurons and neuroendocrine cells produced opposing views on the underlying mechanisms how Cpx is able to hinder premature fusion, a result that at least in part may be due to experimental inconsistencies like an imperfect control of intercellular Ca^{2+} -levels. In this thesis, experiments employ high-resolution membrane capacitance measurements in combination Ca^{2+} -imaging and – ‘uncaging’ to study the function of CpxII and its mutant variants in front of a well-defined Ca^{2+} -stimulus. Using these experimental strategies and in the framework of a detailed structure–function analysis, the impact of CpxII on the size of the primed vesicle pool and the stimulus secretion coupling shall be studied.

Based on previous findings that the CpxII CTD inhibits premature fusion in chromaffin cells (Dhara et al., 2014), the first part of thesis sets out to identify mechanisms by which CpxII CTD clamps asynchronous exocytosis. Further experiments will address the important question of whether and if so how CpxII cooperates with the main Ca^{2+} -sensors Syt1 and Syt7 (present in chromaffin cells) to govern the timing of synchronized Ca^{2+} triggered exocytosis.

The second part of this work studies the role of SybII TMD in regulated synchronized exocytosis. Specifically, these experiments are designed to elucidate important structural determinants and properties of the SybII TMD that have a potential role in facilitating membrane fusion.

4 Materials and methods

4.1 Materials and reagents

All reagents and chemicals were obtained from Sigma-Aldrich (St. Louis, MO, U.S.A.) unless otherwise noted. In addition, all allied products (falcon tubes, Petri dishes, six-well plates, etc.) were from Life Technologies (Carlsbad, California, U.S.A.).

4.2 Transgenic mice and genotyping

All experiments were performed on chromaffin cells prepared from wild type, and a mutant (CpxII ko, Syt7 ko, Syt1 ko, Syt1 Tm3, Syt1 Tm5) littermates of either sex at P0-P2. For prenatally lethal knockouts (Syb/Cel), pregnant mothers were sacrificed at E18; doubleknockout pups showing a distinctive phenotype of an arched back and smaller stature are prepared with a proper littermate. Animals were kept according to German Animal Health Care regulations and sacrificed according to the German animal care, and humane sacrificing regulations.

Genotyping

instruments

PCR thermocycler	Biometra	T3000 thermocycler
Heating Block	HLC	HBT 130
Table top centrifuge	Thermo Scietific	Heraeus Biofuge Pico
Balance	Mettler	PI200
Power supply	BioRad	Power Pac 300
Geldock	PeqLab	
Gel block	BioRad	

Mouse lines

C57BL/6N (wt)	The Jackson Laboratory	Stock No: 005304
CpxII ko	Dr. N. Brose (MPI Gottingen, Germany)	Reim et al., 2001
Syt1 Tm3 (R233Q KI)	The Jackson Laboratory	Stock No: 006385
Syt1 Tm5 (D232N KI)	The Jackson Laboratory	Stock No: 006386
Syt VII ko	The Jackson Laboratory	Stock No: 004950

Primers (25 pM/μL):

Fw Cpx mut	Eurofins MWG Operon	5'- CGC GGC GGA GTT GTT GAC CTC G -3'
Rev Cpx mut	Eurofins MWG Operon	5'- CAG GCA CAC TAC ATC CCA CAA ACA -3'
Fw Cpx wt	Eurofins MWG Operon	5'- CGG CAG CAG ATC CGA GAC AAG -3'
Rev Cpx wt	Eurofins MWG Operon	5'- GAG AGG GGC ATG AAG TCA AGT CAG -3'
Fw Syt7 mut	Eurofins MWG Operon	5'- CCT ACC TGA AGC CTG TGT TCAC - 3'
Rev Syt7 mut	Eurofins MWG Operon	5'- CAG CTG TGC TCG ACG TTG TCA CTG -3'
Fw Syt7 wt	Eurofins MWG Operon	5'- CAT CCT CCA CTG GCC ATG AATG - 3'
Rev Syt7 wt	Eurofins MWG Operon	5'- GCT TCA CCT TGG TCT CCA G -3'
Fw Syt1 mut	Eurofins MWG Operon	5'- GAG CGC GCG CGG CGG AGT TGT TGA C - 3'
Rev Syt1mut	Eurofins MWG Operon	5'- AAC TAT AAT TTG TCA CAG GCA TTG CCT TTC A -3'
Fw Syt1wt	Eurofins MWG Operon	5'- GTA TTC AGT GCG TCT CAG AGA C - 3'
Rev Syt1wt	Eurofins MWG Operon	5'- AAC TAT AAT TTG TCA CAG GCA TTG CCT TTC A -3'
Fw SytI Tm3/Tm5 mut	Eurofins MWG Operon	5'- CAG CTG TGC TCG ACG TTG TCA CTG - 3'
Rev SytI Tm3/Tm5 mut	Eurofins MWG Operon	5'- CTA TTA GGG GTC TGA AGC - 3'
Fw SytI Tm3/Tm5 wt	Eurofins MWG Operon	5'- GGA TCT CTA TGT ATA ATA GTC TCT CTG - 3'
Rev SytI Tm3/Tm5 wt	Eurofins MWG Operon	5'- GAA TTG ACA TCA GTA TTA G - 3'
Fw SybII wt	Eurofins MWG Operon	5'- GCC CAC GCC GCA GTA CCC GGA TG - 3'
Rev SybII wt	Eurofins MWG Operon	5'- GCG AGA AGG CCA CCC GAT GGG AG - 3'
Fw SybII mut	Eurofins MWG Operon	5'- CAC CCT CAT GAT GTC CAC CAC - 3'
Rev SybII wt	Eurofins MWG Operon	5'- CAG CAG ACC CAG GCC CAG CG - 3'

DNA extraction**Materials:**

DNA Extraction buffer	Quanta Bio, 95091-025	100 μl per tail
DNA Stabilization buffer	Quanta Bio, 95091-025	100 μl per tail
Tail	1 - 3 mm	

Genotyping mix 25μl (per tail):

DDH ₂ O	Sigma, W4502	11.5 μl
Green Kappa Mix		10 μl
Forward primer (25 pM/μL)		1.25 μl
Reverse Primer (25 pM/μL)		1.25 μl
Extracted DNA		2 μl

PCR programs

CpxII/SytVII wt reaction:

94°C	5 minutes	41 cycles
94°C	30 seconds	
64°C	45 s	
72°C	1 min	
72°C	7 min	
4°C	Pause	

CpxII/SytVII mutant reaction:

94°C	5 minutes	41 cycles
94°C	30 seconds	
59°C	30 s	
72°C	1 min	
72°C	7 min	
4°C	Pause	

SytI tm3/tm5 wt reaction:

95°C	5 minutes	35 cycles
95°C	30 seconds	
65°C	30 s	
72°C	2 min 30 s	
72°C	10 min	
4°C	Pause	

SytI tm3/tm5 mutant reaction:

95°C	5 minutes	35 cycles
95°C	30 seconds	
60°C	30 s	
65°C	2 min 30 s	
65°C	10min	
4°C	Pause	

SybII wt reaction:

95°C	5 minutes	35 cycles
95°C	50 seconds	
55°C	45 s	
65°C	1 min 30 s	
65°C	10 min	
4°C	Pause	

SybII mutant reaction:

95°C	4 minutes	40 cycles
95°C	30 seconds	
60°C	30 s	
72°C	2 min	
72°C	10min	
4°C	Pause	

Syt1 wt reaction:

94°C	5 minutes	35 cycles
94°C	30 seconds	
60°C	45 s	
72°C	1 min 30 s	
72°C	10min	
4°C	Pause	

Syt1 mutant reaction:

94°C	5 minutes	35 cycles
94°C	30 seconds	
60°C	45 s	
72°C	1 min 30 s	
72°C	10min	
4°C	Pause	

Gel electrophoreses:

Materials:

Agarose powder	Biozym, 840004	1.8 %
Ethidium Bromide	Sigma Aldrich, E1510	0.0008 %
DNA Ladder	New England Biolabs, N0553G	8 µL/lane
Tris-Acetate-EDTA running buffer	40mM TRIS, 20mMacetic acid, and 1 mM EDTA	

Procedure:

Off springs of heterozygous parents from mouse lines carrying mutations were used for the electrophysiological recordings. Homozygous wild type or mutant littermates were identified using the Polymerase Chain Reaction (PCR). The presence of a mutation was detected using well-designed primers flanking a reporter (neomycin cassette), giving a specific molecular weight. Statistically, the ratio of null mutants was in accordance with Mendel's law.

Mice tails were digested for 30 minutes at 95°C with the extraction buffer, followed by addition of the Stabilization buffer 1:1 at room temperature. The extracted DNA was then diluted 1:1 with DDH₂O and centrifuged at 13000 RPM for 2 minutes. 2 µl of the supernatant having the extracted DNA was added into a 200 µl Eppendorf tube containing 25 µl genotyping mix and placed in the PCR Thermocycler running the program corresponding to the reaction in use. The amplified DNA was migrated on a 1.8% agarose-TAE gel supplied with ethidium bromide for 30 minutes at 5V/cm. DNA bands were resolved by UV illumination that allowed the determination of their molecular weight in reference to the DNA ladder bands running along at the first well.

4.3 Mouse chromaffin cell preparation

Instruments:

Dissection forceps	AESCALP	BD331R
Cleaning forceps	Dumont	Dumostar 09-55
Microscope	Zeiss	Stemi 2000
Laminar flow sterile hood	Thermo Scientific	Safe 2020
Cell incubator	Thermo Scientific	Hera cell 150

Solutions:

1. Lock's Solution

NaCl	Roth, 9265.2	58.44 g / mol	154mM
KCl	Sigma, P4504	74.55 g / mol	5.6mM
NaHCO ₃	Merck, 1.06329.1000	84.01 g / mol	3.6mM
D(+)-Glucose	Sigma, G6152	180.16 g / mol	5.6mM

HEPES	Sigma, H7523	238.30 g / mol	5.0mM
pH=7.3 NaOH	340mOsm/kg		

2. Digestion Solution (Freshly made, batched, and stored at -20°C)

DMEM	Fisher, 1074-8424		250mL
L- cysteine	Sigma, C7352	121.16 g/mol	1.65mM (50mg)
CaCl ₂ .H ₂ O	Sigma, 21115	110.98 g/mol	100mM
Na ₂ EDTA	Roth, 8043.3	372.24 g/mol	100mM
Papain suspension	Worthington, LS003126	100 mg	20 units/ml
pH=7.3			

3. Inactivation Solution (Freshly made, batched, and stored at -20°C)

DMEM	Fisher, 1074-8424	225mL
Fetal Calf Serum	Fisher, 1066-4083	25ml
Trypsin Inhibitor	Fisher, 1077-9414	
pH=7.3		

4. Culture Medium

DMEM	Fisher, 1074-8424	100mL
Penicillin-Streptomycin	Fisher, VX15140122	4000units & 4000 µg
Insulin-Transferrin-SeleniumX 100X	Gibco, 51500056	1ml (1:100)

Materials:

Petri Dishes	FALCON, 351008
Filter unit	Millipore, SCGVU02RE
Tubes	Greiner Bio-One, 188271 & 227261
6 Well Plates	FALCON, 353224
Glass Cover slips	Hecht ASSISTANT, 41001125

Procedure:

Adrenal glands were extracted from P0-P2 pups, the excess connective tissue is removed in an ice cold Locks' solution without damaging the cortex. Glands are then submerged with digestion solution and incubated in a shaking water bath at 37° C for 20 minutes. The digestion solution is then replaced with an inactivation solution and incubated again at 37° C for 5 minutes. The glands are then washed with the culture medium before the trituration step. Afterwards, the glands are then triturated in 200 µl culture medium and further diluted by the addition of 400 µl of culture medium. The cell suspension is then distributed equally on six glass cover slips in a six well plate and incubated for 30 minutes at 37° C, 11 %CO₂. 3 ml of culture medium are then added to each well and the cells are kept in the incubator until the day of measurement. Note that from the

digestion step onward, all the steps were performed in a sterile laminar flow hood. Electrophysiological measurements were carried out on DIV 2.

4.4 Electrophysiology

Instruments:

The flash uncaging - calcium imaging patch clamp setup.

Microscope	Zeiss	Axiovert 200
Objectives	Zeiss	FLUAR 40x/1.30 oil 440255
Fura Filter set	Till photonics	DCLP 410/LP 440
FITC Filter (GFP Filter)	Zeiss	BP 450-490/FT 510/LP515
Lock-in Amplifier	HEKA	Double Patch Clamp EPC9/2
Monochromator	Till Photonics	Polychrome IV
UV Flash lamp	Rapp Optoelectronics	Xenon flash lamp system JML-C2
UV Flash filter	Analysetechnik AG	UV-3, FT 400, AHF
Photodiode detector	Till Photonics	Photodiod detector head SN0210016
Camera	WATEC AMERICA Corp.	LCL-902C
Micromanipulator	Piezosystem Jena	TRITOR100
Air table	Technical Manufacturing Corporation USA	

Fabrication of the Glass Micro Pipettes.

Micropipette puller1	Sutter Instruments	BROWN/FLAMMING Model P87
Micropipette puller1	Sutter Instruments	BROWN/FLAMMING Model P1000
Filaments	Sutter	FB255B
Borosilicate glass capillaries	HARVARD APPARATUS	30-0057capillaries GC150F-10
Microforge		
Upright Microscope	Zeiss	
Objective 1 (Low mag.)	Zeiss	Acrostigmat 5X/0.12 440120
Objective 2 (High mag.)	Zeiss	Epiplan50X/0.50 442850
Platinum Filament	Alfa Aesar GmbH	D=0.25mm PN: 10288

Ringer Solution (extracellular recording bath solution) 2 mM free Ca²⁺:

NaCl	Roth, 9265.2	58.44 g / mol	140 mM
KCl	Sigma, P4504	74.55 g / mol	4 mM
CaCl ₂	Sigma, 21115	110.98 g/mol	2 mM
MgCl ₂	Sigma, M2393	203.30 g / mol	1 mM

D-Glucose	Sigma, G6152	180.16 g / mol	30 mM
HEPES	Sigma, H7523	238.30 g / mol	10 mM
pH =7.4 with NaOH	Osmolarity 330 mOsm/kg		

ATP-GTP Stock solution

ATP magnesium salt	Sigma, A9187	507.18 g / mol	20 mM
GTP-Disodium salt	Sigma, G8877	523.18 g / mol	3 mM
HEPES	Sigma, H7523	238.30 g / mol	20 mM
pH =7.4 with CsOH			

Fura- Mag Fura Stock solution

Fura-2, Pentapotassium Salt	Thermo Fisher, F1200	831.996 g / mol	2 mM
Mag-Fura-2, Tetrapotassium Salt	Thermo Fisher, M1290	586.68 g / mol	3 mM
HEPES	Sigma, H7523	238.30 g / mol	10 mM
pH =7.4 with CsOH			

NP-EGTA Stock solution (1:1) dilution with HEPES solution

NP-EGTA	HOM made	653.8 g / mol	50 mM
HEPES	Sigma, H7523	238.30 g / mol	50 mM
pH =7.4 with KOH			

Viral activation: (200µl)

Opti-Mem (1X)	Gibco, 31985-062	- (175 µl)
α-Chymotrypsin from bovine pancreas	Sigma, C4129	2 mg/ml (55µl)
Aprotinin from bovine lung	Sigma Aldrich, A1153	6 mg/ml (55µl)
Bovine Serum Albumin	Sigma-Aldrich, A7906	6.5 % (55µl)

Peptide dissolution solution

KCl	Sigma, P4504	74.55 g / mol	20mM
HEPES	Sigma, H7523	238.30 g / mol	40mM
pH=7.4 KOH			

Data acquisition and analysis software:

Pulse	HEKA
Igor	Wave Metrics Software
Sigma Plot 12	Systat Software Inc.(SSI)

4.4.1 Primer on the patch clamp technique

Patch clamp is an electrophysiological method that allows to detection of the macroscopic whole cell and the microscopic single channel currents in isolated living cells and tissue sections. This technique was first used to identify single-channel conductance and mean open times under a constant voltage (voltage-clamp), and the changes in the current indicated the channel activity (Neher et al., 1976). The electrical signals resulting from the cell's activity are minute, scaling from the femto (10^{-15}) to the nano (10^{-9}) range. Thus, reducing the electrical noise and increases the temporal resolution is necessary for detecting those changes in electrical signals. Therefore, isolating a patch of the cytoplasmic membrane inside the glass tip of a patch pipette allows for low noise recordings of the biological activity (Sakmann 2009). Due to the high precision and high

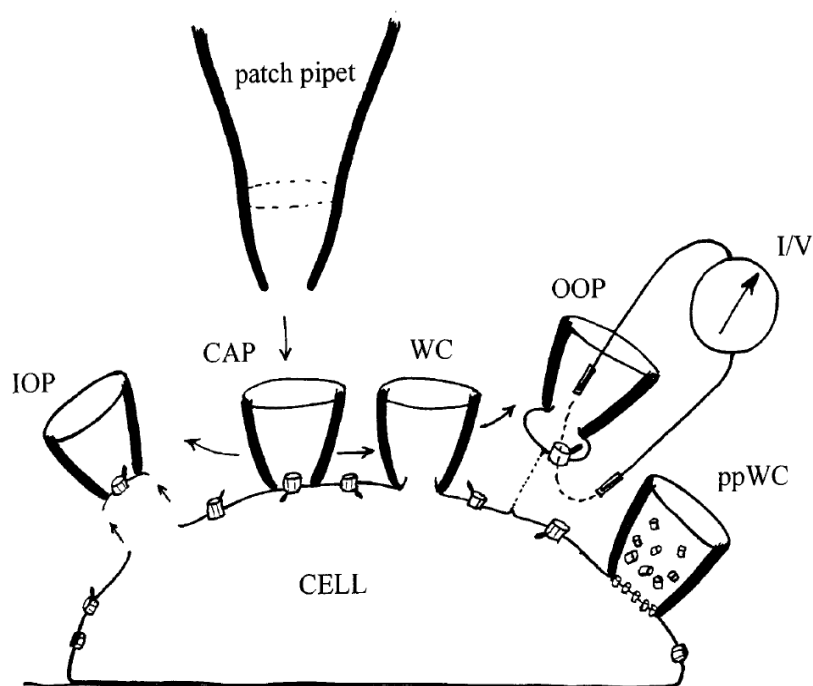


Figure 8. The five configurations of the patch clamp recording. The diagram represents a side view of an exemplary living cell, with ion channels represented as the barrel like structures on the membrane. Five configurations of the patch technique each represented with a pipette. From left to right starting with the inside out patch (IOP), cell attached patch (CAP), whole cell (WC), outside out patch (OOP), permeabilized-patch whole cell configuration (ppWC). These configurations are not practically possible at the same time, a maximum of 2 electrodes have been used in measuring cellular exocytosis and activity (DeFelice 1997).

resolution of the patch clamp technique, this diversified its use from quantifying the voltage dependence of single ion channels activation up to measuring the changes in membrane potential as well membrane surface area. As a technical approach, the diversity of the patch clamp technique comes from the different configurations it can be used in (Figure 8), wherein the selected configuration depends on the model system of choice and on the scientific question under investigation.

The first configuration is the cell-attached patch (CAP) which is used for the detection of currents through a single channel in an intact cell membrane, this is made possible by isolating the channel in a tight seal formed between the glass pipette and the cell membrane (Gigaseal). Unlike the CAP, the whole cell (WC) configuration requires breaking the cell membrane after the gigaseal is achieved, creating a continuity between the pipette and the cell lumen, which drives a dialysis-like solution exchange between the pipette and the inside of the cell. This approach is widely used to infuse cells with defined components as calcium concentrations, calcium dyes, deliver peptides and other components, which can modulate exocytosis in excitable cells. A second method allows the exchange between the cell lumen and the patch pipette solution while keeping the cells relatively intact is the permeabilized-patch whole cell configuration (ppWC). This is achieved by supplying the patch pipette solution with antibiotics that serve the role of ion transporters across the cell membrane without the need to break it (Figure 8). Two patch clamp configurations are used to measure isolated single channel activity, in which the ion channel is excised from the cell membrane and its activity monitored in response to changes in their surrounding microenvironment. An inside out patch (IOP) excision of the channel with the previously intracellular region now exposed to the extracellular environment is accomplished by retracting the patch pipette from the cell membrane after the gigaseal has formed. On the other hand, the channel orientation can be maintained as it was in the cell membrane by using 'the outside-out patch (OOP)'. To achieve this, the channel is excised by maneuvering the pipette away from the cell membrane after achieving the whole cell configuration. In the OOP the ion channel is oriented with its extracellular compartment is exposed to the same phase and the previously intracellular domain becomes exposed to the pipette solution (DeFelice 1997) (Figure 8).

4.4.2 Principle of whole cell voltage clamp for membrane capacitance measurements

Low noise whole cell recording requires a tight seal and continuity between the patch pipette and the cell membrane, as well as a low resistance connection between the lumens of the pipette and

the cell that allows for modifications in the intracellular environment by exchanging it with the solution in the patch pipette. Simultaneously, membrane voltage is held constant to monitor membrane electrical properties under resting or depolarized conditions. Here we use voltage clamp with the cell with membrane potential held at resting value (-70 mV) to avoid the activation of voltage gated calcium channels. The changes surface area of the cell membrane is reported as capacitance variations in response to stimulus which represents the dynamic equilibrium between the processes of exocytosis and endocytosis in secretory cells like chromaffin cells.

4.4.2.1.1 The cellular cytoplasmic membrane is equivalent to an RC circuit model

The lipid bilayer membrane outlining the cell is an electrical insulator. In excitable cells, the intracellular concentration of negatively charged ions (Cl^-) is kept higher than the extracellular one, and vice versa for the positively charged ions (Na^+). Essentially this accumulation of opposite charges separated by an insulating lipid membrane defines an electrical capacitor (Figure 9 A). The membrane capacitance is directly proportional to the surface area of the cell, given by the equation:

$$C = \frac{A * \epsilon_r}{d}$$

Where C is the capacitance (in Farads) A is the area of the membrane (in square meters), ϵ_r is the membrane's dielectric constant (Farads per meter) (ϵ_r is 2-3), and d is the separating distance between the opposite charges (thickness of the membrane uniform from 5 to 10 nm) in meters.

The channels embedded in the cell membrane act as resistors (Figure 9 A), and R_M is the total resistance of the membrane coming from the ion channels. The magnitude of R_M depends on the type of the ion channels and the ions they are permeable to; usually R_M is in the range of 1 G Ω (Chen et al., 2000). The lipid membrane and the channels embedded in it, allow the electrical representation of a patch-clamped cell membrane by a capacitor and a resistor connected in parallel to a power source also known as an RC circuit (Figure 9 B). In whole-cell configuration, a voltage is applied by the patch electrode to the cell membrane (RC circuit), the voltage passes through the capacitor first then makes its way to the resistor.

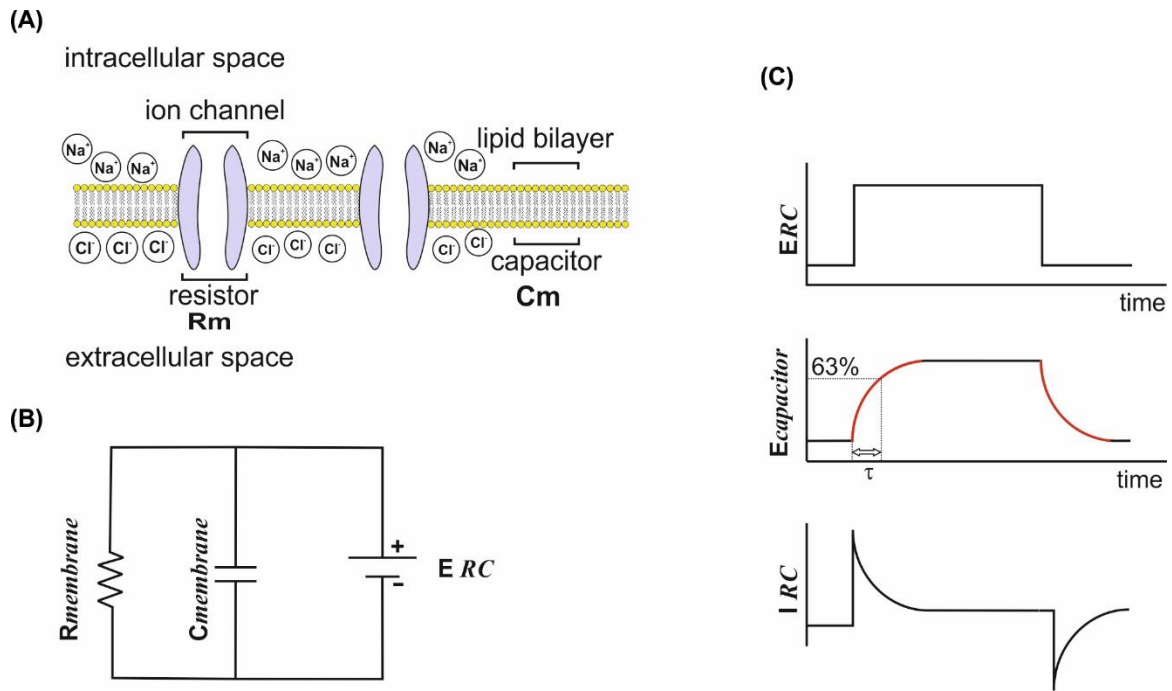


Figure 9. The RC circuit representation of the cell membrane and the corresponding electric signals in whole cell recording. (A) The lipid membrane acts as a capacitor separating positive and negatively charged ions on the intra and extracellular spaces respectively, with ion channels acting as resistors. **(B)** Representation of the cell membrane as an RC (resistor-capacitor) electrical circuit **(C)** ERC is the voltage supplied via the power source as a stepwise increase. $E_{capacitor}$ is the voltage passing through the capacitor causing a transient increase in potential with a defined τ . IRC current flowing through the RC circuit which decreases with the same τ as the capacitance transient in the $E_{capacitor}$.

The voltage applied to the cell membrane is in a square step fashion (Figure 9 C upper panel). This causes a slow increase in the voltage across the capacitor with a time constant τ (time needed to fill 63% of the maximum available capacity) (Figure 9 C middle panel). The voltage across a capacitor at a time (t) is given by the equation:

$$Vm(t) = V(1 - e^{-\frac{t}{\tau}})$$

With $\tau = R_c * C$

R_c being the internal resistance in Ohm of the capacitor and C is the capacitance in Farad.

The current across the membrane IRC has two components (Figure 9 C lower panel)

$$IRC = I_r + I_c$$

The first is the capacitive current I_c resulting from the voltage changes across the capacitor

$$I_c = C_m \frac{dV}{dt}$$

In addition, the second component of the membrane circuit is the current across a resistor I_r :

$$I_r = \frac{V}{R_m}$$

with the current being proportional to the voltage when applied across the resistor.

The electrical connection between the voltage-recording electrode and the membrane also has a resistance in series to the cell circuit (Figure 11 A) R_{series} (R_s). When the voltage V_c surges through the membrane, the true potential across the membrane changes equivalent to the series resistance $I_x R_s$. There for it is highly desirable for R_s to have low values in the whole-cell

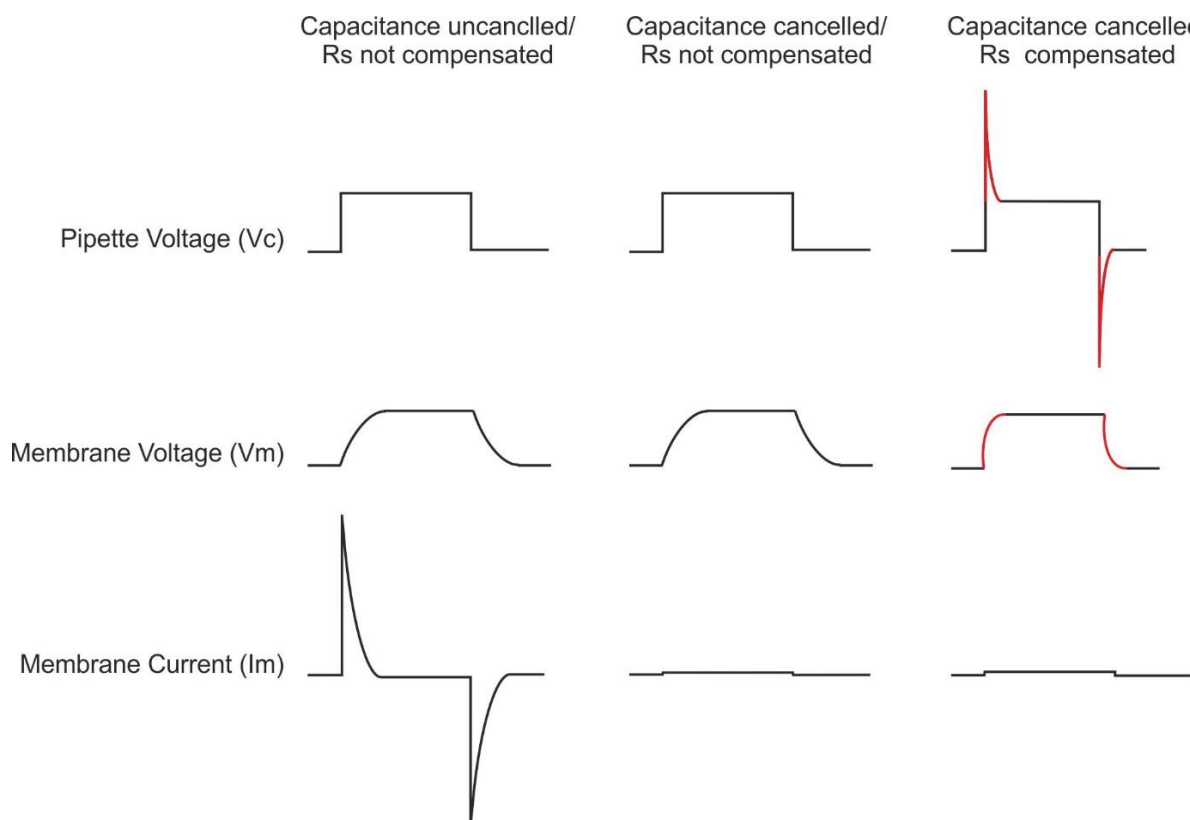


Figure 10. Compensation of membrane capacitance and series resistance R_s in voltage clamp recordings. The applied square like step voltage to the pipette (V_c) causes a transient exponential increase in the membrane capacitive voltage $V_m(t)$ and produces a membrane capacitive current I_m . Canceling the membrane capacitive current I_m does not change the time course of the membrane voltage $V_m(t)$. On the other hand, compensation for R_s by injecting overshooting voltage pulses (red peaks in the pipette voltage), accelerates the charging and discharging phases of $V_m(t)$ (reduction in the time constant τ of the capacitive transients) which increases the temporal resolution for detection of changes in membrane capacitance C_m .

configuration to ensure a proper electrical continuity between the patch pipette and the cell membrane. In whole cell recordings, the access resistance of the pipette as well as the leakage resistance contributes to the R_s . Thus, it is critical to compensate for R_s in whole cell voltage clamp

recordings. To compensate for R_s effects, the amplifier injects additional current translated to overshooting potential pulses (the red peaks in V_c) equivalent to the current drop caused by the series resistance (Figure 10).

4.4.2.1.2 Assessing the size of the cell membrane using electrical capacitance

A command sine-wave voltage (**V-command**) ($V(t)=V_0 \cdot \cos \omega t$) with a frequency (ω) is supplied to the cell membrane after the whole cell configuration by the amplifier in a lock-in configuration (Figure 11 B). The virtue of using the sine-wave voltage input comes from the nature of the sine-wave signal itself, having an inflection point (where the net applied voltage across the membrane is zero), and a peak (where the voltage value is constant) (Figure 11 C). Using Ohm's Law, the capacitance and the resistance parameters of the cell membrane can be determined. Determination of the membrane capacitance is at the inflection point of the I_{Rm} where the voltage and the resistive current I_{Rm} values are zero. Thus the capacitive current is given by:

$$I_c(t) = C_m \frac{dV}{dt} = C_m \frac{dV_0 \cos \omega t}{dt} = -\omega \cdot C_m \cdot V_0 \cdot \sin \omega t$$

The resulting capacitive current is shifted by 90 degrees due to the nature of the applied sine-wave voltage, which is then processed by the phase sensitive detector in the lock-in amplifier, and the capacitance of the membrane can be now determined by the equation:

$$C_m = \frac{-I_c(t)}{2\omega \cdot V_0 \cdot \sin \omega t}$$

On the other hand, determination of the resistive current I_{Rm} is performed when the voltage has a constant value, which is the maximum value at the peak of the sine-wave signal where the I_{Cm} is at zero (Figure 11 C). Given by Ohm's Law:

$$I_{Rm} = \frac{V(t)}{R_m} = \frac{V_0 \cdot \cos \omega t}{R_m}$$

Then R_m would be:

$$R_m = \frac{V_0 \cdot \cos \omega t}{I_{Rm}}$$

It is worth mentioning that the phase shift and amplitude of a sine wave are determined from one sine wave period. The time resolution of capacitance measurement using sine wave is determined by the frequency of the applied sine wave (one data point per sine wave). The accuracy (noise reduction) of capacitance measurements depend on the amplitude of the sine wave, although one

should choose the magnitude of the sine wave with care, to avoid activation voltage-gated channels.

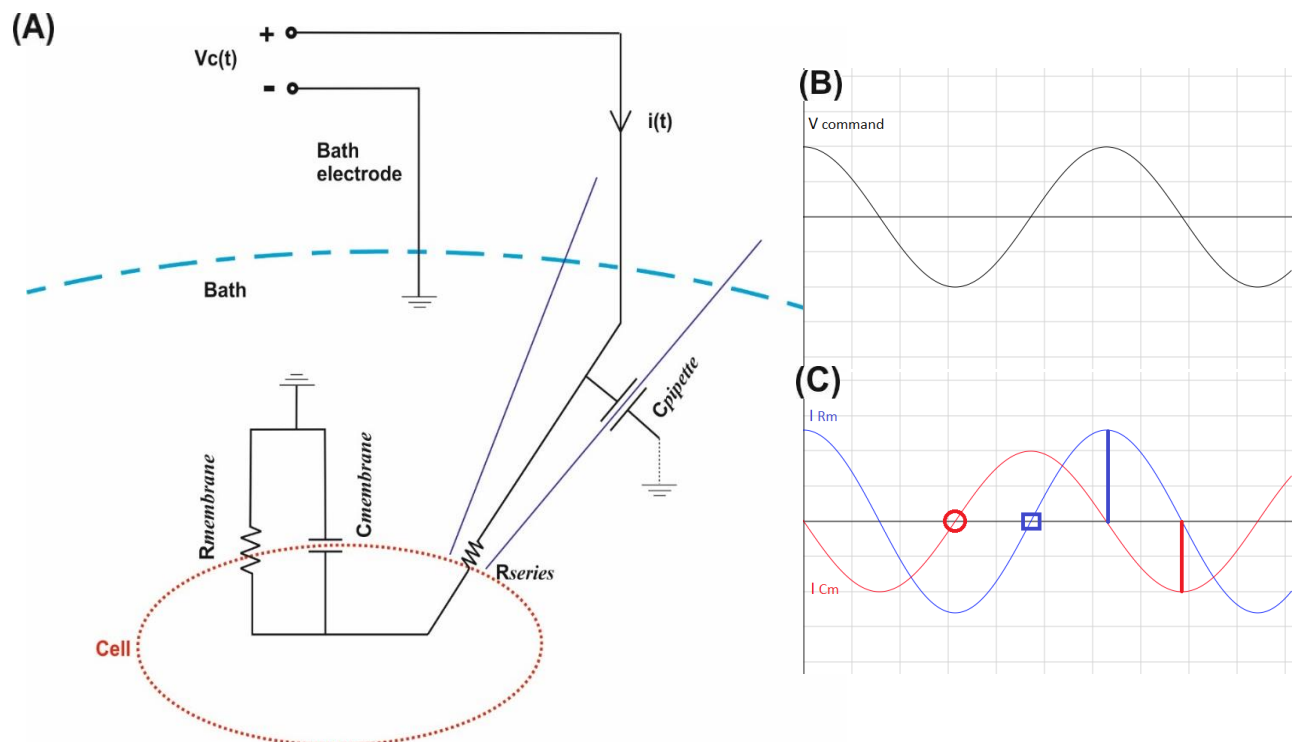


Figure 11. Electrical circuit representation of a voltage clamp in a whole cell configuration. (A) Representation of a cell membrane (red) in a bath (blue stripe), in a whole cell configuration with a patch pipette (violet). **R pipette**: is the pipette resistance when immersed in the bath solution without touching the cell. **C pipette**: pipette capacitance. **R leak**: leakage resistance. **R access**: resistance of the connection between the cell lumen and the pipette solution. **C membrane**: membrane capacitance of the cell reporting the cell size. **R membrane** resistance generated by the ion channels in the cell membrane. The probe is the detector for the returned voltage returning from the pipette-cell circuit. Amplifier controlling holding potential and injecting current to compensate the loss by the pipette-cell circuit. **(B)** Sine wave voltage applied by the amplifier to the cell membrane. **(C)** Detected currents from the **RC** circuit are the current through the capacitor I_{Cm} with a phase shift and amplitude changes from the V_{command} in (B), and an I_{Rm} in phase with the original V_{command} in (C) (blue sine wave). The obtained I_{Rm} current has an inflection point (blue square) at which the voltage and resistance are zero at which membrane capacitance is constant at its maximum value (red line), and a peak (indicated by the blue line) at which the voltage is constant. Vice versa, membrane resistance I_{Rm} is determined at the peak where the I_{Rm} is constant at its maximum value (blue line), and the capacitive current is at zero (red circle).

Unlike the capacitive current, the resistive current of the membrane is in phase with the sine-wave voltage signal. With the utilization of sine-wave potential signal, two (C_m , R_m) of the three important parameters (C_m , R_m , and R_s) of the whole cell voltage clamp recording are resolved. For this end, two methods were proposed to estimate the third parameter R_s (series resistance).

The first known as the "Piecewise-Linear technique", is by assuming that changes in the membrane resistance and in the access resistance have minimal effect on the membrane capacitance estimation, rendering the identification of the series resistance unnecessary. In addition, a second more preferred, and widely used "sine-wave + DC" approach by which the introduction of an additional direct current to the circuit can be used to quantify the series resistance of the cell-membrane connection. In this work, a "sine wave + DC" voltage clamp was applied to the chromaffin cells in the whole cell configuration to measure the increase in membrane surface area because of calcium driven vesicle fusion.

Experimental Procedure:

In this work, Capacitance measurements were performed according to the Lindau-Neher technique. Parameters were set for all electrophysiological recordings DC-holding potential at -70 mV, with sine wave stimulus to 1000 Hz and peak-to-peak amplitude was set to 35 mV. Whole-cell recordings were performed with patch pipettes with a resistance $R_p = 4 - 6 \text{ M}\Omega$. Current signals were digitized at 20 kHz and R_s , R_m , and C_m were calculated with the use of implemented lock-in module in the pulse software. The inverse of the R_s , and R_m are displayed on the X chart recording table which are the series conductance $G_s = \frac{1}{R_s}$ and the membrane conductance $G_m = \frac{1}{R_m}$ respectively. Cells were selected for averaging based on their electrical properties after visual inspection, cells with G_m higher than 200 nS, or cells displaying a decrease in series conductance G_s greater than 30% over the recording period were discarded. Current signals were digitized at 20 Hz and membrane capacitance was analyzed with custom-made Igor Pro routines Recordings were performed at room temperature.

4.5 Measuring exocytosis and determination of vesicle pools in chromaffin cells

Chromaffin cells evolved from the same neuronal crest as the sympathetic neurons (Doupe et al., 1985), and they share similar proteins that mediate regulated exocytosis as in neurons. Unlike neurons though, these cells lack specialized release sites "active zone" and instead release neurotransmitters at any site on their plasma membrane (Angleton et al., 1999).

Owing to similarities in the exocytotic mechanism and the identity of the proteins mediating vesicular exocytosis in both chromaffin cells and neurons, chromaffin cells serve as a model system which provides several advantages over their closely related neuron for studying exocytosis (Rettig

et al., 2002). Firstly, chromaffin cells are spherical, relatively small sized cells (8-10 μm in diameter) in contrast to neurons, making them well suited for voltage clamp experiments (Hamill et al., 1981). High resolution membrane capacitance measurements can be utilized to estimate vesicle fusion in chromaffin cells (Moser et al., 1997), which can be coupled with several techniques to study aspects of fusion based on the question at hand. Some of which can estimate vesicles pool sizes and their subsequent kinetics of release in response to intracellular calcium uncaging by an ultraviolet (UV) flash (Neher et al., 1993; Voets et al., 1999; Voets 2000). Secondly, given the oxidizable cargo of the chromaffin cell granules (adrenaline and noradrenaline), carbon fiber amperometry can be used to measure the kinetics of cargo discharge through a dilating fusion pore as well as the quantal catecholamine release from single vesicles (Wightman et al., 1991; Bruns 2004). In a different approach, vesicle fusion and cargo discharge from chromaffin cells as well as the post-fusion translocation of synaptic proteins can also be determined using total internal reflection microscopy (TIRF) (Basso et al., 2004). Furthermore, chromaffin cells lack a post synapse, which makes it possible to study the functional aspects of presynaptic proteins independently from postsynaptic adaptations. These advantages make of chromaffin cells a well-adapted and controlled model system for electrophysiological measurements to study exocytosis.

4.1 Flash photolysis of caged Ca^{2+} and the calibration curve for intracellular calcium estimation

The basis to study calcium stimulus-secretion coupling in chromaffin cells was established by Thomas Voets and Erwin Neher about two decades ago (Voets et al., 1999; Voets 2000). In short, a photo labile calcium chelating agent Nitrophenyl-EGTA (Figure 12 B) having a calcium affinity of K_d 8.0×10^{-8} M in its native form is supplied to the pipettes solution, an application of an intense UV light decreases its calcium affinity to 1.0×10^{-3} M (Ellis-Davies et al., 1994) resulting in an instantaneous liberation of the caged calcium. Additionally, calcium reporters Fura2 and Mag-Fura2 (Grynkiewicz et al., 1985) were used in the pipette solution to continuously monitor calcium levels in the cell. The calcium indicators show a shift in their spectral properties upon calcium binding (Figure 12 A). Fura2 with K_d close to the basal calcium in mammalian cells $\sim 224\text{nM}$ (Grynkiewicz et al., 1985) that can report with high fidelity the calcium concentration in the submicromolar range required for vesicle priming in chromaffin cells, and Mag-Fura2 $K_d \sim 20$ mM

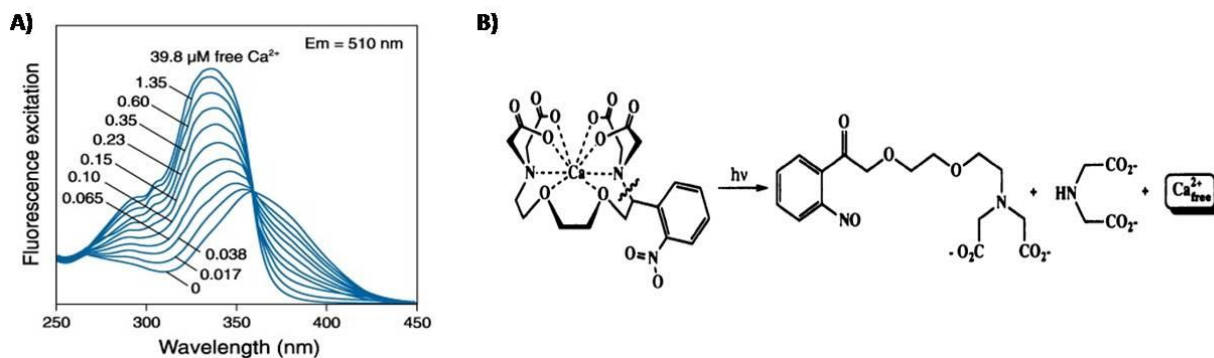


Figure 12. Florescence profile of Fura2 and the reversible Ca^{2+} buffering by NP-EGTA. (A) Spectral emission properties of the calcium dye Fura2 measured at 510 nm at increasing free calcium concentrations. Intensities of the emission increase with the increase of the free Ca^{2+} in the range of excitation wavelengths 300-350 nm with the highest difference in the emission is when Fura2 is excited at 340nm (Hyrc et al., 2000). (B) The photo labile calcium chelator NP-EGTA which liberates calcium after the break of its backbone by a short intense UV flash (Ellis-Davies et al., 1994), the byproduct of this breakage has a 12500 times less affinity to calcium than NP-EGTA.

reporting over the range of calcium concentrations that induce fusion (1- 100 μM) in this model system (Hyrc et al., 2000). In our experiments, we use a combination of both calcium indicators in the intracellular solution allowing for a reliable estimation of the intracellular Ca^{2+} concentration in patch-clamped chromaffin cells.

4.1.1 Calcium calibration curve for intracellular calcium imaging

Free calcium concentrations in the cell can be continuously monitored comparing the ratio metric emissions of the calcium indicators Fura-2 and Mag-Fura-2. The outcome ratio is compared with a calibration curve made with irreversible calcium chelators BAPTA and DPTA to have 11 solutions with increasing free calcium concentrations.

Stock Solutions:

4X Cs-Glutamate (440 mM) 100 ml:

L-Glutamic acid (Potassium free)	Sigma, G1251	147.13 g / mol	440 mM
NaCl	Roth, 9265.2	58.44 g / mol	32 mM
HEPES	Sigma, H7523	238.30 g / mol	80 mM
pH =7.4 with CsOH			

BAPTA (100 mM) 5 ml:

BAPTA, tetrapotassium salt	Invitrogen, B1204	628.8006 g / mol	100 mM
HEPES	Sigma, H7523	238.30 g / mol	264 mM
pH =7.4 with CsOH			

DPTA (100 mM) 100 ml:

DPTA	Aldrich, 158178	322.27 g / mol	100 mM
HEPES	Sigma, H7523	238.30 g / mol	10 mM
pH =7.4 with CsOH			

Calcium calibration solutions**Solutions containing BAPTA**

Sol.Nb.	Ca ²⁺ (mM)	CaCl ₂ ,μl(100mM)	BAPTA,μl(100mM)	4x Cs glut,μl	H ₂ O,μl	Osmolarity	pH
1	0	0	328	267	405		
2	13,7	137	328	252	283		
3	19,2	192	328	231	249		
4	23,0	230	328	224	218		
5	25,0	250	328	220	202		

The five solutions above represent the five calcium concentrations, each of which is one point on the calibration curve. The osmolarity is between 350 to 380 mmol/kg. The pH is adjusted to 7.4 with CsOH. Later a very small amount of the solutions (64μl) is added to 10 μl 10x ATP/GTP solution (8μl) and 10x fura-2/mag-fura solution (8μl).

Sol. Nb	Ca ²⁺ (mM)	Ca ²⁺ - BAPTA Sol (μl)	10x ATP/GTP (μl)	10x fura-2 /Mag-Fura2 (μl)	Ca ²⁺ free calculated (nM)	Mg ²⁺ free calculated(nM)	Osmolarity Mmol/Kg	pH
1	0	64	8	8	1e ⁻⁹			7.29
2	13,7	64	8	8	1.5439 e ⁻⁷			7.29
3	19,2	64	8	8	3.0254 e ⁻⁷			7.37
4	23,0	64	8	8	4.8839 e ⁻⁷			7.36
5	25,0	64	8	8	6.7004 e ⁻⁷			7.33

6 solutions containing DPTA are made to determine the ratio of high calcium range on the calibration curve. Osmolality and pH are measured and a small fraction (64µl) will be added to 10 µl 10x ATP/GTP solution (8µl) and 10x fura-2/Mag-fura solution (8µl).

Solutions containing DPTA

Sol.Nb.	Ca ²⁺ (mM)	Mg ²⁺ (mM)	CaCl ₂ , µl (100mM)	MgCl ₂ , µl (100mM)	DPTA, µl (100mM)	4x Cs-glut, µl	H ₂ O, µl DDW	Osmolarity	pH
1	2.8	6.5	28	65	400	205	302		
2	5.3	6.0	53	60	400	201	286		
3	9.0	5.5	90	55	400	195	260		
4	20	3.5	200	35	400	182	183		
5	25	2.5	250	25	400	175	150		
6	35	0.5	350	5	400	163	82		

Sol Nb.	Ca ²⁺ (mM)	Mg ²⁺ (mM)	Ca ²⁺ DPTA Sol (µl)	10x ATP/GT P (µl)	10x fura-2 /Mag-Fura2 (µl)	Ca ²⁺ free calculated (nM)	Mg ²⁺ free calculated (nM)	Osmolarity	pH
1	2.8	6.5	64	8	8	4.971 e ⁻⁶			7.2
2	5.3	6.0	64	8	8	8.370 e ⁻⁶			7.3
3	9.0	5.5	64	8	8	1.609 e ⁻⁵			7.3
4	20	3.5	64	8	8	5.804 e ⁻⁵			7.3
5	25	2.5	64	8	8	9.165 e ⁻⁵			7.2
6	35	0.5	64	8	8	3.138 e ⁻⁴			7.3

Ratio metric measurements are performed by infusing at least 4 chromaffin cells per free calcium solution. An averaged ratio is obtained. Both osmolality and pH are measured again. Osmolality around 280 to 320mOsm/kg and pH 7.4. The efficiency of the calcium chelators is assumed at 99.9%, concentrations of the free calcium and magnesium are then assessed by using the program “freecon-3” extension in Igor.

Calcium points are plotted against the ratio 380/340 and fitted with the double sigmoidal function (Figure 13):

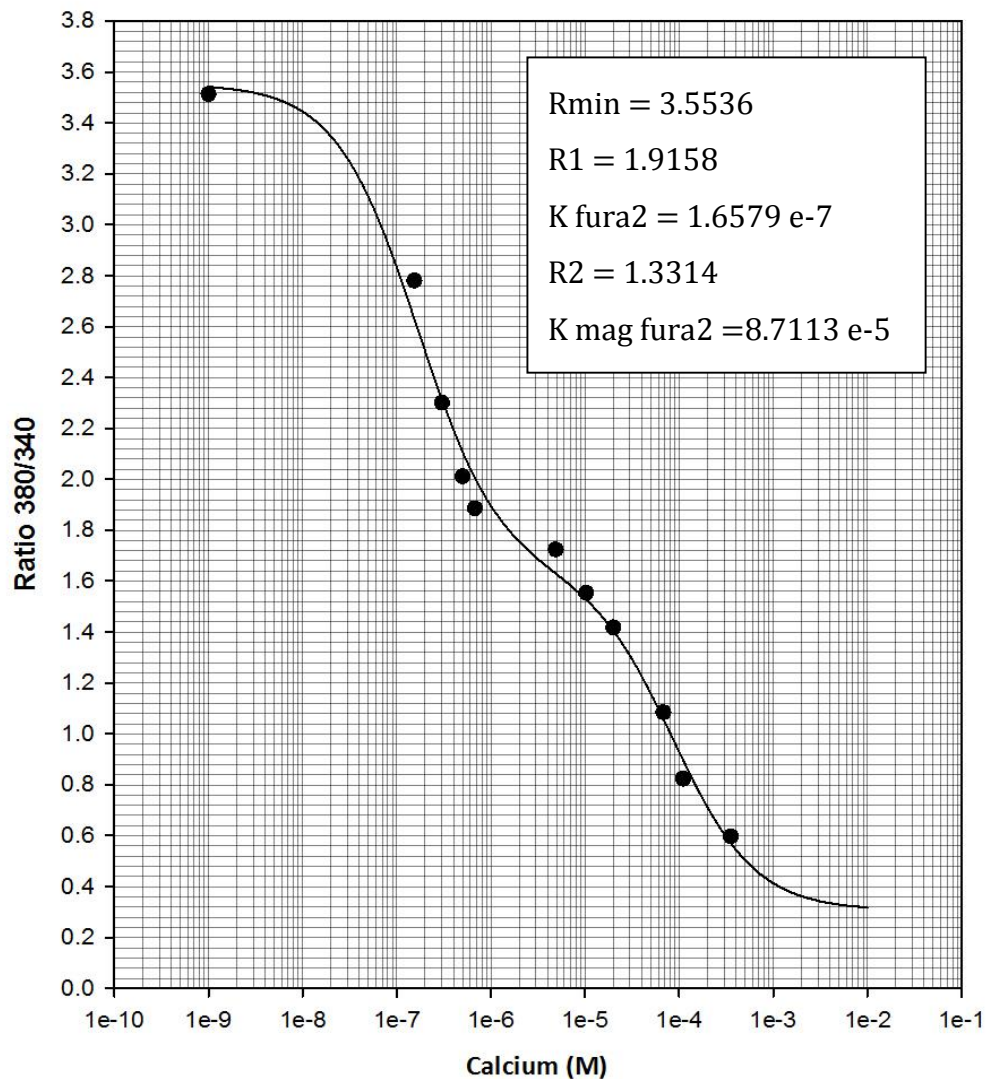


Figure 13. Calcium calibration curve for calcium imaging. The 11 calcium values in molar plotted on a logarithmic X-axis vs the ratio of the average readout values from the wavelength 380 / 340 on the Y-axis. Values of R1 and R2 are determined by fitting the curve with a double sigmoid function.

$$R = R_{min} - R_1 \frac{x}{x + K_{fura2}} - R_2 \frac{x}{x + K_{mag\ fura2}}$$

The fitted values from are used as reference to assess the concentration of the free intracellular calcium throughout the electrophysiological recordings.

4.1 Kinetic model of priming and fusion in chromaffin cells

The spacing of Ca^{2+} channels in the plasma membrane of chromaffin cells is variable, which allows for tonic fusion of vesicles but not the synchronization of exocytosis in response to Ca^{2+} influx through the calcium channels (Klingauf et al., 1997). In order to build up pool of vesicles, chromaffin cells can be infused with an intracellular solution containing submicromolar free Ca^{2+} , in addition to Calcium that is caged by a photo labile Ca^{2+} chelator such as NP-EGTA (Ellis-Davies et al., 1994). Degradation of NP-EGTA that instantaneously liberates the bound Ca^{2+} upon the UV application causing a stepwise increase in intracellular $[\text{Ca}^{2+}]_i$ from hundreds of nM/L to tens of $\mu\text{M/L}$ (Figure 15 A). This method bypasses the requirement of calcium influx through calcium channels; moreover, it provides a homogeneous elevation of calcium levels inside the cell to synchronize vesicle exocytosis. Voltage-clamp membrane capacitance measurements coupled with flash photolysis of caged calcium experiments in chromaffin cells able us to identify changes in the sizes and fusion kinetics of different vesicle pools. In response to calcium uncaging, chromaffin cells showed a triphasic increase in their membrane capacitance (Neher et al., 1993; Voets et al., 1999; Voets 2000), based on which vesicle pools were categorized into a readily releasable pool of vesicles (RRP), a slow releasable pool of vesicles (SRP), and those in the

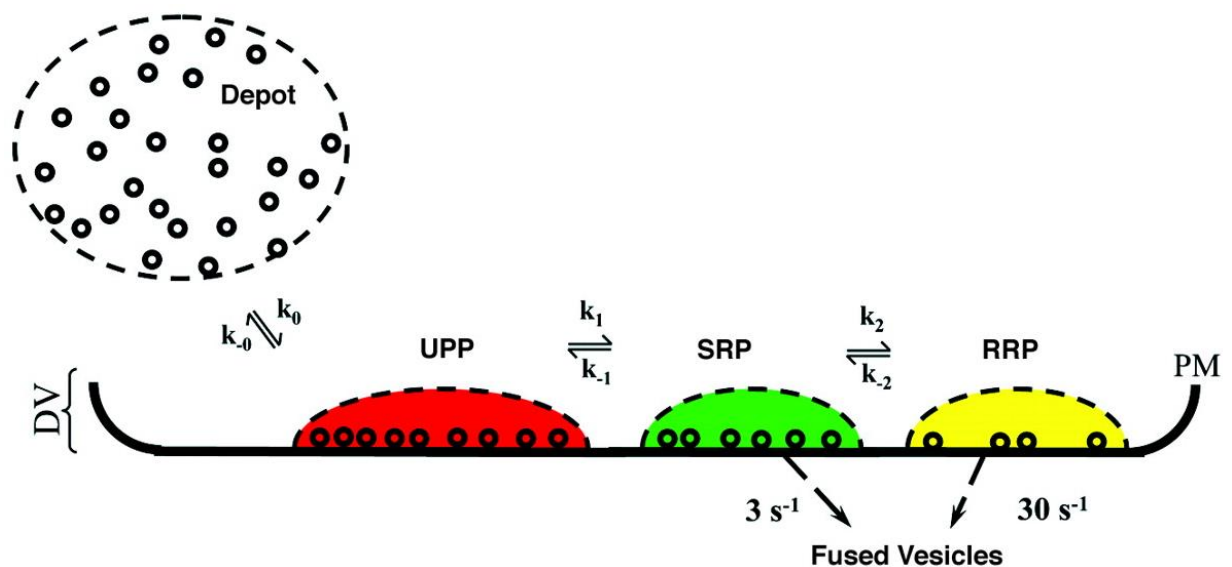


Figure 14. Schematic representation of vesicle pools. Vesicles from the depot pool reversibly dock to the plasma membrane (PM) forming a pool of docked but unprimed vesicles (UPP, red). Docked vesicles reversibly prime in a $[\text{Ca}^{2+}]_i$ -dependent manner, forming the SRP (green). From the SRP, vesicles either undergo fusion or transit into the RRP (yellow). Sequential elevation of $[\text{Ca}^{2+}]_i$ triggers fusion of vesicles from the RRP and the SRP. Vesicles from the RRP fuse faster than those coming from SRP, producing two distinct kinetic components in the exocytotic burst. It is also possible for vesicles from SRP to undergo maturation into RRP and then fuse (Rettig et al., 2002).

unprimed pool (UPP). A molecularly primed Readily Releasable Pool (RRP) (Figure 14), which is a population of vesicles that is held near the plasma membrane, which has a high fusion probability upon calcium trigger and constitute the majority of the fast release phase in synchronizes secretion (Figure 15 B) (Rettig et al., 2002; Stevens et al., 2011). A second pool having slower release kinetics known as the Slow Releasable Pool (SRP) (Figure 14), consisted of those vesicles that are not molecularly primed even though they reside within a close distance to the plasma membrane (docked), and have ten times slower fusion kinetics than the RRP (Figure 15 B) (Rettig et al., 2002; Stevens et al., 2011). After the fusion of the RRP and the SRP from chromaffin cells, the elevated intracellular calcium drives the maturation of vesicles from the UnPrimed Pool (UPP) (Figure 14) forward to the RRP and the SRP. Some of those vesicles that are undergoing molecular maturation will undergo exocytosis and appear as a linear increase in membrane capacitance (Figure 15 B). This phase of secretion in chromaffin cells is known as a sustained rate of release, that be an indicative for the forward priming rate of vesicles from the UPP to the RRP and the SRP (Rettig et al., 2002; Stevens et al., 2011). Combining whole-cell capacitance measurements and flash photolysis of caged Ca^{2+} allows for the identification of vesicle pools with different kinetics in chromaffin cells (Voets 2000; Rettig et al., 2002).

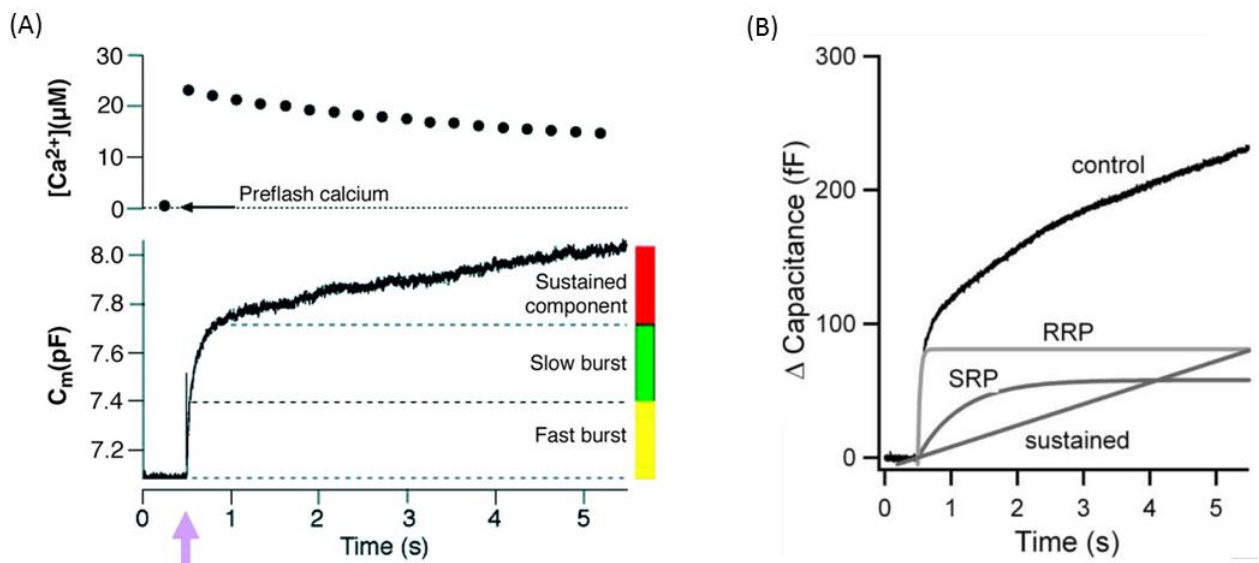


Figure 15. Synchronized exocytosis in chromaffin cells is composed of three kinetically distinct phases. (A)

Upper panel shows $[\text{Ca}^{2+}]_i$ before and after flash. The second panel is the increase in membrane capacitance, in response to the instantaneous calcium rise resulting from photolysis of the calcium chelator NP-EGTA, an Initial burst is fast (yellow) with a time constant $\tau \sim 10\text{-}30$ ms followed by a slower phase with $\tau \sim 100\text{-}300$ ms. Sustained rate is measured as femtoFarad per second and ranges from 5-50f F/s (Rettig et al., 2002). **(B)** The membrane capacitance increase is dissected into two exponentially fitted phases, a fast RRP and a slow SRP, followed by a linear sustained phase of release (Stevens et al., 2011).

The secretory response of a wild type chromaffin cell can be divided into two kinetically distinct phases (Heinemann et al., 1994; Voets et al., 1999). A fast phase (also referred to as exocytotic burst) lasting ~ 1 s after the flash, that contains both the RRP and the SRP (Figure 15 A), and a subsequent sustained phase that is thought to represent the release of newly recruited vesicles into the exocytosis competent primed state (Figure 15 A). The synchronous exocytotic response can be fitted with a double exponential and constant phase equation mentioned in the previous section, reflecting the sustained rate of secretion.

$$F(t) = A_0 + A_1 \left(1 - e^{-\frac{t}{\tau_1}}\right) + A_2 \left(1 - e^{-\frac{t}{\tau_2}}\right) + kt$$

Where A_0 represents the cell membrane capacitance before the flash. The parameters A_1 , τ_1 , and A_2 , τ_2 represent the amplitudes and time constants of RRP and SRP respectively, and k is the sustained release done by the cell when calcium levels remain high after UV flash, representing the fusion of newly coming vesicles (Figure 15 B). By increasing $[Ca^{2+}]_i$ above $1 \mu M$, the rate of vesicle fusion exceeds the refilling rate of the primed pool and therefore leads to pool depletion revealing a bell-shaped dependence of the RRP and SRP size on the concentration of intracellular Ca^{2+} (Voets et al., 1999; Voets 2000). Thus it is crucial to maintain the intracellular free Ca^{2+} concentration within the priming range of 500-900 nM to achieve efficient priming of vesicles and consequently able us to properly asses the synchronous exocytosis from chromaffin cells. After its exhaustion, the RRP is refilled by vesicles from the SRP, thus it is likely that these pools are in dynamic equilibrium and therefor it is conceivable that these two pools represent different maturation steps of secretory vesicles (Rettig et al., 2002).

4.1.1 Calcium imaging and calcium uncaging procedure

Pipette solution (intracellular recording solution) 500-900 nM free Ca^{2+} :

Glutamic acid (potassium free)	Sigma, G1251	147.13 g / mol	110 mM
NaCl	Roth, 9265.2	58.44 g / mol	8 mM
CaCl ₂	Sigma, 21115	110.98 g/mol	3.5 mM
HEPES	Sigma, H7523	238.30 g / mol	20 mM
Fura-2, Pentapotassium Salt	Thermo Fisher, F1200	831.996 g / mol	0.2 mM
Mag-Fura-2, Tetrapotassium Salt	Thermo Fisher, M1290	586.68 g / mol	0.3 mM
Mg-ATP	Sigma, A9187	507.18 g / mol	2 mM
Na ₂ -GTP	Sigma, G8877	523.18 g / mol	0.3 mM
NP-EGTA	HOM made	653.8 g / mol	5 mM
pH =7.4 with CsOH	Osmolarity 310 mOsm/kg		

Flash photolysis of caged calcium coupled with calcium imaging and in combination with whole-cell voltage clamp was performed on DIV 2 chromaffin cells. A pipette solution having 500 nM-900 nM free calcium (priming calcium) was infused into the chromaffin cells for duration of 120 s. Membrane capacitance was monitored during this time period to assess asynchronous vesicle exocytosis. In parallel, we monitored the intracellular free calcium concentration using 0.5 Hz sequential illuminations with wavelengths 340 and 380 nm were applied by the monochromator to excite Fura2 and Mag-Fura2, the resulting emission at 510 nm is detected by the photodiode and converted into voltage values. The calculated ratio of emission intensities resulting from the 340/380 illumination are transformed to Electrical signals by the photodiode and compared to values determined by a calibration curve to identify calcium levels in the cell at each time point. Membrane electrical properties were simultaneously recorded (Cm, Gm, Gs) to estimate the magnitude of the asynchronous release at submicromolar calcium concentrations. Cells with calcium levels outside the range of calcium for priming, or with fluctuating electrical properties (Gm, Gs) were discarded during the data analysis phase.

The UV flash and the monochromator illumination systems are coupled via a dual port containing a quartz beam splitter. Such a port allows the transition of about 20 % of light source at the side port (used for monochromator illumination) and 80 % of the light source at the back port (used for flashlight) independent of wavelength.

After monitoring the tonic release in the first two minutes of recording, the NP-EGTA is photolysed by a short pulse of high-energy UV flash is applied to the cell. NP-EGTA photolysis results in an instantaneous and homogeneous step-like increase in the intracellular calcium levels, pushing the pool of primed vesicles to fuse which confer to the synchronized phase of release from the chromaffin cells (Figure 15).

4.1.2 Tonic exocytosis

High Ca²⁺ pipette solution (intracellular recording solution) 19 μM free Ca²⁺:

L-Glutamic acid (Potassium free)	Sigma, G1251	147.13 g / mol	110 mM
DPTA	Aldrich, 158178	322.27 g / mol	20 mM
HEPES	Sigma, H7523	238.30 g / mol	40 mM
CaCl ₂	Sigma, 21115	110.98 g/mol	5 mM
Mg-ATP	Sigma, A9187	507.18 g / mol	2 mM
Na ₂ -GTP	Sigma, G8877	523.18 g / mol	0.3 mM
pH =7.4 with CsOH	Osmolarity 310 mOsm/kg		

When paired with capacitance measurement, the total ability of the cell to release vesicles under long-lasting stimulation conditions can be studied by infusing the chromaffin cell with a pipette solution containing 19 μM free Ca^{2+} . Such a strong and long-lasting calcium stimulus is beneficial for overcoming any restrictions on exocytotic events that may result from low intracellular Ca^{2+} concentrations.

4.2 Data acquisition and analysis

Electrophysiological data were acquired through a low-resolution X-chart plug-in module of the Pulse software in order to monitor C_m changes with low time resolution during the stimulation (0.5 Hz). Capacitance measurements were performed according to the Lindau-Neher technique (sine wave stimulus: 1000 Hz, 35 mV peak-to-peak amplitude, DC holding voltage -70 mV). Current signals were digitized at 20 Hz and membrane capacitance was analyzed with customized IgorPro routines. Recordings were performed at room temperature.

4.3 Peptide dissolution and infusion

Infusion of molecules through a patch pipette is one of the feasible methods used to internalize agents that monitor, aid, or modify the efficiency of the exocytosis machinery. We already use this method in controlling the levels of Ca^{2+} inside the cell by chelating factors as NP-EGTA and BAPTA, and Ca^{2+} indicators as Fura-2 and mag-Fura-2 each of which has its own molecular and diffusion properties. In the carried out experiments, we took advantage of this method to study the role of a synthesized peptide comprising the last 34 amino acids of the C-terminus of CpxII on the exocytotic machinery in mice chromaffin cells. Prof. Martin Jung provided lyophilized peptides, having the sequences:

CpxII CTD: ¹⁰¹ IPAGCGDEEEEEESILDTVLKYLPGPLQDMFKK ¹³⁴ (M.W.3824.4 Daltons)

CpxII Scrambled: KVPYELGGQLPELKTSDPIEGEDEDELFMKEIAC (M.W.3824.4 Daltons)

CpxII CTD + Cys: IPAGCGDEEEEEESILDTVLKYLPGPLQDMFKK**C** (M.W.3927.4 Daltons)

After total dissolution, the solved peptides had a final concentration of 470.6744 μM in a 50mM KCL, 50mM HEPES solution, and batched into 20 μL aliquots, snap frozen, and preserved at -80 C°. On the day of measurement, peptides were added to the pipette solution to constitute a sufficient final concentration of 10 μM . Such a concentration is required to avoid a reduction in the rate of peptide diffusion than expected due to hindrance from the interaction with intracellular

organelles before reaching the site of action, so the delay caused by hindrance is negligible (Pusch et al., 1988).

The diffusion constant of the peptides into the lumen of the chromaffin cells is correlated to two parameters first is the molecular weight of the peptide and the second is access resistance describing the ease of exchange between the pipette's solution and the cell's lumen. Diffusion time constant " τ " can be determined by the use of the equations:

$$\tau_0 = (78.4 \pm 6.6) * \frac{R_a}{D}$$

$$\tau_0 = (0.60 \pm 0.17) * R_a * M^{1/3}$$

Where τ_0 is the diffusion time constant in seconds, R_a is the access resistance in $M\Omega$, D is the diffusion coefficient in $10^{-7}cm^2s^{-1}$, and M is the molecular weight in Daltons.

τ_0 is the diffusion time constant for the original cells studied by Pusch and Neher in 1988 where their estimate was based on a mean membrane capacitance $C_0 = 5.91$ pF. Having different cell sizes than the original C_0 but with the similar spherical geometry, the following transformation can be used to correctly quantify the diffusion time constant " τ " meeting the average size of our cells:

$$\frac{\tau}{\tau_0} = \left(\frac{C_m}{C_0}\right)^{1.5}$$

In the presence of the peptide in the intracellular solution, the peptide tends to cover the pipette's tip and reduces the chance of obtaining the Giga-seal by 50%. Additional help can be applied to reach the on-cell configuration (Pusch et al., 1988). One aiding method is applying some negative pressure after the contact between pipette's tip and the cell membrane, another method is to hyperpolarize the pipette by decreasing the holding voltage to -70mV to speed up the Giga-seal formation (Sakmann 2009).

4.4 BIOCHEMISTRY

Solutions

Equipment:

Balance	Sartorius	
pH Meter	WTW	InoLab PH7110
Osmometer	WESCOR	Vapro vapopressure osmometer 5520

Stirrer	Roth	MH 15 Rotilabo Magnetic Stirrer
---------	------	---------------------------------

Protein assays:

Equipment:

Nanophotometer	IMPLEN	NP 80
Tabletop centrifuge	Thermo Scientific	Biofuge PRIMOR centrifuge
Eppendorf tubes agitator	IKA	VIBRAX VXR Basic
End over end mixer	Fröbel Labortechnik	
Electrophoreses chamber	BioRad	MINI PROTEAN 3 CELL
Power supply	BioRad	POWER PAC 300
Rotating shaker	Benchmark	ORBI-SHAKER JR

Materials:

BSA	Sigma Aldrich	A7906
Bradford	BioRad	5000205
Protein Ladder low range	Cell signalling	13070
Protein Ladder	Fisher scientific	BP36031
SulfoLink™ Immobilization Kit	Thermo Fisher Scientific	44999
GST Beads	Millipore	70541
Ni-NTA His•Bind® Resin	Millipore	70666

4.4.1 Recombinant protein production and purification

Equipment:

Ultra-centrifuge	Sorvall	RC5B Plus
Rotor1	Sorvall	SS-34
Rotor2	Sorvall	SLA-3000
Bacterial culture incubator	New Brunswick Scientific	C25KC INCUBATOR SHAKER classic
Sonicator	Bandelin electronic	UW 2070

Materials:

Ecoli DH5-alpha		
Ecoli BL21		
IPTG	VWR	A1008.0005
GST Beads	Millipore	70541
Spectra/Por 1 Dialysis Tubing	Spectrum labs	132655

Solutions and Media:

Antibiotics (1000X):

Ampicillin	Sigma Aldrich, A9518	150 µg / ml
------------	----------------------	-------------

Kanamycin	Sigma-Aldrich, K4000	50 µg / ml
-----------	----------------------	------------

LB Medium:

Bacto Tryptone	Fisher, 214010	-	1%
Yeast extract	Roth, 2904.2	-	0.5%
NaCl	Roth, 9265.2	58.44 g / mol	1%
NaOH (1n)			0.01%

Sinification solution:

NaCl	Roth, 9265.2	58.44 g / mol	300 mM
NaH ₂ PO ₄ *H ₂ O	Merck, 1.06580.1000	177.99	50 mM
Imidazol	Sigma, I202	68.08 g / mol	10 mM
Lysozyme	Millipore, 5501	-	1 mg / ml
Protease inhibitor	Roche, 11836170001	25 tabs	1 tab/ 15 ml
PMSF	Thermo, 36978	174,2 g/mol	1 mM
Benzonase	Millipore, 70746	-	10-20mg
MgCl ₂	Sigma, M2393	203.30 g / mol	1mM
pH = 8 NaOH			

GST wash Buffer:

NaCl	Roth, 9265.2	58.44 g / mol	100 mM
EDTA	Roth, 8043.3	372.2 g / mol	1 mM
Tris-HCL	Roth, 9090.3	157,60 g / mol	20 mM
DTT	VWR, A1101.0025	154,25 g / mol	1 mM
pH = 7.4 NaOH			

GST elution Buffer:

NaCl	Roth, 9265.2	58.44 g / mol	100 mM
EDTA	Roth, 8043.3	372.2 g / mol	1 mM
Tris-HCL	Roth, 9090.3	157,60 g / mol	50 mM
L-Glutathione	Sigma Aldrich	G4251	30 mM
pH = 8 NaOH			

Hexa-His tag wash Buffer:

NaCl	Roth, 9265.2	58.44 g / mol	300 mM
NaH ₂ PO ₄ *H ₂ O	Merck, 1.06580.1000	177.99	50 mM
Imidazol	Sigma, I202	68.08 g / mol	10 mM
DTT	VWR, A1101.0025	154,25 g / mol	10 mM
pH = 8 NaOH			

Hexa-His tag elution Buffer:

NaCl	Roth, 9265.2	58.44 g / mol	300 mM
------	--------------	---------------	--------

Na ₂ HPO ₄ *H ₂ O	Merck, 1.06580.1000	177.99 g / mol	50 mM
Imidazol	Sigma, I202	68.08 g / mol	80 mM/ 120 mM/ 160mM/ 200mM/ 250mM.
DTT	VWR, A1101.0025	154,25 g / mol	10 mM
pH = 8 NaOH			

Dialysis Buffer:

NaCl	Roth, 9265.2	58.44 g / mol	130 mM
HEPES	Sigma, H7523	238.30 g / mol	50 mM
EDTA	Roth, 8043.3	372.2 g / mol	1 mM
DTT	VWR, A1101.0025	154,25 g / mol	1 mM
Triton X 100	Merck, 1.08603.1000		0.5 %
pH = 7.3, NaOH			

Competent bacteria are transfected by heat shock with the DNA for protein production and plated on agar supplied with the selective antibiotic (Kanamycin or Ampicillin) overnight at 37°C. One colony is picked for an overnight culture in 20 ml LB medium + antibiotic (at 200 RPM, 37°C). Pre-cultures are transferred to 250 ml LB + antibiotic and incubated at 200 RPM, 37°C, bacterial growth is monitored by OD at 600 nm to a value of 1-1.2. IPTG (1 µM) is added to initiate protein production by the bacteria and incubated for 4-5 hours at 200 RPM, 37°C. Bacteria is then centrifuged at 6000 RPM, 4°C for 20 mins, and then frozen at -80°C overnight. Frozen bacteria is quickly thawed, suspended and incubated at RT for 30 mins in the sonification buffer (15 ml/pellet), then sonified on ice to break down the bacterial membrane. Sonified bacteria were then incubated for 30 mins at RT before centrifugation at 16000 RPM, 4°C, 20 mins. The supernatant is then incubated with prewashed beads (Nickle beads for Hexa-His tagged proteins, or GST coupled beads for GST- proteins) on a rocker for 2 hours at 4°C. Beads are then centrifuged and washed with the respective wash buffer to discard unwanted proteins, and then proteins are eluted from the column, with the concentration determined by OD, and then ran on a denaturing SDS gel where its integrity is determined by coomassie staining according to its expected molecular weight. The obtained proteins are then dialyzed once overnight and then twice for 1 hour each over day against the dialysis buffer before snap freezing and storage at -80°C.

4.4.2 Gel electrophoresis

Equipment:

Electrophoreses chamber	BioRad	MINI PROTEAN 3 CELL
Power supply	BioRad	POWER PAC 300

Glass Plates	BioRad	MINI PROTEAN 3 system 1mm Spacer
Gel comb	BioRad	Mini Protean comb 10 well 1 mm thickness

SDS poly-acrylamide gel

Materials:

Poly acrylamide	BioRad	3029.1	0.5 mM
APS	Sigma Aldrich	A7460	0.4%
TEMED	BioRad	1610801	0.004%

Solutions:

Stacking gel buffer (4X):

Tris-Base	VWR, 1083872500	121.14 g / mol	0.5 mM
SDS	Serva/ZHCL, 20765.03	288.38 g / mol	0.4%
pH = 6.8			

Separating gel buffer (4X):

Tris-Base	VWR, 1083872500	121.14 g / mol	0.5 mM
SDS	Serva/ZHCL, 20765.03	288.38 g / mol	0.4%
pH = 8.8			

Electrophoresis buffer (10X):

Tris-Base	VWR, 1083872500	121.14 g / mol	250 mM
SDS	Serva/ZHCL, 20765.03	288.38 g / mol	1 %
Glycine	Applichem, A1067	75.07 g / mol	1.9 M
pH = 8.8			

SDS Sample Buffer (5X):

Tris-Base	VWR, 1083872500	121.14 g / mol	300 mM
SDS	Serva/ZHCL, 20765.03	288.38 g / mol	10 %
Glycine	Applichem, A1067	75.07 g / mol	25 %
Bromophenol Blue	Tocris, 5218	669.96 g / mol	0.1 %
β -mercaptoethanol	Sigma Aldrich, M6250	78.13 g / mol	14.4 mM
pH = 6.8			

Coomassie Stain (1L):

Coomassie Blue R250	Thermo fisher, 20278	1 g
Methanol	VWR, 20847360	450 ml
Glacial acetic acid	MERCK, 1.00063.2511	100 ml

Double Distilled Water	-	450 ml
------------------------	---	--------

Coomassie Destain solution (1L):

Methanol	VWR, 20847360	400 ml
Glacial acetic acid	Merck, 1.00063.2511	100 ml
Double Distilled Water	-	500 ml

4.4.3 Native protein extraction

Equipment:

Glass pestle tissue grinder		
Tabletop centrifuge	Thermo Scientific	Biofuge PRIMOR centrifuge

Homogenization Buffer:

NaCl	Roth, 9265.2	58.44 g / mol	130 mM
HEPES	Sigma, H7523	238.30 g / mol	50 mM
EDTA	Roth, 8043.3	372.2 g / mol	1 mM
Triton X 100	Merck, 1.08603.1000		2 %
PMSF	Applchem,A0999,0025	174.19 g/mol	1 mM
Protease inhibitor	Roche, 11836170001	25 tabs	1 tab/ 15 ml
pH = 7.3 NaOH			

4.4.4 Western Blot

Materials

Protein ladder	Fisher scientific	BP36031
Extra thick blot paper	BioRad	1703967
Milk	Applchem	A0830.1000
Whatman paper	BioRad	1703967
Developer	Sigma Aldrich	P7042-1GA
Fixer/Enhancer	Sigma Aldrich	P7167-1GA
ECL	Thermo Scientific	32209
Films	Amersham Hyperfilm	70001
Ponceau solution	Sigma Aldrich	P3504

Transfer Buffer:

NaCl	Roth, 9265.2	58.44 g / mol	150 mM
------	--------------	---------------	--------

Tris-HCL	Roth, 9090.3	157,60 g / mol	20 mM
Tween	Sigma, P7949	-	5%
pH = 8 NaOH			

TBS-Tween:

NaCl	Roth, 9265.2	58.44 g / mol	150 mM
Tris-HCL	Roth, 9090.3	157,60 g / mol	20 mM
Tween	Sigma, P7949	-	5%
pH = 8 NaOH			

Primary antibodies:

Anti Cpx I-II	Synaptic Systems	122002	1:1000
Anti Syntaxin	Synaptic Systems	78.2, 110 001	1:1000
Anti Synaptobrevin II	Synaptic Systems	69.1	1:1000
Anti-SNAP-25	Synaptic Systems	CL 71.1, 111 011	1:1000
Anti Synaptotagmin I	Synaptic Systems	41.1, 105 011	1:1000
Anti Synapsin	Synaptic Systems	CL 46.1, 106 001	1:1000

HRP-conjugated secondary antibodies:

Goat anti Mouse	Thermo Fisher	10158113	1:1000
Goat anti Rabbit	Thermo Fisher	A-21428	1:1000

4.5 Immunocytochemistry

Solutions:

PBS:

NaCl	Roth, 9265.2	58.44 g / mol	137 mM
KCl	Sigma, P4504	74.55 g / mol	2.7 mM
Na ₂ HPO ₄	Merck, 1.06580.1000	177.99 g / mol	10 mM
KH ₂ PO ₄	Merck, 1.04873.1000	136.09 g / mol	2 mM
pH = 7.4, HCL			

PFA 4% in PBS:

PFA	Merck	1.04005.1000	0.4%
pH = 6.8			

Blocking buffer in PBS:

Triton X 100	Merck, 1.08603.1000	0.15 %
BSA	Sigma Aldrich, A7906	3 %
pH = 6.8, HCl		

Quenching buffer in PBS:

NH4Cl	Sigma, A9434	53.49 g/mol	0.25 %
-------	--------------	-------------	--------

Procedure:

DIV2 cells from wt and knockout cells were infected with mutant for 5 hours. Coverslips were washed with PBS 3X and fixed with PFA for 1 hour at RT with shaking. Coverslips were then washed with PBS and then quenched for 15 minutes at RT followed with 3 washes with PBS. Blocking buffer is applied for 1 hour followed by incubation overnight at 4 degrees with the primary antibody anti-CpxII 1-100 (1:5000) in blocking buffer. The excess primary antibody is washed away with 3 washes using the blocking buffer. Cells are then incubated with the secondary antibody conjugated with an Alexa 488 fluorophore in the darkroom for 1 hour at RT. 4 washes with PBS are then applied to remove the unbound secondary antibody. Afterwards, coverslips were dried and placed upside down on a drop of glycerol on a glass plate and insulated by applying nail polish to the edges of the coverslip.

4.6 Chemical fixation of chromaffin cells for Electron Microscopy imaging

Solutions:

Cacodylate buffer (0.2 M):

Cacodylate sodium salt	Sigma aldrich O250	214.03 g / mol	200 mM
Cacodylate acid (free acid)	Sigma aldrich C0125	138 g / mol	200 mM
pH = 7.4 NaOH			

PFA 100 ml

PFA		15 ml	15 %
pH = 7.4 with NaOH			

Fixative Buffer (30ml):

Cacodylate buffer	15 ml	100 mM
PFA (15%)	5 ml	2.5%
Gluteraldehyde (10%)	10 ml	3.3%

Osmiumtetroxide solution 2%, 10ml:

Osmium tetroxide	5 ml	4%
Cacodylate buffer	5 ml	

Uranyl acetate solution (2%):

Uranyl acetate		1.093g
DDW	50 ml	2.5%

Filtered and covered in aluminum foil.

Graded ethanol for dehydration:

	Ethanol	DDW
100 % Ethanol	50 ml	0 ml
96 % Ethanol	48 ml	2 ml
90 % Ethanol	45 ml	5 ml
80 % Ethanol	40 ml	10 ml
70 % Ethanol	35 ml	15 ml
50 % Ethanol	25 ml	25 ml

Epon embed mixture:

Embed	20 ml
Nadic Methyl	8 ml
DDSA	16 ml
BDMA	1.3 ml

Acetone - Epon mixture:

Acetone : Epon	Acetone	Epon
3:1	22.5 ml	7.5 ml
1:1	15 ml	15 ml
1:3	7.5 ml	22.5 ml

Procedure:

High-density Chromaffin cell cultures were plated on Flour petriperu and infected with either SybII wt or with SybII polyL for 6 hours, cells are then washed with ringers' solution and stimulated twice for 20 seconds with high K⁺ solution separated by a washing step with ringer. Cells are then fixed with Glutaraldehyde-PFA solution for 1 hour at room temperature, or overnight at 4°C with gentle shaking. Fixative was discarded then cells are washed 3x with cacodylate buffer and 1x with osmium tetroxide. Osmium tetroxide is added to the cells and incubated for 1 hour at RT. A step of cacodylate buffer wash is then applied followed by 2 washed with DDW. Cells are then washed once with uranyl acetate and then incubated with uranyl acetate for 1 hour at RT. Wash with cacodylate buffer and then twice with DDW 5 mins each. Dehydrate the cells sequentially by incubation with increasing ethanol concentrations 50% to 100% 15 minutes each at RT. Cells are then gradually fixed with Epon-acetone mixture (3:1, 1:1, then 1:3) for 30 minutes each before the addition of 100% epon and let them stand at RT for 2 hours. Then petri dishes are placed at 60°C

for 48 hours to harden. Cells are then visually selected, cut out and sliced with a diamond tipped knife at 70 μm and fixed on a grid for imaging.

5 Results

5.1 Complexin II inhibits premature exocytosis in chromaffin cells via its carboxyl-terminal domain

5.1.1 Complexin II regulates exocytosis in chromaffin cells

Complexin is a small cytoplasmic protein that regulates SNARE mediated vesicle fusion (Mohrmann et al., 2015; Lai et al., 2017). Only the CpxII isoform is expressed in chromaffin cells (Cai et al., 2008; Makke and Bruns unpublished observation) and no compensatory changes in the expression of other Cpx isoforms in CpxII ko mice could be detected (Yang et al., 2013; El-Brolosy et al., 2017). In order to elucidate the mechanism by which Cpx regulates exocytosis, we detected vesicle fusion from chromaffin cells using high-resolution membrane capacitance measurements. By combining this technique with calcium uncaging, we could determine how chromaffin granules fuse with the plasma membrane in response to a rapid elevation of $[Ca^{2+}]_i$ (Voets et al., 1999; Voets 2000). To promote vesicle priming, chromaffin cells are infused with sub-micromolar free $[Ca^{2+}]_i$ (500 nM free Ca^{2+}), (Voets et al., 1999; Voets 2000). Under those conditions, not only priming but also exocytosis of granules takes place, albeit at a slow rate, representing an asynchronous phase of secretion in chromaffin cells (Dhara et al., 2014) (Figure 16 F). To trigger synchronous fusion of vesicles, Ca^{2+} is uncaged by applying a short intense UV flash producing a step-like increase in intracellular $[Ca^{2+}]_i$ from nanomolar levels of about 500 nM up to the μM range (20 μM) (Figure 16 C, upper panel). As a consequence, membrane capacitance increases rapidly in proportion to the number of vesicles that undergo exocytosis (Rettig et al., 2002). This synchronous exocytosis (Figure 16 C, lower panel) is also referred to as exocytotic burst (EB), in which two components can be kinetically distinguished as Readily-releasable (RRP) and Slowly-releasable pool (SRP) (Figure 16 D, E). The Ca -stimulus leads to pool depletion and the subsequent sustained phase of secretion (SR) reflects exocytosis of newly primed vesicles at elevated $[Ca^{2+}]_i$ (Stevens et al., 2011).

Loss of CpxII caused a pronounced reduction in the size of the EB in chromaffin cells (Figure 16 C). In comparison to Cpx ko cells, expressing the wild type protein (CpxII ko+CpxII) both components of the synchronous response the RRP as well as the SRP were significantly reduced, but no changes in the sustained release phase were observed (Figure 16 D). Furthermore, loss of CpxII slowed down the kinetics of the synchronized fusion and prolonged the secretory delay. Moreover,

asynchronous vesicle fusion before the flash response was significantly increased in the absence of CpxII (Figure 16 F, G). Indeed, an inverse linear correlation has been found between the EB size and the magnitude of the asynchronous (premature) fusion in chromaffin cells (Dhara et al., 2014), indicating that both types of secretion draw vesicles from the same pool of release-competent organelles. Taken together, CpxII plays a dual role in facilitating synchronized exocytosis. On one hand, it inhibits premature vesicle fusion allowing for the build-up of a pool of primed vesicles. On the other hand, it accelerates release kinetics of the primed vesicles.

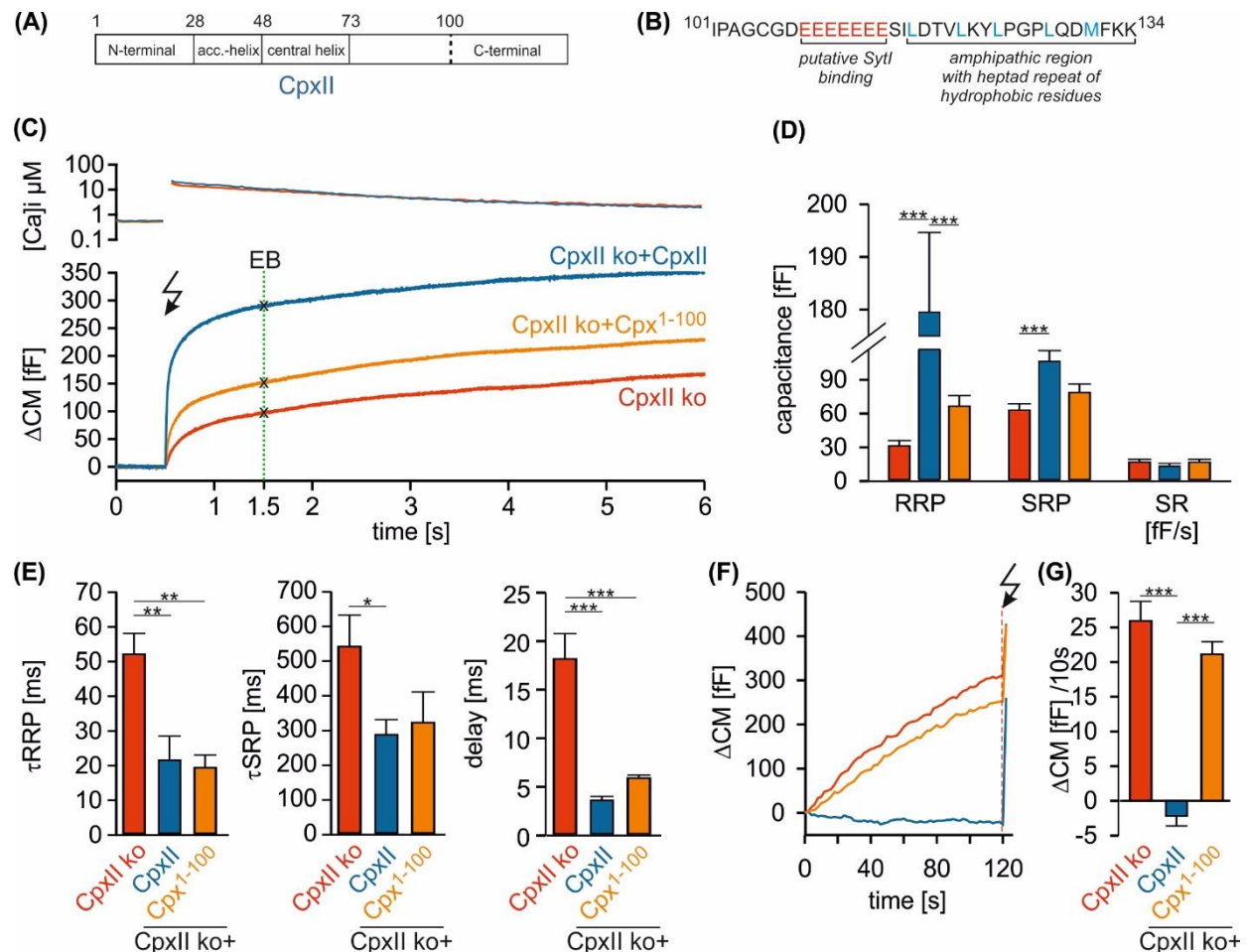


Figure 16. The C-terminal domain of CpxII controls the magnitude of the synchronous secretion. (A) Schematic view on CpxII subdomains (numbers indicate amino acid positions within CpxII). (B) Primary sequence of the CpxII C-terminal region (residue 101–134) highlighting its structural characteristics (glutamate cluster, red; heptad repeat of hydrophobic residues, blue). (C) Mean $[Ca^{2+}]_i$ levels (top) and corresponding CM signals (bottom) of CpxII ko cells (n = 25) and those expressing CpxII (n = 32) or the mutant Cpx1-100 (n = 29). UV flash is at t = 0.5 s (arrow). (D) Amplitudes of RRP and SRP, the rate of sustained release (SR; femtofarad/second) determined for CpxII ko (red), CpxII ko + CpxII (blue), CpxII ko+Cpx1-100 (orange). (E) Time constants for the EB components (τ_{RRP} and τ_{SRP}), and the exocytotic delay. (F) Mean tonic CM traces of the cells shown in (C) before the triggering flash (arrow). (G) The rate of tonic exocytosis (determined at similar $[Ca^{2+}]_i$ in nM, CpxII ko: 714 ± 32 ; CpxII ko + CpxII: 639 ± 23 ; CpxII ko + CpxII1-100: 628 ± 30) is significantly reduced with CpxII but not with its mutant. ANOVA followed by Tukey-Kramer post-hoc test. * $p < 0.05$; ** $p < 0.01$; *** $p < 0.001$. Bars indicate mean \pm SEM.

5.1.2 CpxII clamps premature release via its C-terminal domain (CTD)

Our previous data have shown that the C-terminal half of CpxII (aa 73-134) hinders asynchronous release in chromaffin cells (Dhara et al., 2014) (Figure 16 A). Closer inspection of the primary amino acid sequence revealed that the last 34 amino acid residues at the very end of the C-terminus contains structural features that are conserved throughout the animal kingdom (Figure 16 B). A cluster of glutamate residues (E¹⁰⁸-E¹¹⁴) which has been implicated in binding to the calcium sensor Syt1 (Tokumaru et al., 2008), and an amphipathic α helix which has been proposed to associate with vesicular membranes (Wragg et al., 2013; Snead et al., 2014) (Figure 16 B). In a first set of experiments, we studied the functional impact of these CpxII domains on synchronous exocytosis by viral expression of the truncated mutant (Cpx1-100) in CpxII ko cells. Indeed, the mutant Cpx1-100 largely failed to restore the magnitude of the EB (Figure 16 C). In comparison to the wt rescue, both, the RRP as well as the SRP were significantly diminished and no changes in the SR phase were observed (Figure 16 D). Notably, the Cpx1-100 fully restored exocytosis timing like the wt protein, consistent with our original observation that the N-terminal domain is responsible for speeding stimulus-secretion coupling (Figure 16 E). In contrast, the Cpx1-100 mutant failed to clamp asynchronous exocytosis (Figure 16 F), which is significantly higher than with the wt protein (Figure 16 G). Taken together, these results provide new insight into Complexin's mode of action in exocytosis. They show that the two functions of CpxII (i. e. premature release inhibition and exocytosis speeding) can be molecularly uncoupled. Thus, the very C-terminal end of CpxII (CTD, aa 101-134) specifically regulates the magnitude, but not the kinetics of the synchronized exocytosis, by hindering premature vesicle fusion.

5.1.3 CpxII 1-100 competes with endogenous CpxII for binding to SNARE proteins

The results above show that CpxII lost its ability to clamp premature fusion by truncation of the CTD. This phenotype may indicate that the CTD confers structural properties that are crucial for hindering exocytosis. Alternatively, one might speculate that the observed loss of function phenotype is simply the result of protein misfolding. To distinguish these possibilities, we virally expressed the mutant in wt cells. We found that Cpx1-100 greatly reduces the magnitude of synchronous release compared the wt protein (Figure 17 A). The amplitudes of the RRP and the SRP were significantly decreased (Figure 17 B) without changing the timing of synchronized secretion (Figure 17 C). In agreement with our result in CpxII ko cells (Figure 16) Cpx1-100 significantly increased the asynchronous fusion whereas CpxII wt strongly hindered this type of

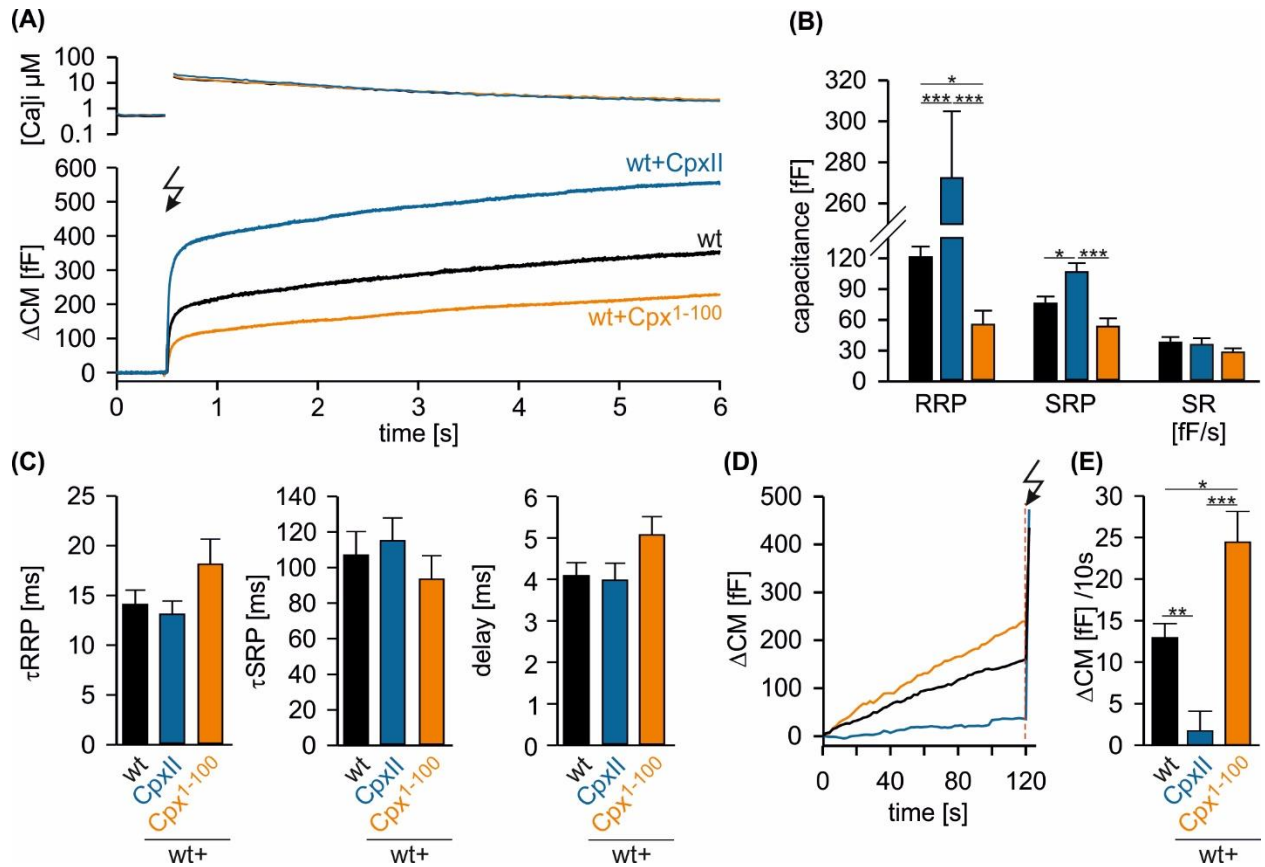


Figure 17. Cpx 1-100 over expression has a dominant negative phenotype in CpxII in wt cells. (A) Mean $[Ca^{2+}]_i$ levels (top) and corresponding CM signals (bottom) of CpxII ko cells (n = 25) and those expressing CpxII (n = 32) or the mutant Cpx1-100 (n = 29). Flash is at t = 0.5 s (arrow). (B) Amplitudes of RRP and SRP, the rate of sustained release (SR; femtofarad/second) determined for CpxII ko (red), CpxII ko + CpxII (blue), CpxII ko+Cpx1-100 (orange). (C) The time constants for the EB components (τ_{RRP} and τ_{SRP}), and the exocytotic delay. (D) Mean tonic CM traces of the cells shown in (C) before the triggering flash response (arrow). (E) The rate of tonic exocytosis (determined at similar $[Ca^{2+}]_i$: in nM, CpxII ko: 714 ± 32 ; CpxII ko + CpxII: 639 ± 23 ; CpxII ko+ CpxII1-100: 628 ± 30) is significantly reduced with CpxII but not with its mutant. ANOVA followed by Tukey-Kramer post-hoc test. * $p < 0.05$; ** $p < 0.01$; *** $p < 0.001$. Bars indicate mean \pm SEM.

secretion (Figure 17 D, E). Taken together, Cpx1-100 acts in a dominant-negative fashion on secretion of wt cells. This data shows that Cpx1-100 is functionally intact and outcompetes the endogenous complexin but fails to suppress the asynchronous fusion. In particular, the latter phenotype illustrates that the mutant variant is able to ‘unclamp’ the exocytotic machinery indicating that the CTD is instrumental for hindering asynchronous vesicle fusion.

5.1.4 The CpxII-CTD reduces tonic release in wt cells

Motivated by these findings we next asked whether the CpxII CTD could on its own hinder tonic secretion. For this, we infused wt chromaffin cells with the synthetic oligopeptide encompassing the entire CTD (CpxII-CTD, MW 3840 Da). As a control, an oligopeptide with a permuted

sequence was used (scrambled pep, Figure 18 A). Peptides were delivered in a solution containing 19 μM free Ca^{2+} to stimulate secretion simultaneously. During the entire recording, the cell's membrane capacitance (CM) together with the electrical access conductance (GS) and membrane conductance (GM) were continuously monitored. The latter properties allowed us to detect and to avoid experimental inconsistencies. In fact, infusion of the CpxII CTD peptide strongly diminished tonic secretion in comparison to its scrambled counterpart (scram pep) (Figure 18 B). Notably, the fusion clamp by the CpxII CTD progressively enhanced with time, showing a stronger relative inhibition when compared with the scram pep (Figure 18 C). This result is not the consequence of different cellular accessibilities, as illustrated by similar GS values for CpxII CTD- and scram-peptide infused cells (Figure 18 D). Taken together, the results show that a surplus of

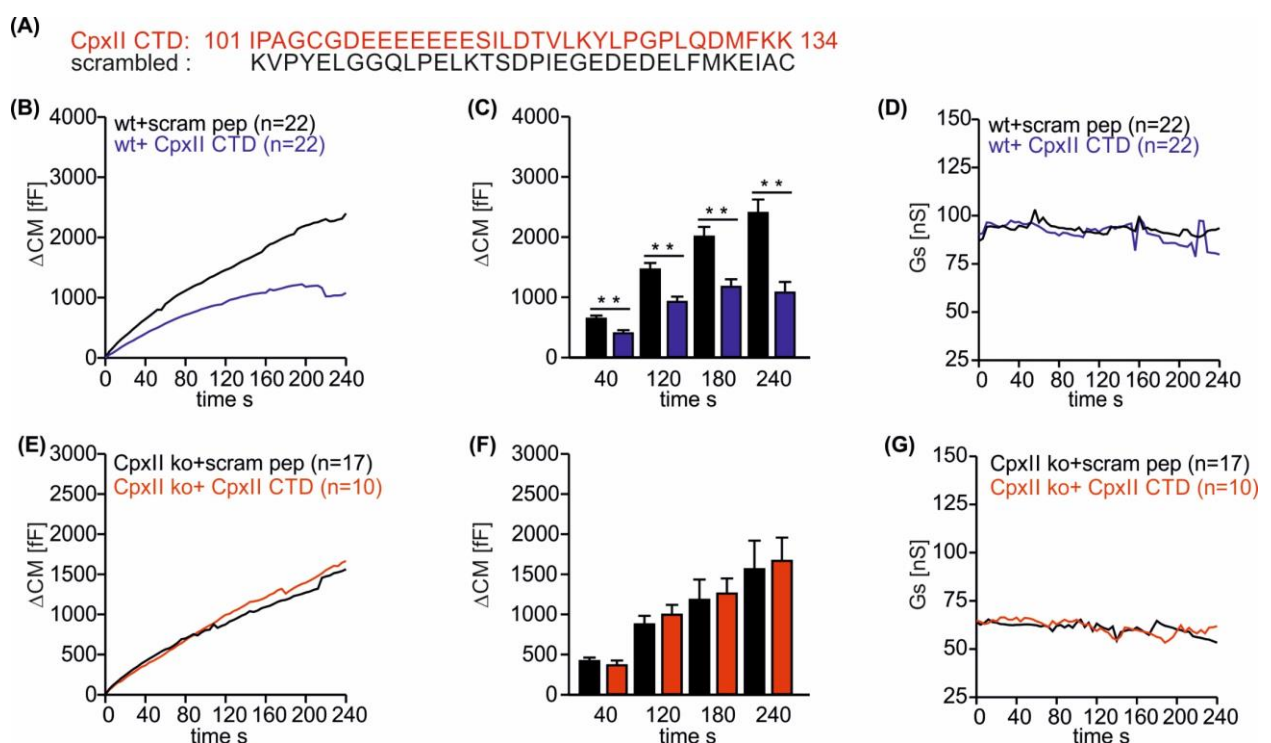


Figure 18. CpxII-CTD inhibits tonic release in wt cells. (A) Sequence of the CpxII-CTD peptide in red and the sequence of the subsequent scrambled peptide (scram pep) in black. (B) Exocytosis assessed by capacitance measurements in wt cells infused with 19 μM free Ca^{2+} having 10 μM of either scrambled peptide in black (n = 22) or the CpxII CTD peptide in blue (n = 22) showing the CpxII CTD peptide hindering release compared to the Scram peptide. (C) Quantification of the capacitance increase at different time points shows significant inhibition of tonic release by the CpxII-CTD in wt cells over time. (D) Average series conductance values of cells measured in (B) showing similar conductance values between the two tested groups in the experiment (E) Capacitance increase in CpxII-ko cells infused with 19 μM free Ca^{2+} intracellular solution having 10 μM of either the scrambled peptide in black (n = 17) or the CpxII CTD peptide in red (n = 10) showing the CpxII CTD does not clamp release in CpxII ko cells. (F) Quantification of the capacitance increase at different time points shows that the CpxII-CTD does not reduce the tonic exocytosis in CpxII-ko cells over time. (G) Average series conductance values of cells measured in (F) showing similar conductance values between the experimental groups.

CpxII CTD strongly impairs tonic secretion, an observation that interestingly mimics the phenotype of CpxII expression in wt cells (Dhara et al., 2014). In sharp contrast, the CpxII CTD failed to clamp tonic exocytosis in the absence of CpxII (Figure 18 E-F). This indicates that the CpxII CTD is essential but not sufficient for hindering asynchronous secretion. It may either require other domains of the CpxII protein or those are needed to establish a molecular stage of the exocytotic mechanism on which the CpxII CTD can exert its clamp action. These questions will be followed up by new experiments, as described below. In any case, the results show that the CpxII CTD is a rate-limiting component for the inhibition of tonic exocytosis in wt cells.

5.1.5 CpxII-CTD reduces the asynchronous release and increases exocytotic burst in wt cells

To investigate how the CpxII CTD peptide might interfere with synchronous secretion, we tested its impact on the flash evoked response in chromaffin cells. For this, wild type chromaffin cells were infused with either CpxII CTD-pep or scram pep containing solution. In comparison to the scram pep, infusion of the CpxII CTD pep strongly boosted the EB (Figure 19 A), increased the RRP and the SRP (without changing their kinetics Figure 19 B, C) and significantly reduced the asynchronous response (Figure 19 D). Again, the effects of the CpxII CTD infusion are remarkably similar to the phenotype of CpxII expression in wt cells (compare with Figure 17 and Dhara et al.,

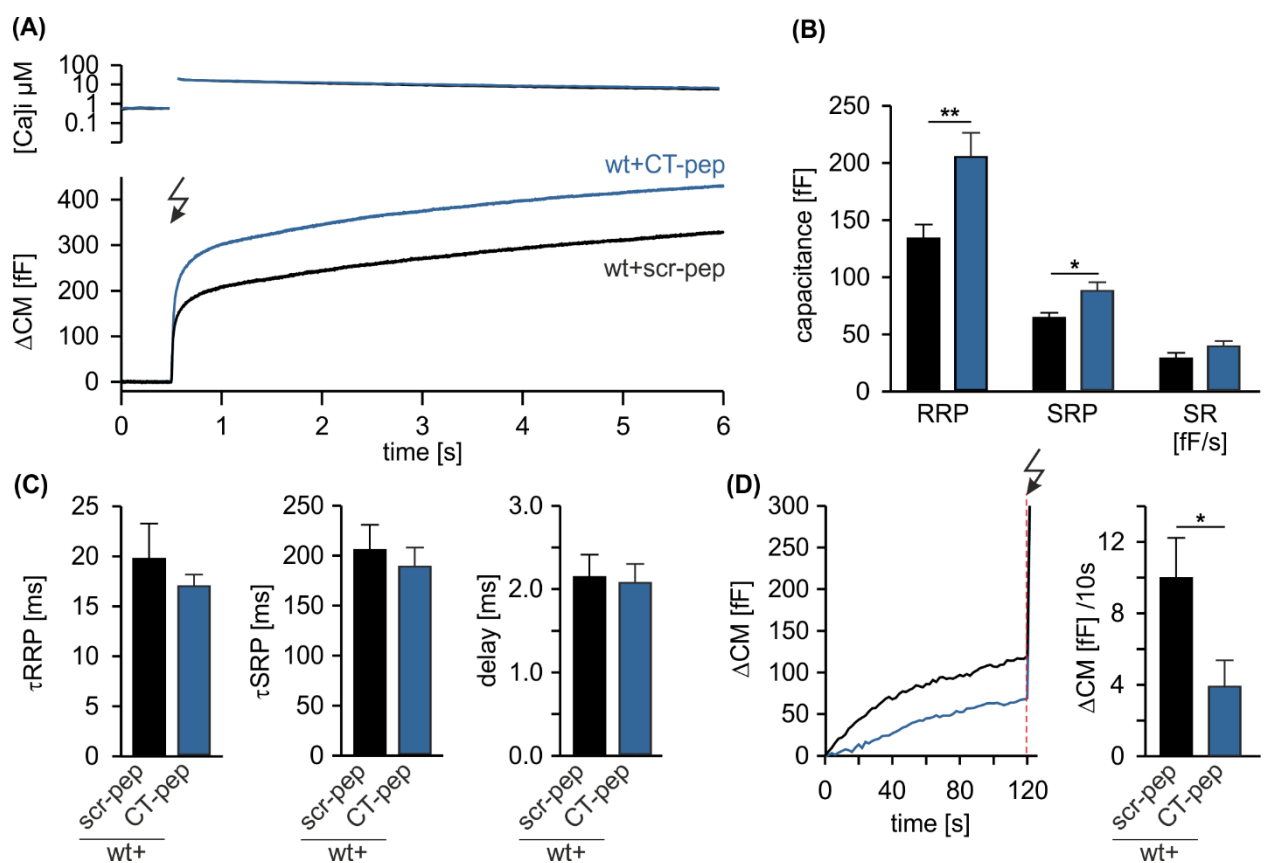


Figure 19. CpxII-CTD in isolation inhibits tonic release and enhances the synchronous release in wt cells. (A) Mean $[Ca^{2+}]_i$ levels (top) and corresponding CM signals (bottom) of wt cells infused with scrambled peptide in black (n = 25) and those infused with CpxII CTD peptide in blue (n = 32). UV flash at t = 0.5 s (arrow). **(B)** Amplitudes of RRP and SRP, the rate of sustained release (SR; femtofarad/second) determined for wt + scram pep, and wt + CpxII CTD pep. **(C)** The time constants for the EB components (τ_{RRP} and τ_{SRP}), and the exocytotic delay. **(D)** Mean tonic CM traces of the cells shown in (A) at similar submicromolar $[Ca^{2+}]_i$ over 120s time before the UV flash triggering response (arrow). The rate of asynchronous release is significantly reduced with CpxII CTD but not with the scram peptide. Student t-test. *p<0.05; **p<0.01; ***p<0.001. Bars indicate mean \pm SEM.

2014). Collectively, this data shows that the CpxII CTD not only inhibited asynchronous fusion in wt chromaffin cells, but also boosted the magnitude of synchronized exocytosis as a gain of function in wt chromaffin cells.

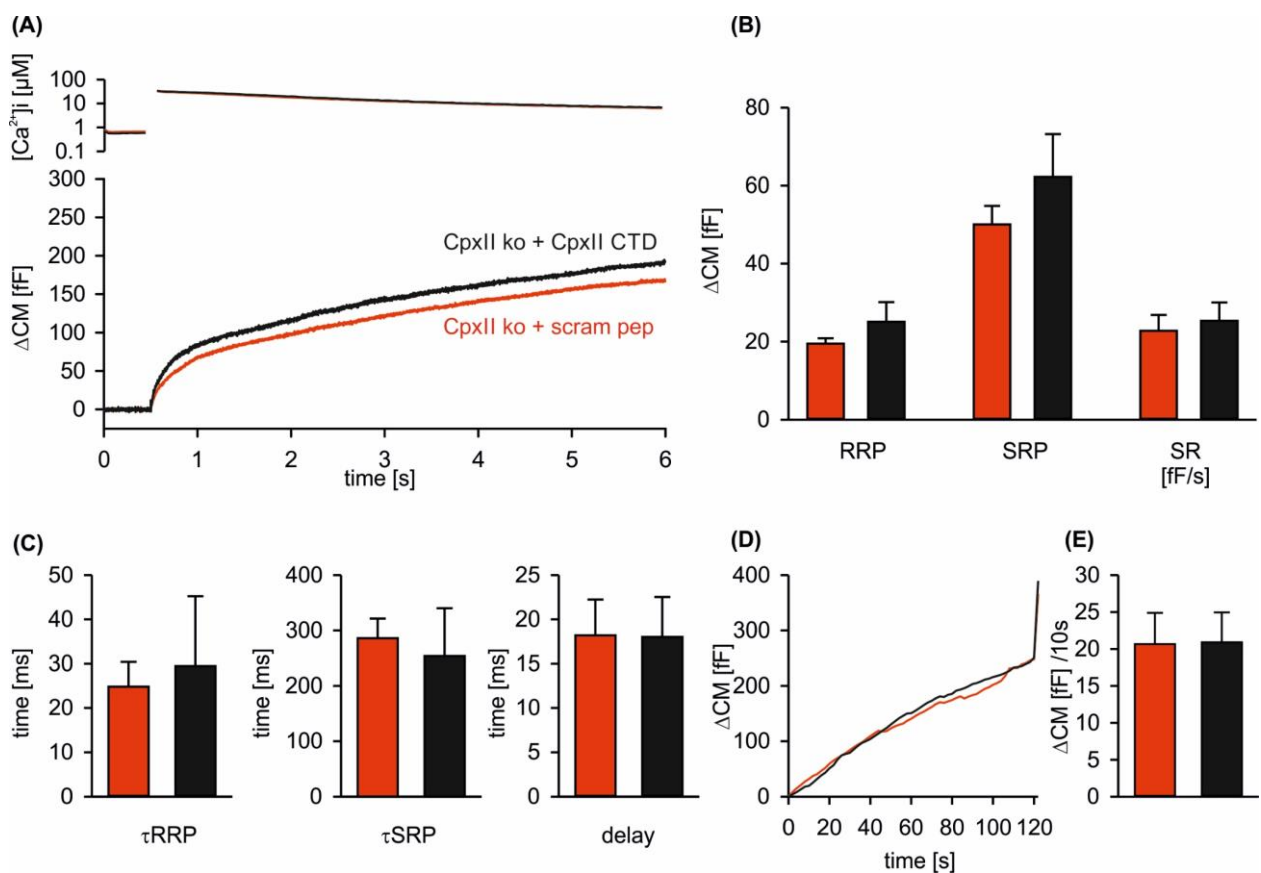


Figure 20. CpxII-CTD does not inhibit premature vesicle fusion in the absence of wt CpxII. (A) Mean $[Ca^{2+}]_i$ levels (top) and corresponding CM increase (bottom) of CpxII ko cells infused with scrambled peptide in red (n = 15) and those infused with CpxII CTD peptide in black (n = 15). UV flash at t = 0.5 s (arrow). **(B)** Amplitudes of RRP and SRP, the rate of sustained release (SR; femtofarad/second) determined for CpxII ko + scram pep, and CpxII ko + CpxII CTD **(C)** The time constants for the EB components (τ_{RRP} and τ_{SRP}), and the exocytotic delay. **(D)** Mean tonic CM traces of the cells shown in (A) at similar submicromolar $[Ca^{2+}]_i$ (CpxII ko + scram pep 862.9 ± 147.5 nM, CpxII ko + CpxII CTD 688.4 ± 82.4 nM) over a 120 s time before the UV flash triggering response (arrow). The rate of the asynchronous fusion is not changed by infusing CpxII ko cells with CpxII-CTD from that of the scram pep infused cells. Student t-test. *p<0.05; **p<0.01; ***p<0.001. Bars indicate mean \pm SEM.

In the same line, we tested if the CpxII CTD could boost the synchronous pool size in the absence of CpxII. In cells lacking CpxII, the CpxII CTD neither enhanced the magnitude (Figure 20 A, B), nor did it speed up the synchronized vesicle fusion (Figure 20 C). In agreement with our previous observation (Figure 18), the CpxII CTD had no effect the asynchronous vesicle release from the Cpx ko cells (Figure 20 D, E).

Taken together, this data shows that the CpxII CTD does not clamp non-synchronized vesicle fusion in the absence of CpxII pointing again to the possibility that the CpxII CTD may require other CpxII domains to exert its clamp function.

5.1.6 The CpxII CTD peptide requires other domains of CpxII to clamp premature vesicle fusion

To test whether the CpxII CTD can act in tandem with the other domains of CpxII to form a fully functional unit, we infused CpxII ko cells that virally express Cpx1-100 with the CpxII CTD peptide (Figure 21 A).

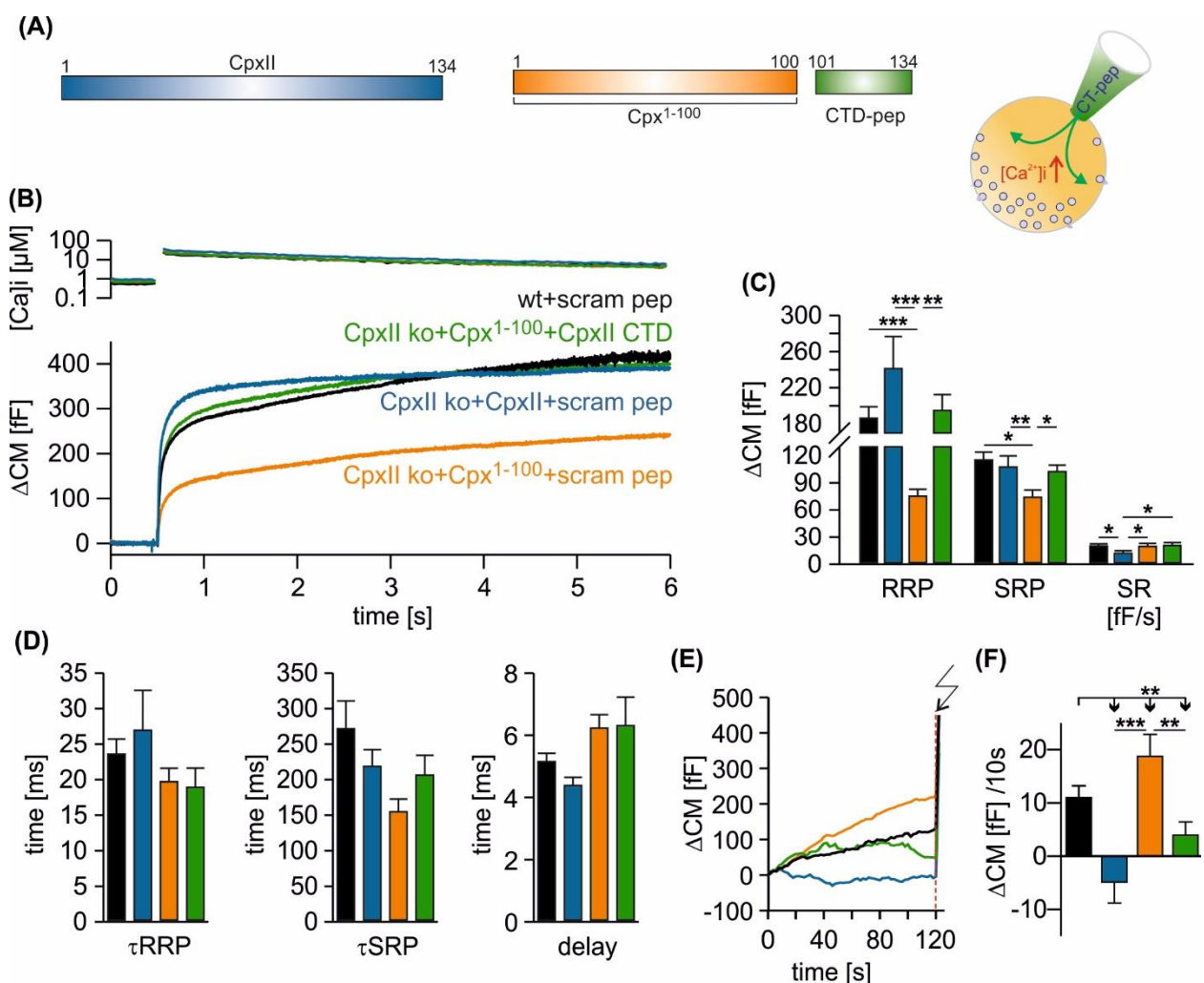


Figure 21. CpxII CTD cooperates with Cpx1-100 to suppress asynchronous vesicle fusion. **(A)** The CpxII CTD-pep (green) or scram-pep is infused into CpxII ko cells expressing either full-length CpxII (blue) or the truncated Cpx1-100 (orange). **(B)** Average $[Ca^{2+}]_i$ levels (top) and corresponding capacitance responses (bottom) for infusion of either scram pep or CpxII CTD-pep in the indicated groups. Data were collected from the following number of cells: wt + scram pep (black, n = 19), CpxII ko + CpxII + scram-pep (blue, n = 15), CpxII ko + Cpx1-100 + scram pep (orange, n = 15) and CpxII ko + Cpx1-100 + CpxII CTD pep (green, n = 18). Flash is at t = 0.5 s. **(C)** The CpxII CTD peptide (green), but not its scrambled variant (orange) recues the RRP and SRP in Cpx1-100 expressing cells, matching nearly the phenotype of full length CpxII expression (blue). The rate of sustained release (SR, fF/s) is slightly reduced with CpxII expression. **(D)** Neither the time constants of the EB components (τ_{RRP} , τ_{SRP}) nor the exocytotic delay are altered for the tested groups. **(E, F)** Contrary to the scram pep infusing the CpxII CTD in Cpx1-100 expressing cells suppresses premature secretion at submicromolar $[Ca^{2+}]_i$ almost like the CpxII protein. ANOVA followed by Tukey-Kramer post-hoc test. * $p < 0.05$, ** $p < 0.01$, *** $p < 0.001$. Error bars indicate mean \pm SEM.

In agreement with our other experiments (Figure 16), Cpx1-100 together with the scram-peptide infusion caused a significant reduction in the size of the exocytotic burst (Figure 21 B, C) without affecting its kinetics (Figure 21 D). This combination of truncation mutant and peptide also failed to suppress the asynchronous vesicle fusion (Figure 21 E, F). The infusion of the CpxII CTD peptide into cells expressing the Cpx1-100, instead, promoted the synchronized fusion like full length CpxII (Figure 21 B), where both the RRP and the SRP were restored to the level of wt cells (Figure 21 C). Notably, infusion of the CpxII CTD together with the Cpx1-100 expression caused only a progressive increase in clamping asynchronous exocytosis (Figure 21 E, F). Such a delayed onset in fusion clamping (~30-40 seconds) might be related to the time needed for peptide infusion (Figure 20 E) and agrees with our theoretical estimates, that a peptide with a molecular weight of 3846 Da can infuse into the cell with a diffusion time constant of 60 s (see Materials and Methods). In close correlation, the expression of the full-length wild type protein hindered asynchronous secretion without any delay (Figure 21 E).

Taken together, these results show that molecular continuity is not required for the CpxII CTD with the rest of Cpx to exert its clamp action. They demonstrate that the separated CpxII CTD cooperates with the N terminal regions of Cpx to form a fully functional entity. Furthermore, this data provides strong evidence against the view that the CTD by binding vesicular membranes concentrates other inhibitory domains of CpxII (e.g. accessory alpha helix) at the site of fusion (Wragg et al., 2013). Again, the gain of function phenotype confirms the view that the CpxII CTD peptide specifically facilitates synchronized exocytosis.

5.1.7 The CpxII CTD peptide rescues the clamp loss by the dominant negative

Cpx1-100 in wt cells

Our results show that the mutant Cpx1-100 is dominant negative in wt chromaffin cells, where truncation of the CpxII CTD unclamped the asynchronous fusion and diminished the size of the EB (Figure 17). On the other hand, separate CpxII CTD and Cpx1-100 are able to rescue secretion in CpxII ko cells, which raised the question if the separate CTD could also functionally revert the

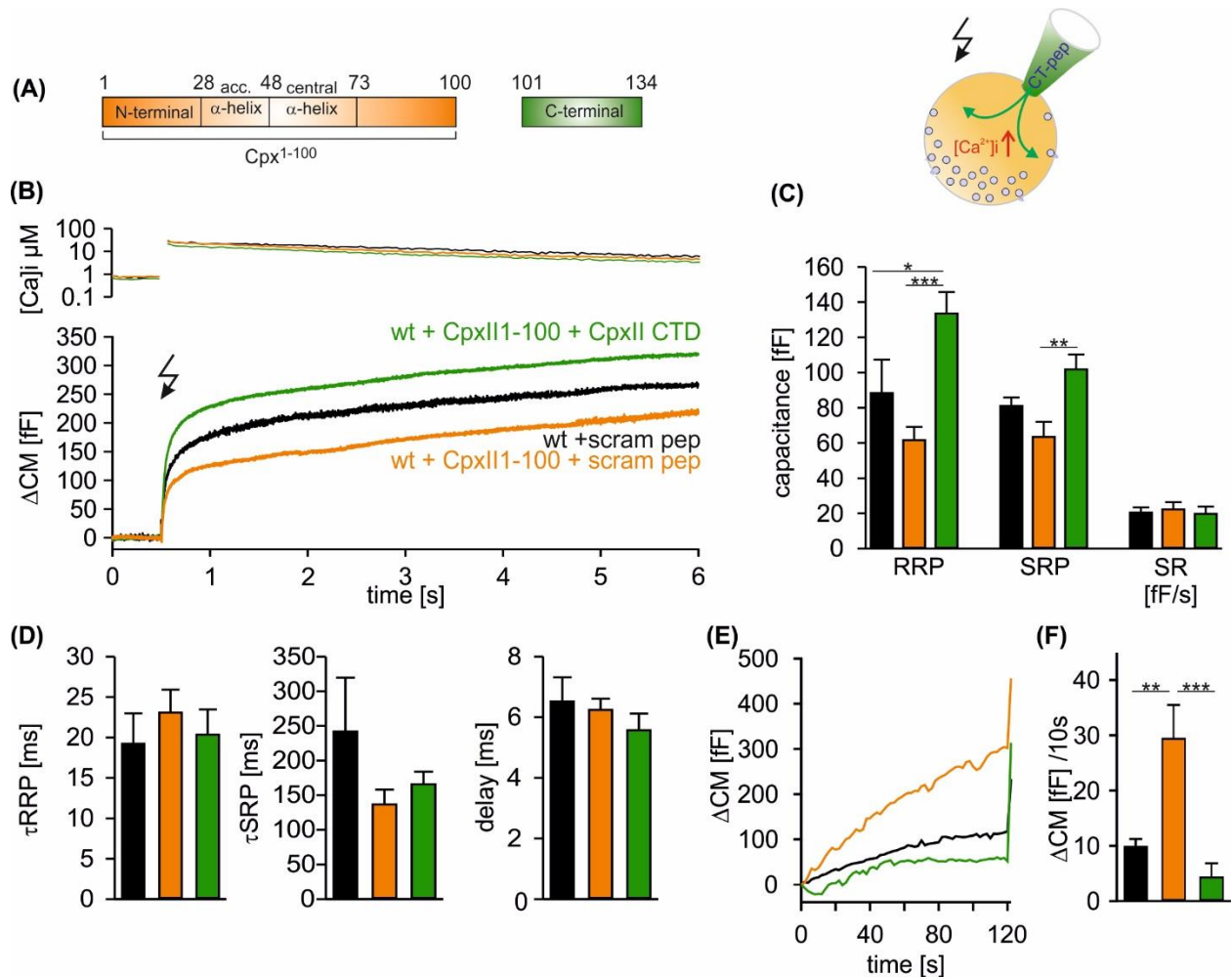


Figure 22. CpxII-CTD rescues the dominant-negative phenotype of Cpx 1-100 in wt cells. (A) Schematic representation of CpxII subdomains (numbers indicate amino acid positions within CpxII). (B) Primary sequence of the CpxII C-terminal region (residue 101–134) highlighting its structural characteristics (glutamate cluster, red; heptad repeat of hydrophobic residues, blue). (C) Mean $[Ca^{2+}]_i$ levels (top) and corresponding CM signals (bottom) of CpxII ko cells (n = 25) and those expressing CpxII (n = 32) or the mutant Cpx¹⁻¹⁰⁰ (n = 29). Flash is at t = 0.5 s (arrow). (D) Amplitudes of RRP and SRP, the rate of sustained release (SR; femtofarad/second) determined for CpxII ko (red), CpxII ko + CpxII (blue), CpxII ko+Cpx¹⁻¹⁰⁰ (orange). (E) The time constants for the EB components (τ_{RRP} and τ_{SRP}), and the exocytotic delay. (F) Mean tonic CM traces of the cells shown in (C) before the triggering flash response (arrow). (G) The rate of tonic exocytosis (determined at similar $[Ca^{2+}]_i$ in nM, CpxII ko: 714 ± 32 ; CpxII ko + CpxII: 639 ± 23 ; CpxII ko+ CpxII¹⁻¹⁰⁰: 628 ± 30) is significantly reduced with CpxII but not with its mutant. ANOVA followed by Tukey-Kramer post-hoc test. * $p < 0.05$; ** $p < 0.01$; *** $p < 0.001$. Bars indicate mean \pm SEM.

dominant phenotype of the Cpx1-100 in wt cells as well. To address this, we recorded secretion from wt cells that virally express Cpx1-100 and are infused with either the CTD, or its counterpart, the scrambled oligopeptide (Figure 22 A).

The results show that the CpxII CTD peptide alongside with the Cpx1-100 strongly boosted the synchronous EB (Figure 22 B), causing significant increases in the magnitudes of the RRP and the SRP compared to Cpx1-100 (Figure 22 C), but without altering the timing of fusion (Figure 22 D). Furthermore, this combination of CpxII domains progressively inhibited the asynchronous exocytosis (Figure 22 E, F). Indeed, infusion of the CTD again clamped the asynchronous fusion with a delayed onset (~30-40 sec), most likely reflecting the time required for the peptide to infuse into the cells, after which the asynchronous fusion was fully inhibited (Figure 22 E).

Oppositely, the scrambled peptide could not alter the phenotype of Cpx1-100 in wt cells (Figure 18) causing a significantly reduced EB from wt (Figure 22 B, C), and unclamped asynchronous fusion (Figure 22 E, F).

This data shows that the CpxII CTD in cooperation with Cpx1-100 reproduces the phenotype of CpxII expression in wt cells (Figure 17). Such a functional restoration of CpxII function in wt cells emphasizes that the molecular continuity of the CTD with the other CpxII regions is not critical to hinder premature vesicle fusion. Taken together, this data supports a mechanism of fusion inhibition by CpxII CTD that is independent from its membrane interaction properties.

5.1.8 Anchoring CpxII to the vesicle membrane aggravates Cpx's functions

Using different approaches, our data provides solid evidence that the function of CpxII CTD in inhibiting asynchronous release can be uncoupled from its role of vesicle membrane anchoring. Nonetheless, tethering CpxII to the site of fusion remains important to concentrate CpxII at the site of fusion in wt conditions (Gong et al., 2016). In a correlation between membrane binding properties and clamping fusion, CpxII CTD was proposed to mediate vesicle targeting of CpxII in order to concentrate other inhibitory domains of Cpx at the release site (Wragg et al., 2013). We tried to address this apparent correlation of membrane tethering by the CTD and the clamp action of CpxII by tethering Cpx1-100 domain to the vesicle membrane via the membrane-associating domain of the cysteine string protein Csp- α (Gong et al., 2016). Indeed, our immune-fluorescence analysis have shown that the generated fusion protein Cpx1-100-Csp- α (Figure 23 A) sorts to

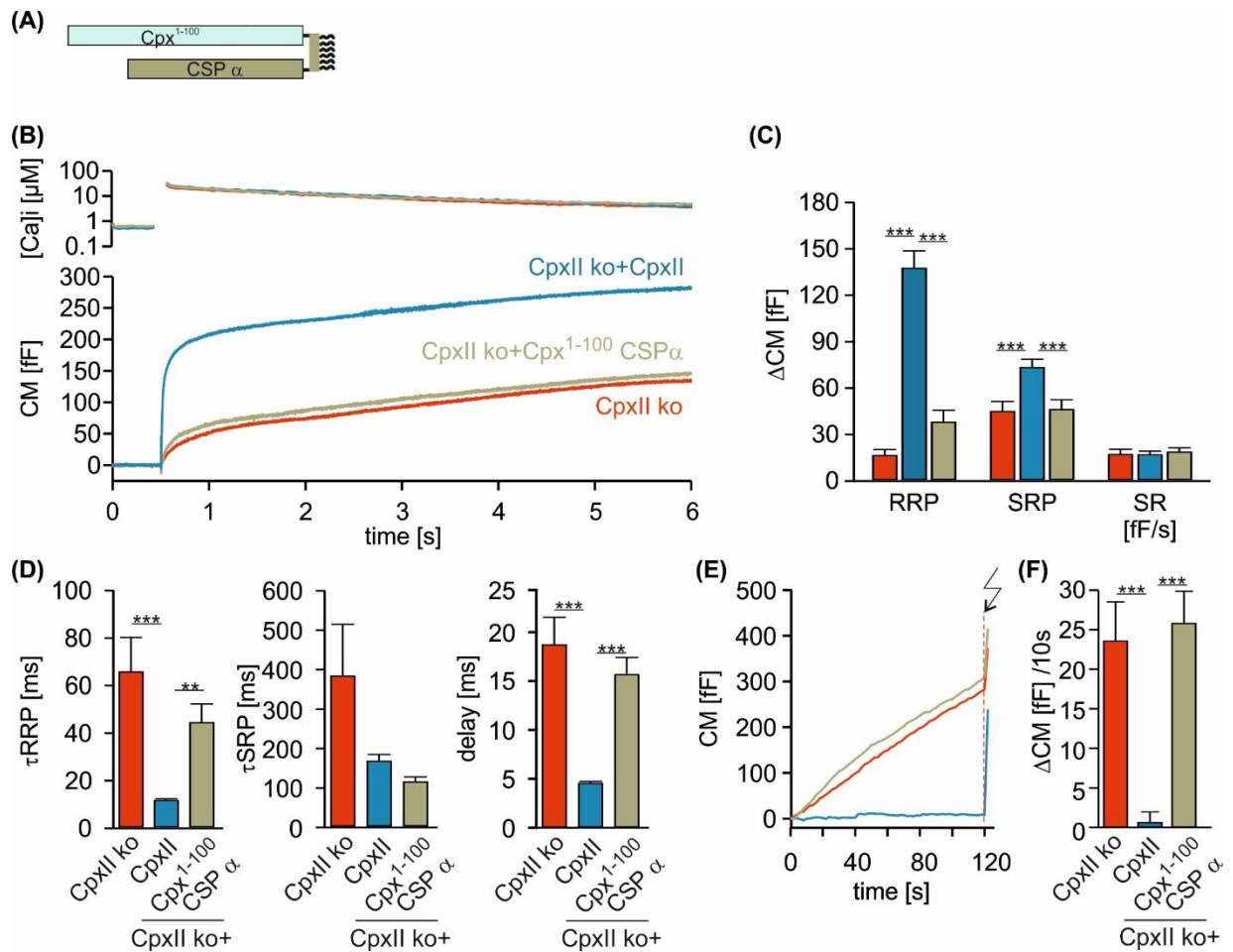


Figure 23. A membrane anchored CpxII 1-100 fails to regulate secretion. (A) Schematic representation of the Cpx¹⁻¹⁰⁰CSP α mutant. **(B)** Average [Ca²⁺]_i levels (top) and corresponding CM signals (bottom) of Cpx ko cells (n = 22) and those expressing CpxII (n = 25) or the mutant Cpx¹⁻¹⁰⁰CSP α (n = 23). Flash at t = 0.5 s. **(C, D)** Expression of CpxII¹⁻¹⁰⁰CSP α (olive) rescues neither the EB (RRP and SRP) nor its kinetics (τ RRP, τ SRP, delay) when compared with CpxII ko cells (red) or those expressing CpxII (blue). **(E, F)** CpxII-100CSP α does not hinder premature secretion like CpxII (arrow vesicle membranes similar to the wt proteins (Dhara et al., 2016; Gong et al., 2016). Yet, functionally, the chimer Cpx1-100-Csp- α failed to boost the EB in CpxII ko cells (Figure 23 B), exhibiting no enhancement of neither the RRP nor the SRP from the CpxII ko level (Figure 23 C). Interestingly, the Cpx1-100-Csp- α mutant also failed to rescue the sluggish exocytosis timing of CpxII ko cells despite the presence of an intact NTD (Figure 23 D).

Nevertheless, these results counter previously proposed function of the CpxII CTD serving as a simple membrane interaction domain to tether other CpxII domains that inhibit exocytosis to the fusion site. They rather support the view, that the CTD of CpxII is instrumental for inhibiting premature secretion at submicromolar [Ca²⁺]_i, leading to the accumulation of exocytosis competent vesicles.

5.2 CpxII CTD interacts with t-SNAREs and Syt1 and is structurally similar to SNAP25-SN1

5.2.1 CpxII CTD interacts with the calcium sensor for fast exocytosis Syt1

Our data presented the CpxII CTD as an independent functional unit that is able to mimic the clamp action of the full-length CpxII regardless of its membrane interaction properties. This observation suggests that the CTD clamps asynchronous fusion by interacting with proteins that mediate and regulate the final steps in the vesicle fusion process. To have a better understanding for the mechanism by which CpxII CTD clamps exocytosis, it is necessary to study how the loss of CpxII CTD interferes with the binding of known interaction proteins. To that end, equal amounts of recombinant bacterially expressed GST-Cpx-wt or GST-Cpx1-100 (as assessed by Coomassie staining, Figure 24-right panel) were immobilized on GST beads. The immobilized proteins were

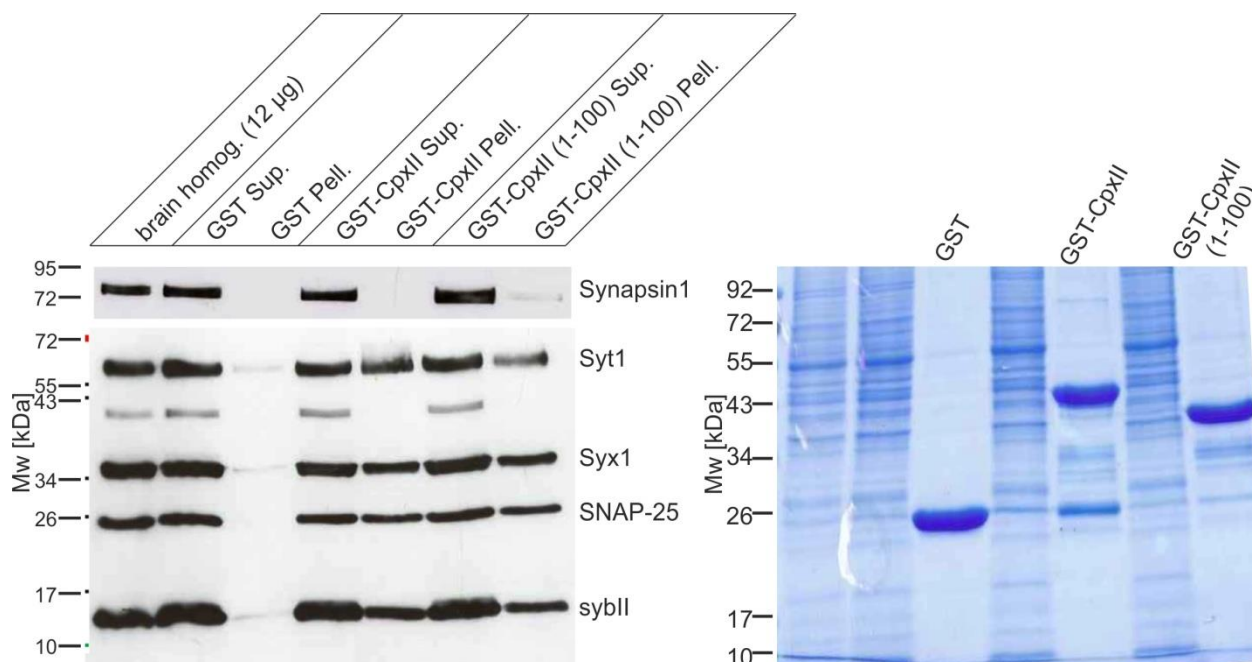


Figure 24. Truncation of CpxII CTD reduces CpxII's interaction with the calcium sensor Syt1. A comparative western blot analysis to identify the protein-protein interactions of the truncated GST-Cpx1-100 in comparison to the full length wt GST-CpxII with full protein extract of wt mouse brain. The results show no change in the interaction of the truncated mutant CpxII 1-100 with the SNARE proteins but a diminished interaction with Syt1 in comparison to wt CpxII. On the right side, a coomassie stained SDS gel showing the equal amounts of proteins loaded into the lanes from each of CpxII1-100 and the CpxII full-length baits.

then incubated with the full protein extract from the brain of a wt mouse in order to detect potential changes in binding affinity of CpxII's interaction partners (Figure 24-left panel). The

resulting Western blots were immune-labelled with antibodies directed against either SNARE protein or Synaptotagmin. The synaptic protein Synapsin which has been reported to show no interaction with CpxII served as a measure for equal protein loading and as a negative control for the specificity of the protein interactions.

We found that the truncation of CpxII CTD reduced the amount of pulled down Syt1 (Figure 24-left panel) confirming the previously reported interaction between CpxII CTD and the calcium sensor for fast fusion Syt1 (Tokumaru et al., 2008). In contrast, the interaction of the truncated Cpx1-100 with the SNARE proteins were was similar to that of full length CpxII (Figure 24-left panel). This unchanged interaction with the SNARE proteins is consistent with the view that Cpx's binding to SNAREs is preferentially mediated by its central α helix (Reim et al., 2001). It verifies that the Cpx1-100 mutant and its variants retain their ability to bind to the SNARE machinery.

5.2.2 The CpxII CTD preferentially interacts with SytI and the t-SNAREs

Given that CpxII-SNARE interactions are largely dominated by the binding of the central alpha helix to the assembled SNARE proteins, interactions by other CpxII domains might have been masked (Figure 24). To report specific interaction partners for the CTD within the secretory machinery, we immobilized similar amounts of the CpxII CTD peptide or its scrambled variant on sulfolink beads. Using a similar approach, the immobilized peptides were incubated with total protein extract from the brain of wt mice to identify potential binding partners (Figure 25). Equal volumes of

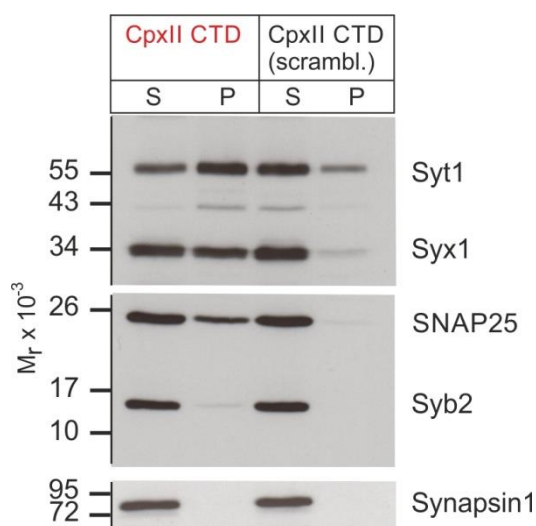


Figure 25. CpxII CTD specifically interacts with the t-SNAREs and Syt1. Western blot analysis of the interaction partners of the CpxII-CTD, by loading equal amounts of Supernatant and pellet, and comparing CTD peptide (red) to the scrambled peptide (black) shows a preferential co-precipitation of the calcium sensor Syt1, and the t-SNAREs Syx1a and SNAP25 by the CpxII-CTD from total protein extract of wt mouse brain. While Synapsin 1 staining shows no unspecific binding and equal loading in both conditions.

supernatant (S) showing unbound proteins and of the pellet fraction (showing co-precipitating proteins) were analyzed by SDS-Page and Western Blot Immunoblotting against Synapsin was again used as a control for similar loading and the specificity of interactions (Figure 25).

CpxII CTD strongly coprecipitated the calcium sensor Syt1 when compared with the scrambled control. The western blot analysis also showed significant bands in the pellet fraction of the CTD peptide at the levels of the SNARE proteins Syx1 and SNAP25 but not for Syb2. In contrast, no signals at comparable strength could be detected with the scrambled peptide. Taken together, these results are consistent with our experiments using recombinant proteins (Figure 24) showing diminished binding between CpxII and Syt1 in the absence of the CTD. They further extend previous observations by Tokumaru et al., 2008, by showing that Syt1 binds specifically to the CTD of CpxII. Yet, we have previously shown that CpxII hinders asynchronous vesicle fusion even in the absence of Syt1 (Dhara et al., 2014) which makes Syt1 an unlikely target for the CpxII CTD clamping effect. Furthermore, these interactions studies show that in addition to its central α helix, the CpxII CTD strongly provides an alternative interaction domain for the SNARE machinery, an observation that may point to the mechanism, by which the CpxII CTD breaks progressive SNARE assembly and hinders premature vesicle secretion.

5.2.3 CpxII CTD slows down the kinetics of SNARE complex formation

Motivated by these findings, we next asked whether Cpx's CTD is able to directly hinder SNARE complex formation. For this, we assessed the formation of SDS-resistant SNARE complexes in the presence of either CpxII CTD or the scrambled oligopeptide. The kinetics of SNARE complex

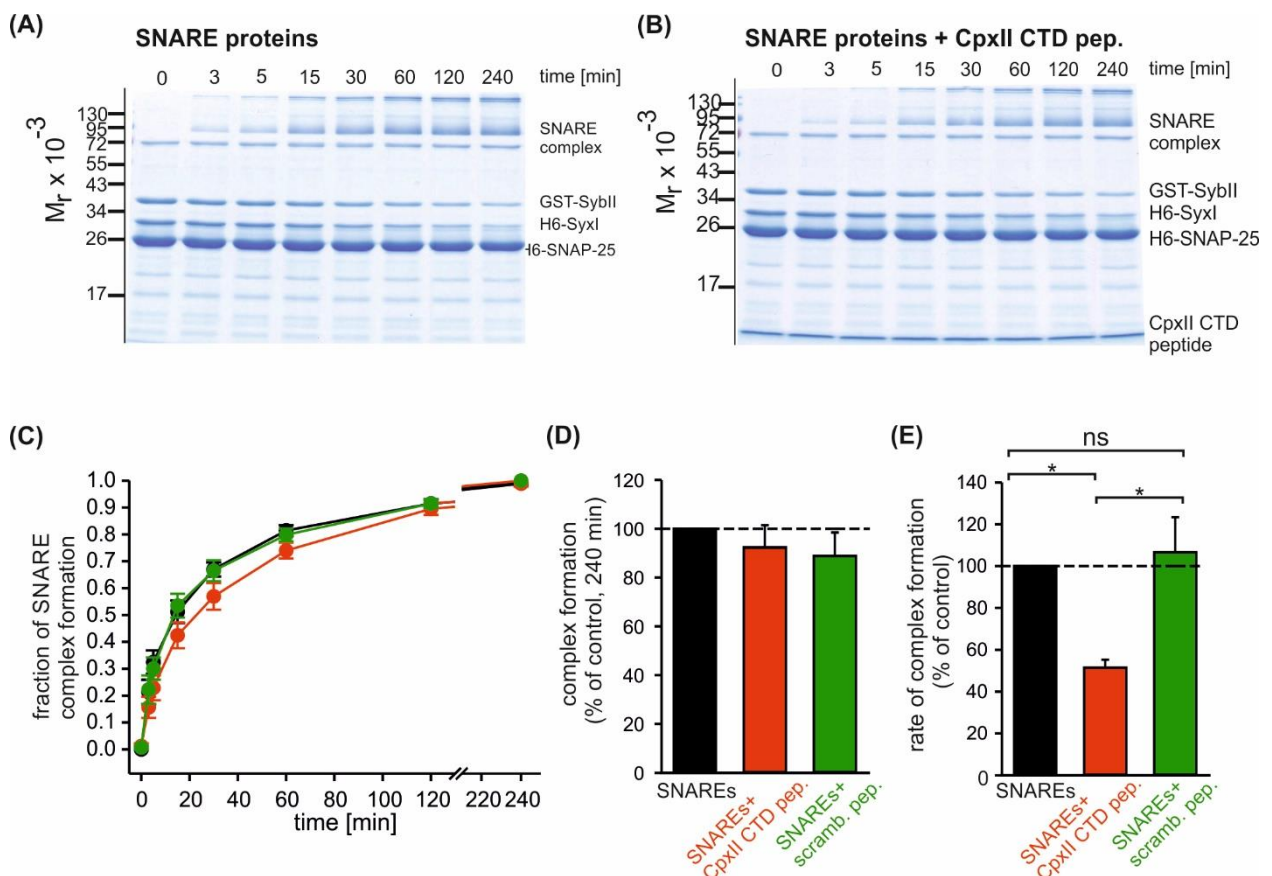


Figure 26. CpxII-CTD slows down the SNARE complex formation in vitro. (A, B) Exemplary coomassie-stained SDS gels are shown of the time-dependent SNARE complex formation between GST-Syb2 (3 mM) and pre-incubated t-SNAREs (Syntaxin 1, amino acids 1–262, 3 mM and SNAP25, amino acids 1–206, 15 mM) in the absence (left-A) and the presence (right-B) of the CpxII-CTD (50 mM). Complex formation was determined at 25°C for the indicated times and analyzed by SDS-PAGE. (C) The CpxII CTD peptide (red) slows down the time course of SNARE complex formation when compared with no peptide (SNAREs alone, black) or the scrambled peptide (green). Data were normalized to the complex formation after 240 min and averaged from the following number of trials (SNAREs, n = 8; SNAREs + CpxII CTD, n = 8; SNAREs + scr pep, n = 7). (D) The total amount of SNARE complexes formed after 240 mins normalized to the average peptide free assay showing similar amounts of SNARE complexes presence of the CTD-peptide 92.3 ± 9.1 p>0.9 and the scr-peptide 88.8 ± 9.6 , p>0.9 in comparison to the peptide free assays at 240 mins. (E) The normalized rate of complex formation to the average peptide free assays in (C) showing a significant reduction in the kinetics of SNARE complex formation with the CpxII CTD peptide ($51.4 \pm 3.8\%$ of the control) but not with the scrambled peptide ($106.6 \pm 16.7\%$ of control). p<0.05, ANOVA on ranks with Dunn's post test.

assembly were determined at different time points by SDS PAGE and Coomassie staining (Figure 26 A, B) and its time course was determined by approximating second order reaction kinetics (Nicholson et al., 1998) (Figure 26 C).

Our experiment revealed that CpxII CTD peptide significantly decelerated the kinetics of SNARE complex formation to 50% compared to the normal rate of SNARE assembly, while the scrambled peptide had no effect on SNARE complex formation (Figure 26 E). Nonetheless, the total amount of formed SNARE complexes formed at 240 minutes was similar under all conditions showing that the hindering of SNARE complex formation by the CTD peptide is transient (Figure 26 D). Thus, we show for the first time that indeed CpxII CTD hinders the progressive SNARE complex assembly.

Collectively, these results provide a first insight into a new mechanism suggesting that CpxII CTD inhibits premature vesicle fusion by transiently hindering the zipping of SNARE proteins.

5.2.4 The sequence of CpxII CTD is highly similar to that of the SNAP25 SN1 motif

Several studies suggested that SNAREs most likely are halfway zipped in the primed state, which makes the unzipped membrane proximal region of the SNARE complex an attractive target for protein-protein interactions (Gao et al., 2012; Li et al., 2014; Li et al., 2016; Zhou et al., 2017). While complexin positions itself by its central helix in a antiparallel orientation to the SNARE motifs (Sutton et al., 1998; Zhou et al., 2017), FRET experiments provided evidence that the amino acid residue Cys 105 in the CTD interacts with the Syx 1a near the ionic 0 layer of the SNARE complex

(Bowen et al., 2005). For the CTD to achieve this proximity to the membrane proximal region of the SNARE proteins it has to fold back and reposition itself in a parallel orientation with the SNARE

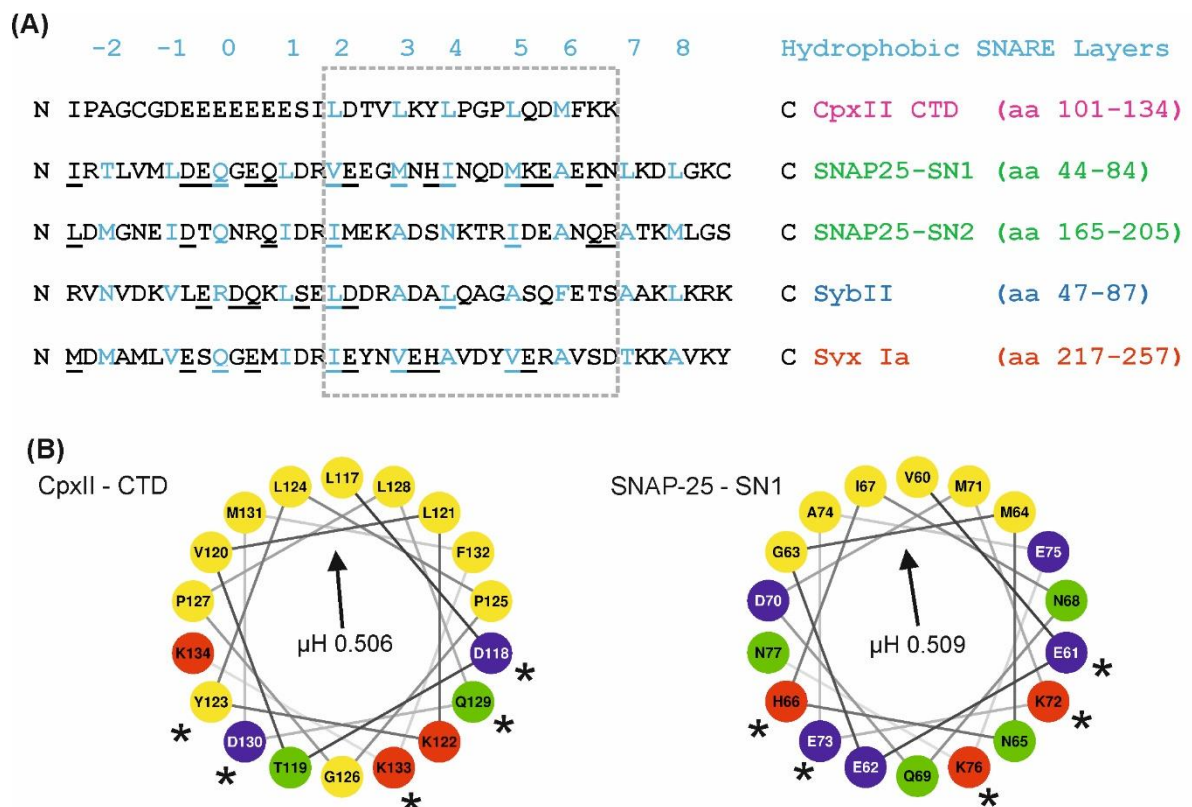


Figure 27. CpxII-CTD shows high sequence similarities with the SN1 motif of SNAP-25. (A) Sequence alignment between CpxII CTD and the SNARE motifs of SNAP25, SybII and Syx1 (hydrophobic layer region -2 to +8, blue). The CpxII-CTD shows a high degree of similarity (underlined residues) to SNAP25-SN1 (50%, calculated for the boxed region, hydrophobic layers +2 to +7, using the BLOSUM62 matrix). **(B)** Helical wheel projections of CpxII CTD (residues 117–134, boxed region in (A) and SNAP25-SN1 (residues 60–77) show the amphipathic nature of the protein regions with similar hydrophobic moments (μH). Similar amino acids in the hydrophilic faces of the helices

proteins. Such a scenario might be possible, because the Intermittent regions between the central alpha helix and the CTD of CpxII are long enough and can provide sufficient conformational freedom for the CTD to fold back on the partially assembled SNARE complex for interaction with its hydrophobic layers. In fact, the CTD may take advantage of the promiscuity of hydrophobic SNARE interactions (Yang et al., 1999; Tsui et al., 2000) to associate by its hydrophobic residues with the membrane proximal layers of the SNARE motifs hindering their progressive zipping. In order to specify how such a hindrance could take place, we investigated based on sequence similarities if there are SNARE motifs that could be targets for competition by CpxII CTD.

Comprehensive sequence alignments of the SNARE motifs near the ionic layer 0 with CpxII CTD showed that the CTD has a high sequence similarity with the hydrophobic layers +2 to +7 of the

SNARE motif SN1 of SNAP25 (50%), higher than with any of the other motifs (SNAP25 SN2 (27.8 %), Syx 1a (38.9 %), and SybII (16.7 %)) (Figure 27 A). Furthermore, the helical wheel projection of the Cpx-CTD aa 117-134 with the similar part of SNAP25 SN1 aa 60-77 showed a similarly angled, and nearly identical hydrophobic moments (μH : CTD 0.506, SN1: 0.509) (Figure 27 B) demonstrating that both sequences have similar orientation of their hydrophobic amino acids. Interestingly, we found that those similarities are shared between the Cpx CTD and its corresponding SNAP25 SN1 to be conserved features among species (i.e. *Drosophila melanogaster*, *Loligo pealeii*, *Hirudo medicinalis*; data not shown). Beside the similarities in the positioning of the hydrophobic residues the helical wheel projections also point out the identical distribution of similar amino acids on the other side of the amphipathic helix (marked by asterisk *Figure 27 B).

Overall, the combined set of data (biochemical data and sequence alignments) allowed for the speculation that the CTD may temporally compete with SNAP25 SN1 for the interaction with the other SNARE proteins at the membrane proximal layers to hinder SNARE assembly and arrest exocytosis.

5.3 CpxII-SNAP25 SN1 chimeras support full regulation of exocytosis

5.3.1 Complexin-SNAP 25 chimeras functionally resemble the wt complexin

To test whether CpxII CTD is functionally interchangeable with the SN1 of SNAP25, we generated the chimeric protein Cpx¹⁻¹⁰⁰LC by replacing the last 34 aa of Cpx with the SNAP25 SN1 44-77 (Figure 28 A). The Cpx¹⁻¹⁰⁰LC chimera largely restored magnitude of the EB and fully rescued the kinetics of the synchronous fusion to the wt level (Figure 28 B, C). Remarkably, the Cpx¹⁻¹⁰⁰LC chimera largely restored magnitude of the EB and fully rescued the kinetics of the synchronous fusion to the wt level (Figure 28 B, C). Cpx¹⁻¹⁰⁰LC also significantly suppressed asynchronous exocytosis at sub-micromolar calcium concentrations (Figure 28 E-G). While the hindrance of asynchronous fusion may simply result from a structural wedging in the presence of a helix Cpx CTD, the gain of function phenotype in the flash-evoked response favors the view that SNAP-25 mimetic C-terminus of CpxII can serve a true substitute for promoting synchronous secretion. To test whether the helical character of the substituting protein domain is the crucial determinant, we replaced the CTD with an artificial stable helix formed by 8.5 repetitions of a Glu-Ala-Ala-Lys

motif (Cpx¹⁻¹⁰⁰Helix) (Radoff et al., 2014) (Figure 28 A). Contrary to the Cpx¹⁻¹⁰⁰LC chimera, replacing the CTD with an artificial helix failed to restore the magnitude of the EB (Figure 28 B). Both, the RRP and the SRP were significantly diminished compared with the wt (Figure 28 C). Nonetheless, the timing of the synchronized release was fully restored by the N terminal domain (Figure 28 D). Moreover, the Cpx¹⁻¹⁰⁰Helix strongly failed to clamp the asynchronous fusion in chromaffin cells in

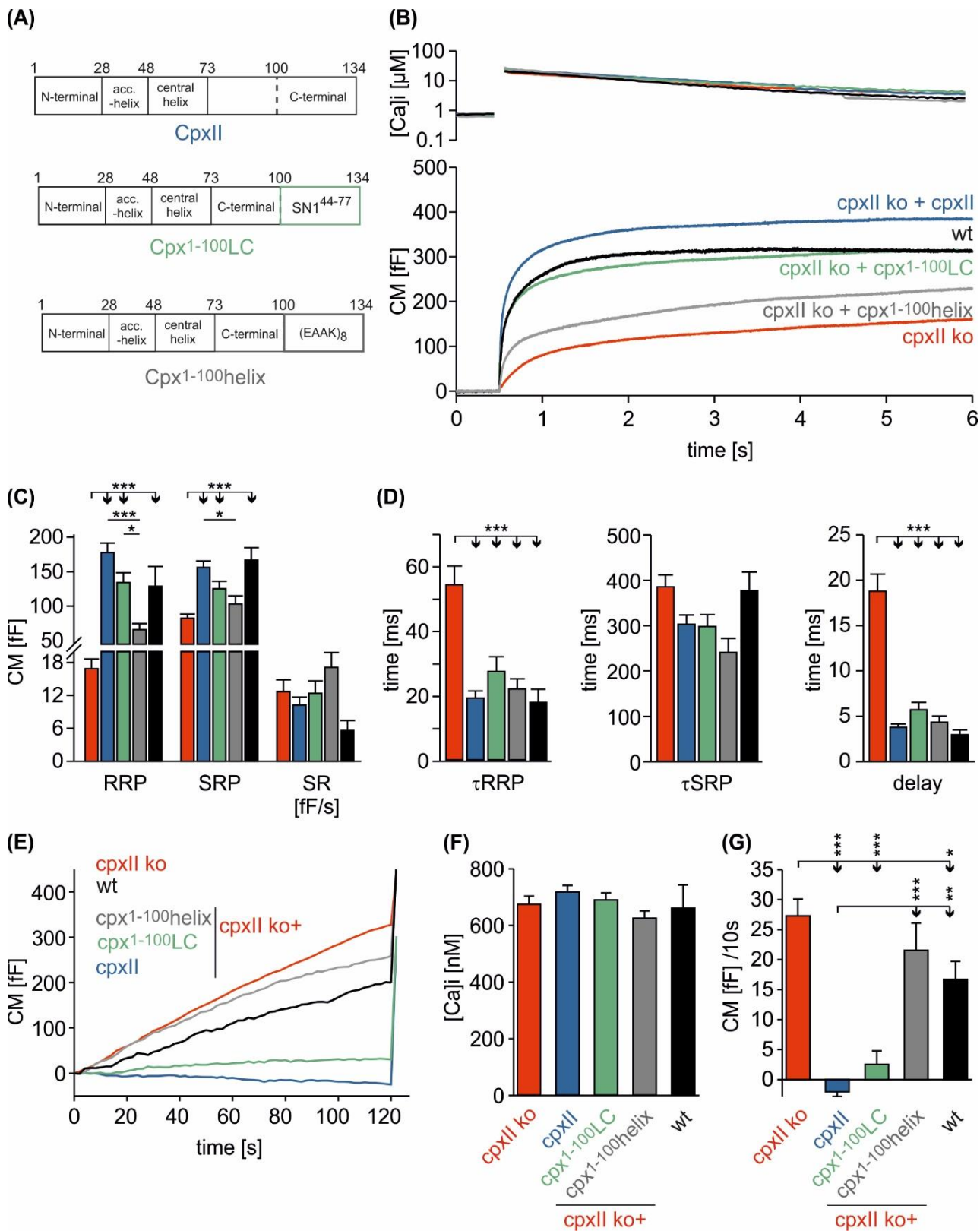


Figure 28. Cpx1-100 - SNAP25 SN1 chimera largely restores the synchronous release. (A) Cartoon illustrates CpxII domains and the structure of the tested mutants. **(B)** Expression of the Cpx¹⁻¹⁰⁰LC largely restores synchronous secretion reaching the response level of wt cells. The Cpx¹⁻¹⁰⁰helix supports exocytosis like Cpx¹⁻¹⁰⁰ (compare with figure 16). Mean [Ca²⁺]_i levels (top) and corresponding CM signals (bottom) of wt cells (n = 11), CpxII ko cells (n = 58), and ko cells expressing CpxII (n = 68) or its mutants (Cpx¹⁻¹⁰⁰LC, n = 41; Cpx¹⁻¹⁰⁰helix, n = 20). Flash, t = 0.5 s. **(C)** quantification of release phases of the synchronous release pools RRP, SRP, and SR. **(D)** The time constants of the EB components (τ_{RRP} and τ_{SRP}), and the exocytotic delay are similarly changed for CpxII and its chimera (color coding as in A). **(F–H)** The Cpx¹⁻¹⁰⁰LC clamps tonic secretion **(G)** of CpxII ko cells at similar [Ca²⁺]_i **(F)** almost like CpxII (F, H). Statistical significance was tested with one-way ANOVA followed by Tukey-Kramer post-hoc test. *p<0.05; **p<0.01; ***p<0.001. Bars indicate mean \pm SEM.

reference to the Cpx¹⁻¹⁰⁰LC (Figure 28 E, G) at similar Ca²⁺ concentrations (Figure 28 F). More importantly, the phenotype of the Cpx¹⁻¹⁰⁰Helix was identical to that by Cpx1-100 on both phases the synchronized as well as the synchronized fusion (Figure 16). The partial but significant restoration of function by the Cpx¹⁻¹⁰⁰LC indicates that CpxII CTD could be functionally replaced by the sequence from SNAP25 SN1 but not by any unrelated stable helix. Collectively, these observations provide strong evidence that the CpxII CTD and SNAP-25 SN1 may compete for the binding to the forming SNARE complex, which may represent an important mechanism by which Cpx hinders SNARE zipping.

5.3.2 A shorter CpxII CTD exchange with SNAP25-SN1 fully restores CpxII's function

To this end, the obtained results indicate that that the CTD and the SNAP25 SN1 are functionally interchangeable. To further narrow down the territory of functionally replaceable amino acids, we generated the chimeric protein Cpx¹⁻¹¹⁵ Short Chimera by exchanging the last 19 aa of the CTD with the stretch of highly similar amino acids at the positions 59-77 of SNAP25 SN1 (Figure 29 A). Cpx¹⁻¹¹⁵SC supported undiminished synchronized EB similar to the wt CpxII (Figure 29 B), and similarly boosted both components of the synchronized fusion the RRP and the SRP (Figure 29 C). Likewise, the secretion timing was also fully restored to the level of the wt (Figure 29 D-E). Furthermore, the efficiency of the Cpx¹⁻¹¹⁵SC to clamp asynchronous fusion paralleled that of wt CpxII (Figure 29 G, H). In a complementary approach, we also tested the functional impact truncating the last 19 amino acids on clamping the asynchronous fusion (Cpx1-115 Figure 29 A), and whether replacement of the CTD by an artificial helix could restore that function (Cpx¹⁻¹¹⁵helix Figure 30 A). The results show that both, Cpx1-115 as well as Cpx¹⁻¹¹⁵helix equally failed to recover

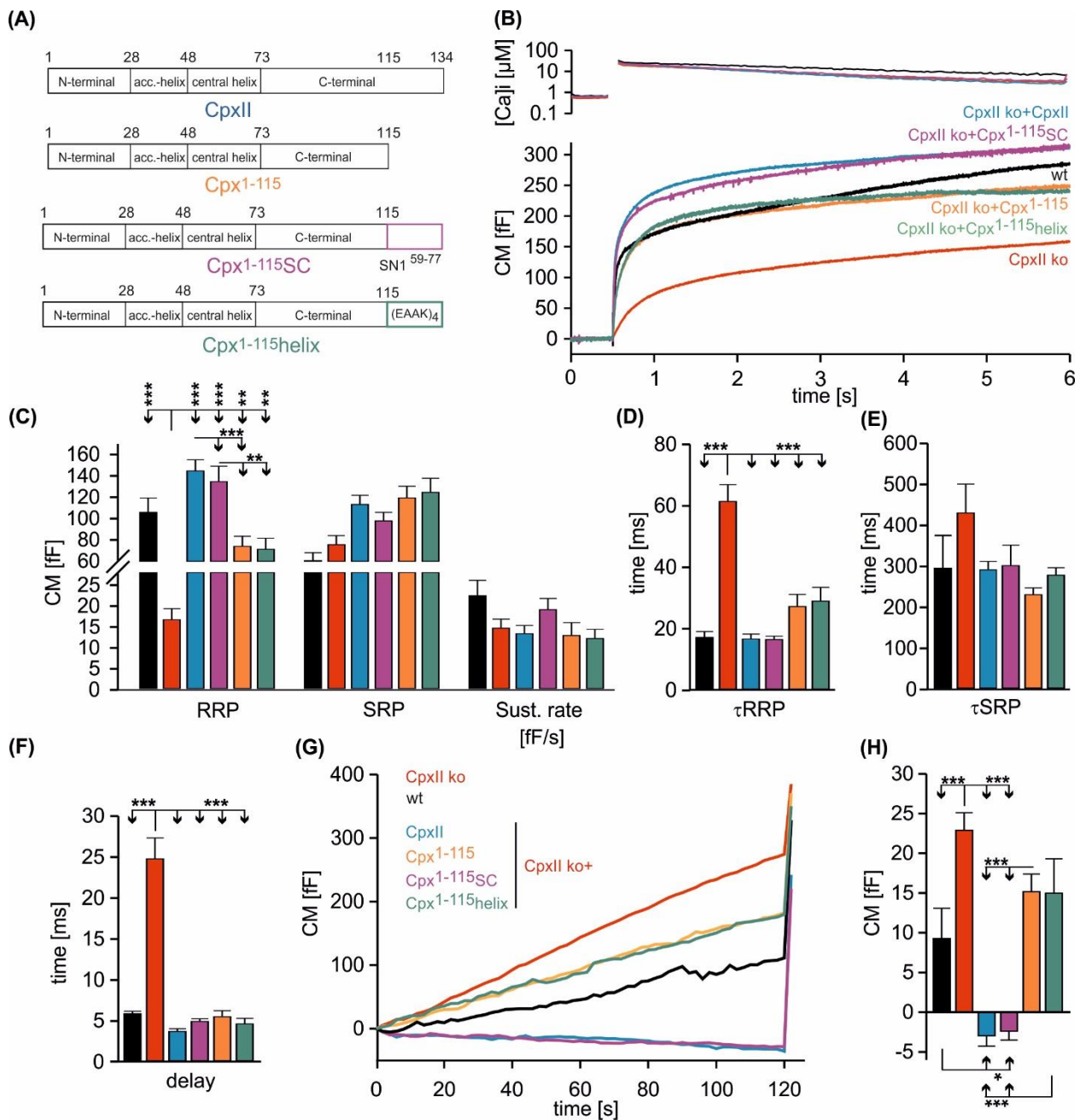


Figure 29. Cpx 1-115 - SNAP25 SN1 fully recovers the synchronous release like wt complexin. (A) Cartoon of the tested truncated and chimera mutants of CpxII. **(B)** Cpx¹⁻¹¹⁵SC but not Cpx¹⁻¹¹⁵helix restores synchronous release like CpxII. Mean [Ca²⁺]_i levels (top) and corresponding capacitance responses (bottom) of wt (black, n = 11), CpxII ko (red, n = 43), CpxII ko expressing CpxII (blue, n = 46), Cpx¹⁻¹¹⁵ (autumn orange, n = 28), Cpx¹⁻¹¹⁵SC (purple, n = 33), Cpx¹⁻¹¹⁵helix (dark green, n = 19). Flash at t = 0.5 s. **(C)** Amplitudes of RRP and SRP, the rate of sustained release (SR, fF/s). **(D–F)** The time constants of the exocytotic burst components (τRRP, τSRP) and the exocytotic delay. C-terminal truncated or mutated CpxII variants restore exocytosis timing like CpxII (see also *Dhara et al., 2014*) **(G)** Cpx¹⁻¹¹⁵SC clamps premature secretion as CpxII. Averaged tonic capacitance responses (same group of cells as in B) over 120 s at sub-micromolar [Ca²⁺]_i infusion (arrow, UV-flash). **(H)** Mean rate of ΔCM before the flash. ANOVA followed by Tukey-Kramer post-hoc test. **p<0.01; ***p<0.001. Bars indicate mean ± SEM.

the magnitude of the EB (Figure 29 B) with a substantial reduction in the RRP from the CpxII rescued cells (Figure 29 C). Still both mutant variants could fully restore the kinetics of synchronous

fusion to the wt level (Figure 29 D-F). Further, the two mutants only partially clamped the premature asynchronous fusion (Figure 29 G, H).

Collectively this data shows that the SNAP25 SN1 motif can functionally replace CpxII CTD. Thus, it is possible that indeed CpxII CTD competes out the SNAP25 SN1 domain serving temporarily as an alternative interaction partner for other cognate SNARE motifs thereby hindering progressive SNARE zipping and subsequent vesicle fusion.

5.4 Two functionally distinct regions reside within the CpxII CTD

5.4.1 The amphipathic character of the last 19 amino acids in CpxII CTD is key for its clamp function

Since our results show that CpxII CTD as an independent entity can hinder premature fusion by preventing the progressive zipping of SNARE proteins, we aim to identify what structural determinants give the CTD its clamping function. To identify the possible secondary structures within the CTD that are crucial for its function, we analyzed its sequence in the tasser 3D prediction program.

Sequence (Tasser 3D protein prediction)

```
IPAGCGDEEEEEESILDTVLKYLPGPLQDMFKK  
CCCCCCCCCHHHHHHHHHHHHHHHHCCC HHHHHHCC Pred.  
9998788701548889999999868469988519 Conf.Sc.  
C:Coil, H:Helix, S:Strand
```

Potential structure of the C-Term peptide

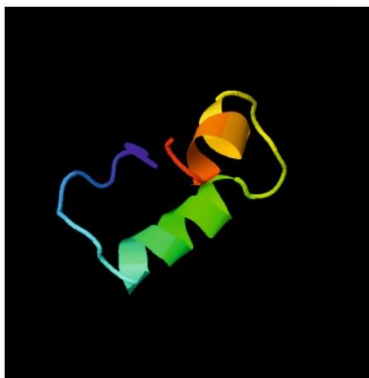


Figure 30. Predicted structure of the CpxII-CTD. The 3D structure prediction based on the Tasser database showing a predominant helical CTD of CpxII, which is intermittently interrupted by coil forming amino acids. The prediction is illustrated as a potential structure representation in the lower box from N terminal amino acid 101 at the dark violet end and the amino acid 134 at the red end.

The structure prediction showed that the CpxII CTD is mostly helical (Figure 30), with a predominant amphipathic helix at the very end of the CTD (residues 116-134) (Figure 30 A). Based

on this information, we want to identify what are the secondary structures important within the CTD for the clamp function of CpxII. This point will be addressed in the following experiments.

Replacing CpxII CTD with an unrelated artificial helix failed to support the synchronized fusion similarly to the equivalent truncated mutants (Figure 28, and Figure 29). Based on this result, it stands to reason whether it is the amphipathic character of the CTD that can be held responsible for mediating the clamp activity of the CpxII protein (Figure 28 A). To address this, we substituted the entire CpxII CTD with a synthetic amphipathic α helix comprising 4.8 repeats of the amino acid sequence (ALEALKA) Cpx¹⁻¹⁰⁰amph helix (Figure 31). Surprisingly, the mutant protein Cpx¹⁻¹⁰⁰amph helix not only failed to restore the EB of synchronous fusion (Figure 31 A, B), but also was unable to accelerate the synchronous release from the CpxII ko (Figure 31 C). The loss of function by the

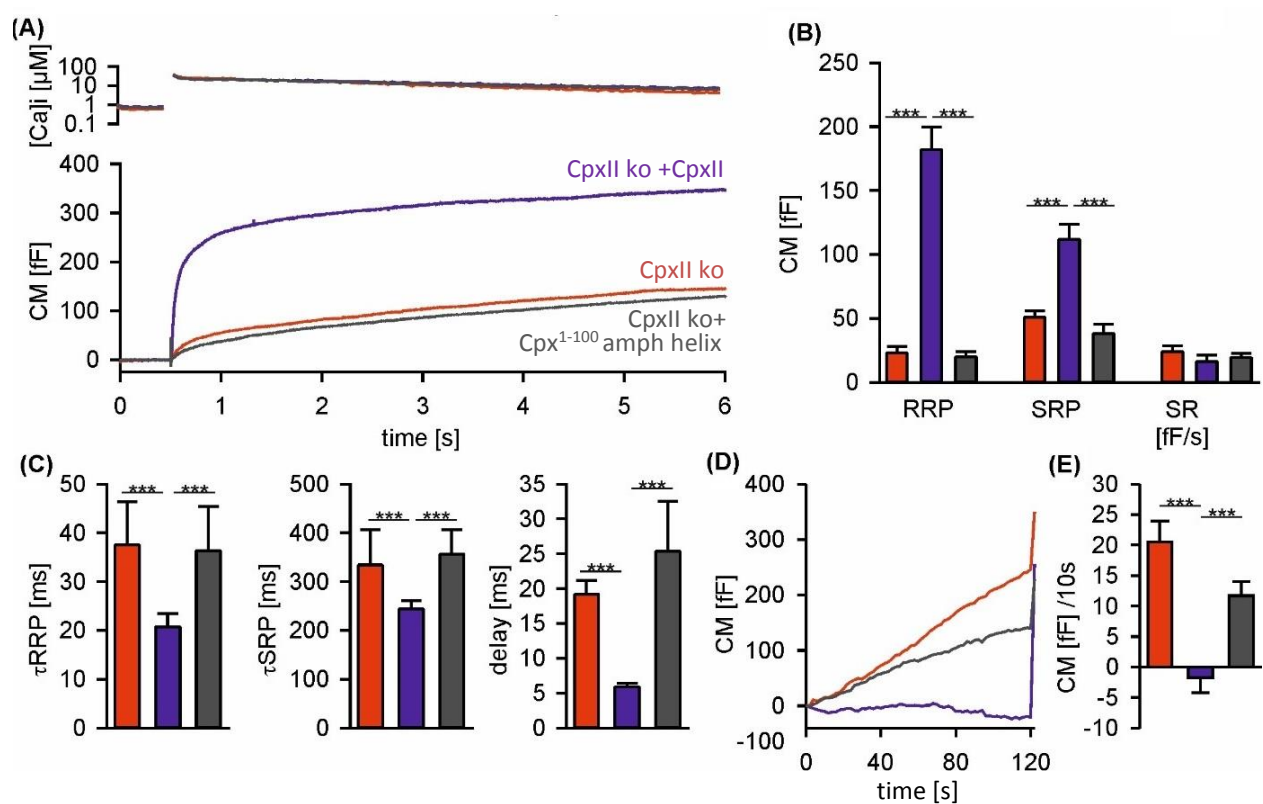


Figure 31. Replacing the CpxII CTD with an amphipathic helix compromises CpxII's functions. (A) Mean $[Ca^{2+}]_i$ levels (top) and corresponding CM signals (bottom) of CpxII ko cells ($n = 18$) and those expressing CpxII ($n = 16$), Cpx¹⁻¹⁰⁰ amph helix mutant ($n = 15$). (B) Amplitudes of RRP and SRP, the rate of sustained release (SR; femtofarad/second) determined for CpxII ko (red), CpxII ko + CpxII (blue), CpxII ko + Cpx¹⁻¹⁰⁰ amph helix mutant (gray). (C) The time constants for the EB components (τ_{RRP} and τ_{SRP}), and the exocytotic delay. (D) Mean tonic CM traces of the cells shown in (A) before the triggering flash. (E) The rate of tonic exocytosis (determined at similar $[Ca^{2+}]_i$ in nM, CpxII ko: 700 ± 38 ; CpxII ko + CpxII: 760 ± 64 ; CpxII ko + Cpx¹⁻¹⁰⁰ amph helix: 869 ± 108) is significantly reduced with CpxII but not with the Cpx¹⁻¹⁰⁰ amph helix mutant. ANOVA followed by Tukey-Kramer post-hoc test. * $p < 0.05$; ** $p < 0.01$; *** $p < 0.001$. Bars indicate mean \pm SEM.

Cpx¹⁻¹⁰⁰ amph helix impairs clamping of asynchronous fusion and hinders also fusion facilitation by the CpxII NTD. This phenotype resembles that of anchoring CpxII to the vesicle membrane via its CTD (Cpx1-100-Csp- α Figure 23 D). Therefore, an attractive explanation could be that the exchange with a long amphipathic sequence Cpx¹⁻¹⁰⁰ amph helix may increase the affinity CpxII to lipids due to its higher content of hydrophobic residues (Datta et al., 2001). Therefore, reversible binding to membranes might be a prerequisite for CpxII to fulfill its function. Alternatively, we cannot rigorously exclude the possibility that that substituting the non-helical region in the CTD with an amphipathic helix (aa 101-115) compromises the overall protein folding.

Revisiting the sequence comparison of the Cpx CTD with the SNARE motifs, revealed the last 19 amino acids stand out by forming an amphipathic helix character (Figure 30) as well as by showing the highest degree of similarity with SNAP25 SN1 motif (Figure 27). To study the importance of the amphipathic character within the CTD for inhibition of premature release, we replaced its last 19 amino acids with 2.7 repeats of the amino acid sequence (ALEALKA) forming a synthetic amphipathic helix (Cpx1-115 amph helix). As shown by our earlier experiments, the truncated Cpx1-115 only partially restored the synchronous fusion (Figure 32 A, B), but it fully restored the exocytosis timing

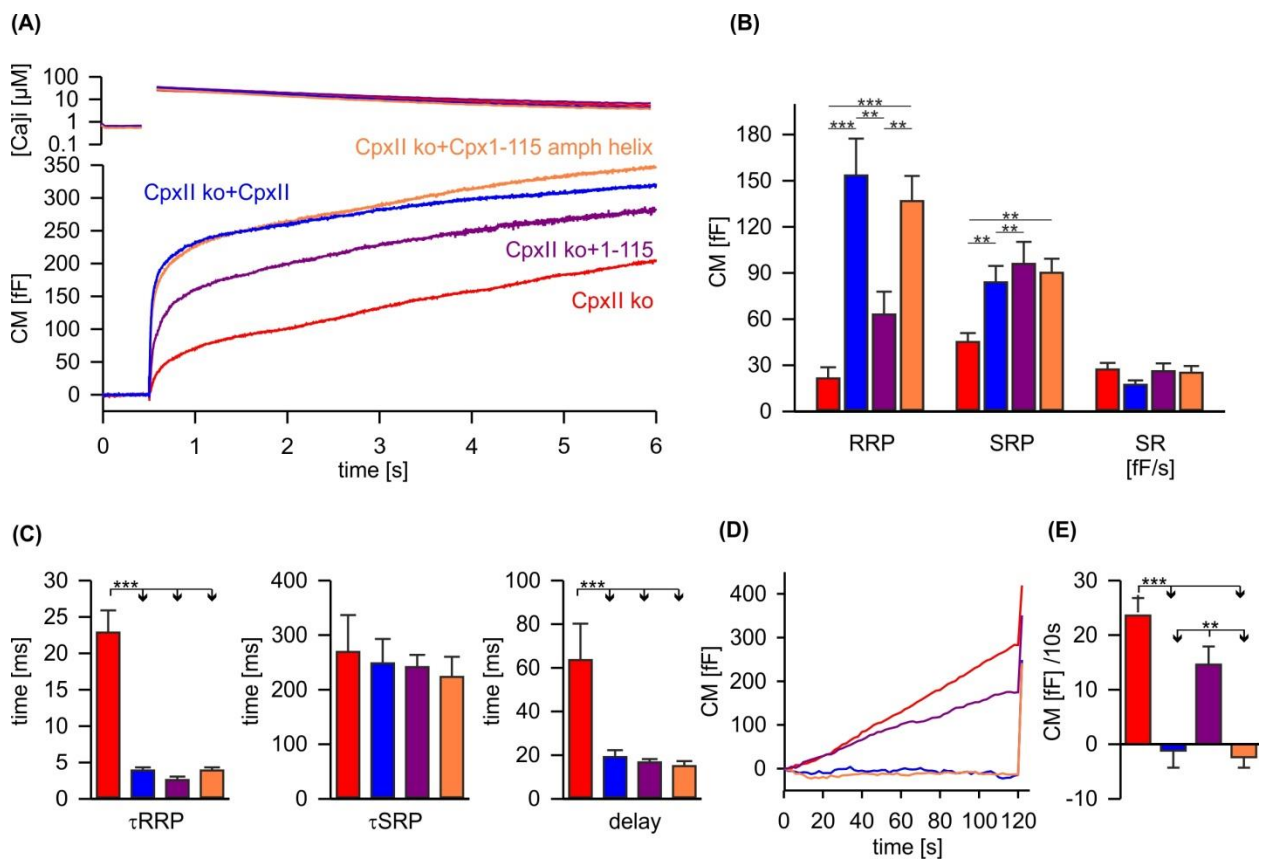


Figure 32. A synthetic amphipathic helix can functionally replace the last 19 amino acids of CpxII CTD in clamping asynchronous fusion. (A) Mean $[Ca^{2+}]_i$ levels (top) and corresponding CM signals (bottom) of CpxII ko cells (n = 15) and those expressing CpxII (n = 15), the truncated mutant Cpx¹⁻¹¹⁵ (n = 15) and the Cpx¹⁻¹¹⁵ amph helix mutant (n = 16). (B) Amplitudes of RRP and SRP, the rate of sustained release (SR; femtofarad/second) determined for CpxII ko (red), CpxII ko + CpxII (blue), CpxII ko+Cpx¹⁻¹¹⁵ (violet), CpxII ko+Cpx¹⁻¹¹⁵ amph helix (light orange). (C) The time constants for the EB components (τ_{RRP} and τ_{SRP}), and the exocytotic delay. (D) Mean tonic CM traces of the cells shown in (A) before the triggering flash. (E) The rate of tonic exocytosis (determined at similar $[Ca^{2+}]_i$: in nM, CpxII ko: 789 ± 120 ; CpxII ko + CpxII: 777 ± 57 ; CpxII ko+ CpxII 1-115: 739 ± 84 ; CpxII ko+ CpxII¹⁻¹¹⁵ amph helix: 796 ± 64) is significantly reduced with CpxII but and CpxII 1-115 amph helix mutant but not with the truncated CpxII¹⁻¹¹⁵ mutant. ANOVA followed by Tukey-Kramer post-hoc test. *p<0.05; **p<0.01; ***p<0.001. Bars indicate mean \pm SEM.

of the synchronously fusing vesicles (Figure 32 C). In addition, the truncation of the last 19 amino acids from Cpx partially clamped the synchronized vesicle fusion (Figure 32 D, E).

In sharp contrast, the chimeric protein Cpx¹⁻¹¹⁵amph helix supported an undiminished synchronized EB (Figure 32 A, B), and sped up the timing of exocytosis (Figure 32 C). Furthermore, it efficiently hindered premature vesicle fusion similar to the wt CpxII (Figure 32 D, E). Taken together, the data shows that the periodic repeats of the hydrophobic amino acids at the C-terminal end of CpxII are sufficient for clamping asynchronous fusion as well as for building up a pool of exocytosis-competent vesicles. Furthermore, the hydrophilic face of the amphipathic helix plays a subordinate role in hindering premature secretion.

5.4.2 The cluster of Glutamate residues E¹⁰⁸-E¹¹⁴ in CpxII CTD facilitates vesicle fusion

The clustering of positively charged glutamates E108-E114 with the CpxII CTD is conserved in both vertebrate and invertebrate Cpx isoforms (Tokumaru et al., 2008). Earlier biochemical experiments provided evidence that this domain of positively charged amino acids mediates a direct interaction with the calcium sensor for fast release Syt1 (Tokumaru et al., 2008). However, the functional significance of this patch of positively charged glutamate residues in the synchronized fusion was not addressed. To clarify the role of this domain in regulated fusion, we substituted the glutamate residues E108-E114 with alanines, a substitution which reduces the interaction of the CTD with Syt1 (Tokumaru et al., 2008). The Cpx E/A mutant expressed in CpxII ko chromaffin cells only partially restored the synchronized pool (Figure 33 A, B). Further, the time constant for RRP was significantly increased and a strong trend in the timing of the SRP release was also prominent (Figure 33 C), indicating that the primed vesicle pool was fusing at a slow rate. Moreover, a

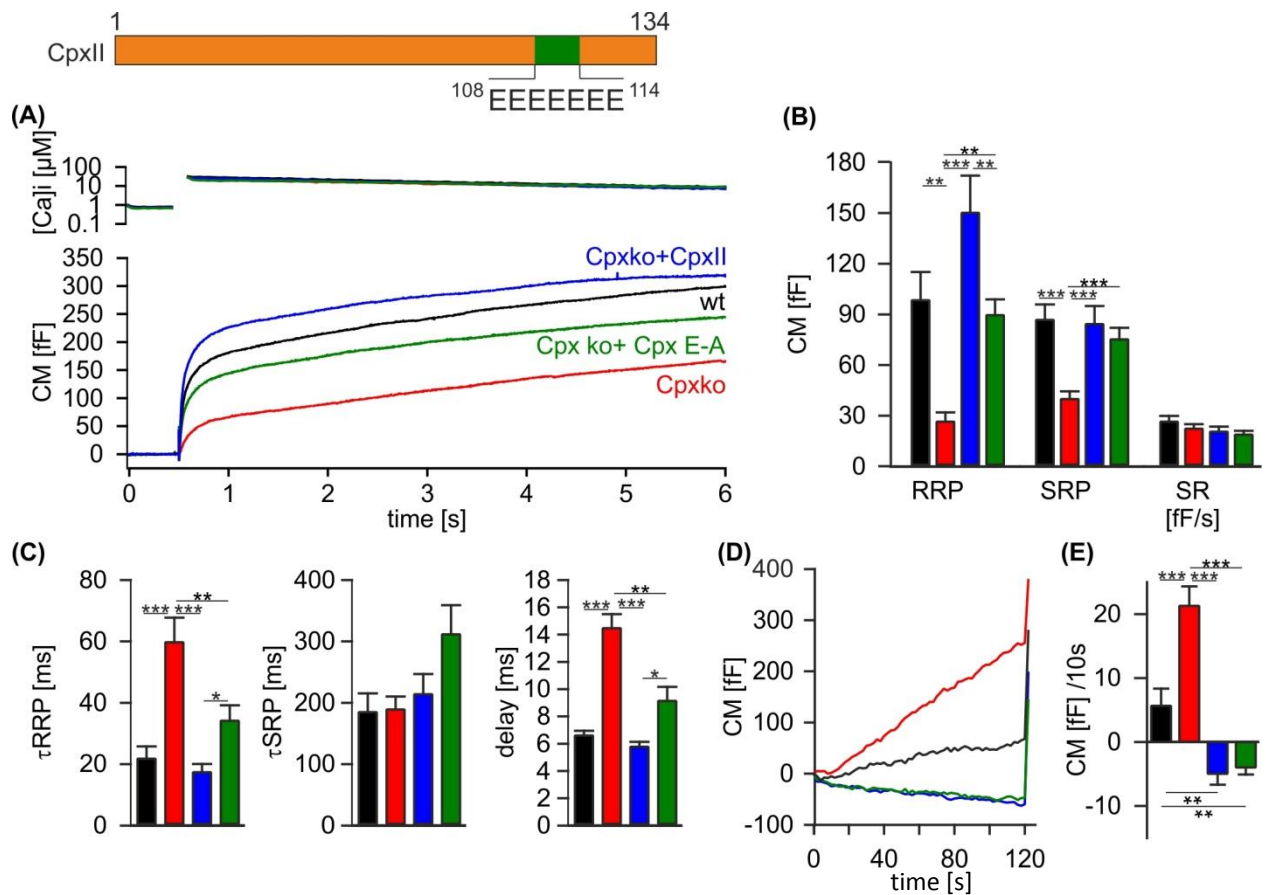


Figure 33. The Glutamate cluster aids in lifting the clamp imposed by the CpxII-CTD. (A) Mean $[Ca^{2+}]_i$ levels (top) and corresponding CM signals (bottom) of CpxII ko cells ($n = 23$) and those expressing CpxII ($n = 24$), the mutant Cpx E-A ($n = 25$) and the wt ($n = 18$). (B) Amplitudes of RRP and SRP, the rate of sustained release (SR; femtofarad/second) determined for CpxII ko (red), CpxII ko + CpxII (blue), CpxII ko+ Cpx E-A (green), wt (black) with an overall reduced exocytotic burst by the Cpx E-A compared to the CpxII rescue. (C) The time constants for the EB components (τ_{RRP} and τ_{SRP}), and the exocytotic delay. (D) Mean tonic CM traces of the cells shown in (A) before the triggering flash. (E) The rate of tonic exocytosis (determined at similar $[Ca^{2+}]_i$: in nM, CpxII ko: 798 ± 36 ; CpxII ko + CpxII: 845 ± 51 ; CpxII ko+ CpxII E-A: 770 ± 29 ; wt: 836 ± 34) is significantly reduced with CpxII and CpxII E-A equally. ANOVA followed by Tukey-Kramer post-hoc test. * $p < 0.05$; ** $p < 0.01$; *** $p < 0.001$. Bars indicate mean \pm SEM.

significant delay in the timing of the stimulus-secretion was observed, despite the presence of the NTD (Figure 33 C). Oppositely, the alanine exchange did not alter the efficiency of CpxII in inhibiting the asynchronous fusion, which remained similar to the CpxII wt rescue (Figure 33 D, E).

Overall, our data shows that the glutamate cluster in the CpxII CTD does not contribute to the clamp function of CpxII. Indeed, the reduced magnitude of the EB accompanied with the increased delay in the stimulus-secretion coupling and slowing of the synchronized fusion kinetics by mutating the glutamate cluster to alanine residue are phenotypes that highly resemble the Syt1 ko phenotype in chromaffin cells (Dhara et al., 2014). This points to the possibility that the cluster of glutamates residues may facilitate fusion by aiding Syt1 to lift the fusion clamp by the CTD,

either by interacting with or recruiting Syt1 to the partially assembled SNARE complex. Alternatively, it is possible that the cluster of glutamates may provide an additional interphase for Syt1's C2 domains to increase the number of coordinated Ca^{2+} , which might increase its efficiency to trigger vesicle fusion.

5.5 The CpxII N terminal domain accelerates exocytosis in cooperation with the calcium sensor Syt1

5.5.1 N-terminal domain of Complexin adapts the calcium sensitivity for exocytosis

The kinetics and timing of the synchronous release are directly proportional to the kinetics of Ca^{2+} binding to the calcium sensors for exocytosis (Voets 2000; Schneggenburger et al., 2005). On the other hand, the CpxII N terminal domain (amino acids 1-26) also accelerates fusion rate in neurons (Xue et al., 2007; Dhara et al., 2014; Lai et al., 2016), as well as in in chromaffin cells by increasing the calcium affinity of synchronous exocytosis (Dhara et al., 2014). Different mechanisms were proposed for the fusion speeding by the NTD, by either interacting with or stabilizing the C-terminal region of the trans-SNARE pin and thereby lowering the overall energy barrier for fusion (Xue et al., 2010). Experiments with liposome fusion assay instead suggested that membrane binding of the N-terminal domain of complexin facilitates fusion (Lai et al., 2016). Furthermore, it is possible that the CpxII NTD adapts the Ca^{2+} -sensor Syt1 and thereby excels fusion kinetics (Neher 2010; Dhara et al., 2014). Still, the possible cooperation between the NTD and the calcium sensors for fast release has not been investigated, and the possibility of a functional interplay remained ambiguous.

5.5.2 CpxII NTD tunes the speed of Syt1 mediated synchronized exocytosis

Two isoforms of Syt are essential for the synchronized fusion in chromaffin cells (Schonn et al., 2008); those are Syt1 for fast release and Syt7 for slow release (Bacaj et al., 2013; Chang et al., 2018; also for review see Mohrmann et al., 2015). As pointed out before, truncation of the CpxII NTD was shown to slow down the rates of RPP release, and to increase the delay for the stimulus-secretion coupling (Dhara et al., 2014). These phenotypes remarkably resemble the loss-of-function phenotype of Syt1-ko cells, suggesting that Syt1 and the CpxII NTD might mechanistically converge in facilitating the calcium triggered synchronized synchronous exocytosis. Alternatively, it is possible that the NTD of CpxII serves as an important molecular switch promoting the use of

Syt1 instead of Syt7 for fusion. To test these hypotheses, we generated the Cpx DN mutant (aa 27-134) by truncating the NTD (aa 1-26) and analyzed its function in Syt7-ko chromaffin cells having only the calcium sensor Syt1 to trigger synchronized fusion. The genetic loss of Syt7 significantly reduced the size of the primed pool compared to the response of wt cells (Figure 34 A, B). Both, the RRP and the SRP component of the EB are similarly affected, indicating that Syt7 exerts its action upstream of pool formation, most likely by serving as a Ca^{2+} -dependent priming factor (Liu et al., 2014; Dolai et al., 2016). Furthermore, the deletion of Syt7 did not affect asynchronous secretion before the triggering flash response (Figure 34 D, E), which favors the view that Syt7 is not the only or preferred Ca^{2+} -sensor for exocytosis at submicromolar $[Ca^{2+}]_i$, despite its high Ca^{2+} -

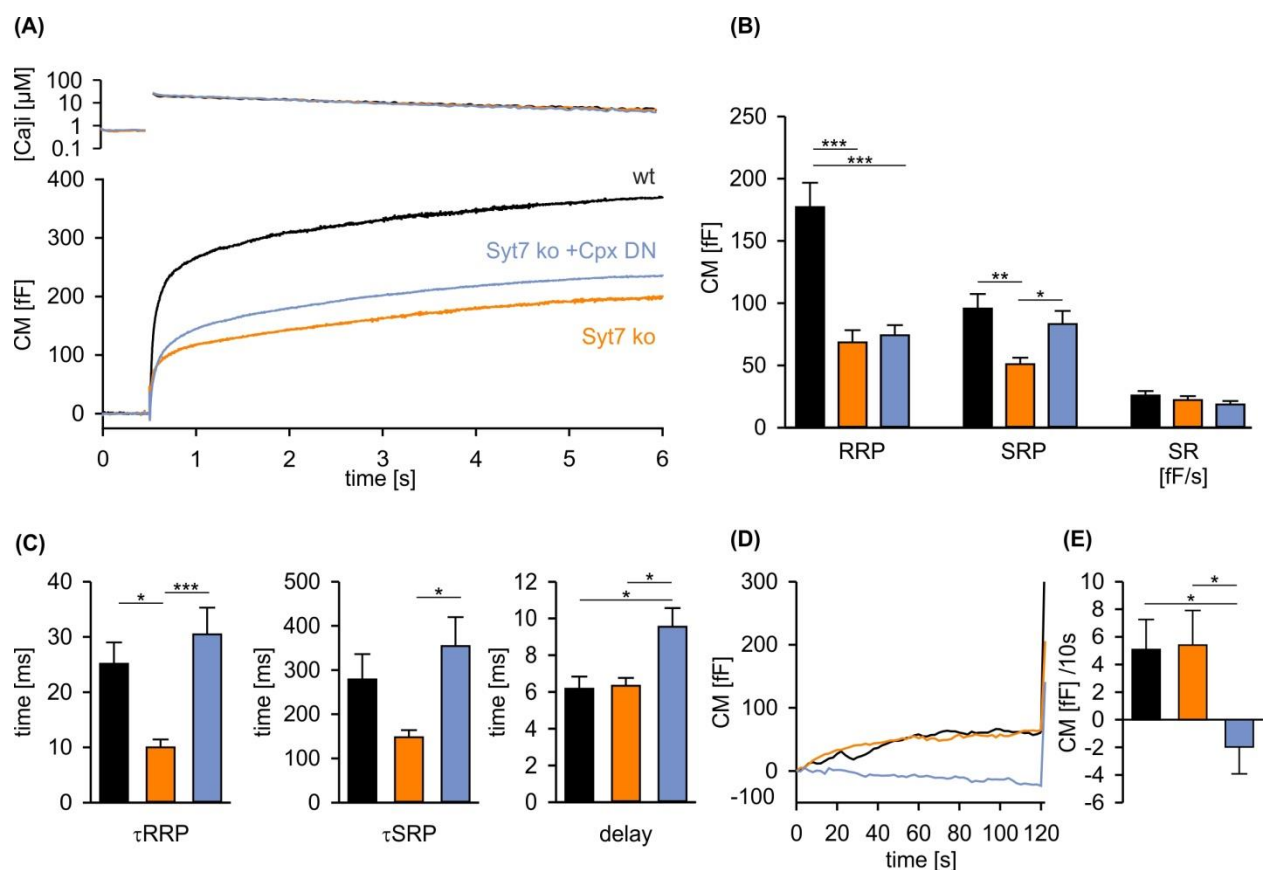


Figure 34. CpxII-NTD supports Syt1 in facilitating synchronized vesicle fusion. (A) Mean $[Ca^{2+}]_i$ levels (top) and corresponding CM signals (bottom) of Syt7 ko cells (n = 15) and those expressing CpxII Δ N (n = 26), and the wt (n = 20). (B) Amplitudes of RRP and SRP, the rate of sustained release (SR; femtofarad/second) determined for Syt7 ko (orange), Syt7 ko + CpxII DN (light blue), wt (black) with an overall reduced exocytotic burst by the Syt7 ko compared to the wt. (C) The time constants for the EB components (τ RRP and τ SRP), and the exocytotic delay. (D) Mean tonic CM traces of the cells shown in (A) before the triggering flash. (E) The rate of tonic exocytosis (determined at similar $[Ca^{2+}]_i$: in nM, Syt7 ko:651 \pm 62 ; Syt7 ko + CpxII Δ N:652 \pm 42; wt:653 \pm 36) is significantly reduced with CpxII Δ N expression. ANOVA followed by Tukey-Kramer post-hoc test. *p<0.05; **p<0.01; ***p<0.001. Bars indicate mean \pm SEM.

affinity (Schneggenburger et al., 2015). The remaining Syt1 mediated synchronized fusion in Syt7 ko cells was significantly faster compared to wt cells (Figure 34 C), consistent with the faster Ca^{2+} -

binding kinetics of Syt1 when compared with Syt7 (Hui et al., 2005). Importantly, the CpxII DN mutant slowed down fusion kinetics (τ RRP, τ SRP and secretory delay) of Syt7-ko cells like it did in wt cells (Figure 34 C, compare Dhara et al., 2014). These results render the possibility unlikely that the CpxII NTD catalyzes the preferred use of Syt1 instead of Syt7. It rather suggests that the NTD of CpxII directly adapts Syt1 and thereby speeds up fusion kinetics. Furthermore, the results show that expression of CpxII DN efficiently clamped asynchronous release in the absence of Syt7, agreeing with the hypothesis that CpxII prevents premature exocytosis by hindering SNARE assembly rather than the Ca^{2+} -sensing Syt proteins (Dhara et al., 2014). Collectively, loss of CpxII NTD clearly slows down the Syt1 mediated vesicle fusion, making it unlikely that CpxII NTD takes the role of a potential switch that preferentially shifts control of the synchronous release to Syt1 rather than to Syt7. It indeed indicates that the CpxII NTD adapts Syt1 in order to speed up fusion.

In following up on this, we next asked to what extent the CpxII NTD is able to modify also the kinetics of the Syt7 mediated exocytosis. For this, we comparatively analyzed the functional impact of expressing either CpxII wt or its N-terminally truncated variant in Syt1 ko cells.

Our data shows that the deletion of the calcium sensor Syt1 in chromaffin cells greatly reduced the magnitude of the EB compared to wt (Figure 35 A). Specifically the fast phase of the RRP was nearly abolished with no observed alteration in the magnitude of the SRP (Figure 35 B) agreeing with previous observations by others as well as our lab (Dhara et al., 2014; Li et al., 2017). Furthermore, loss of Syt1 significantly slowed down the fusion kinetics of both the RRP as well as the SRP components of the synchronized exocytosis and caused a prolonged delay in the stimulus secretion coupling (Figure 35 C). Nonetheless, despite the loss of the calcium sensor Syt1, the premature vesicle exocytosis remained similar to that of wt at submicromolar calcium concentrations (Figure 35 D, E).

In contrast to our published results in wt cells (Dhara et al., 2014), and in Syt7 ko cells (Figure 34), the expression of the CpxII Δ N mutant did not slow down the kinetics of synchronized exocytosis nor did it delay the timing of fusion in the absence of Syt1 (Figure 35 C). In addition, the wt CpxII could not accelerate the slow Syt7 mediated exocytosis, which indicates that CpxII cooperates with Syt1 to determine the speed of synchronous exocytosis. It is important to note that neither CpxII nor the N-terminal domain truncation mutant CpxII Δ N in Syt1 ko cells could rescue the magnitude of the synchronous fusion from the Syt1 ko level (Figure 35 A, B) despite the fact that both CpxII variants fully suppressed the asynchronous release (Figure 35 D, E). This data shows that CpxII

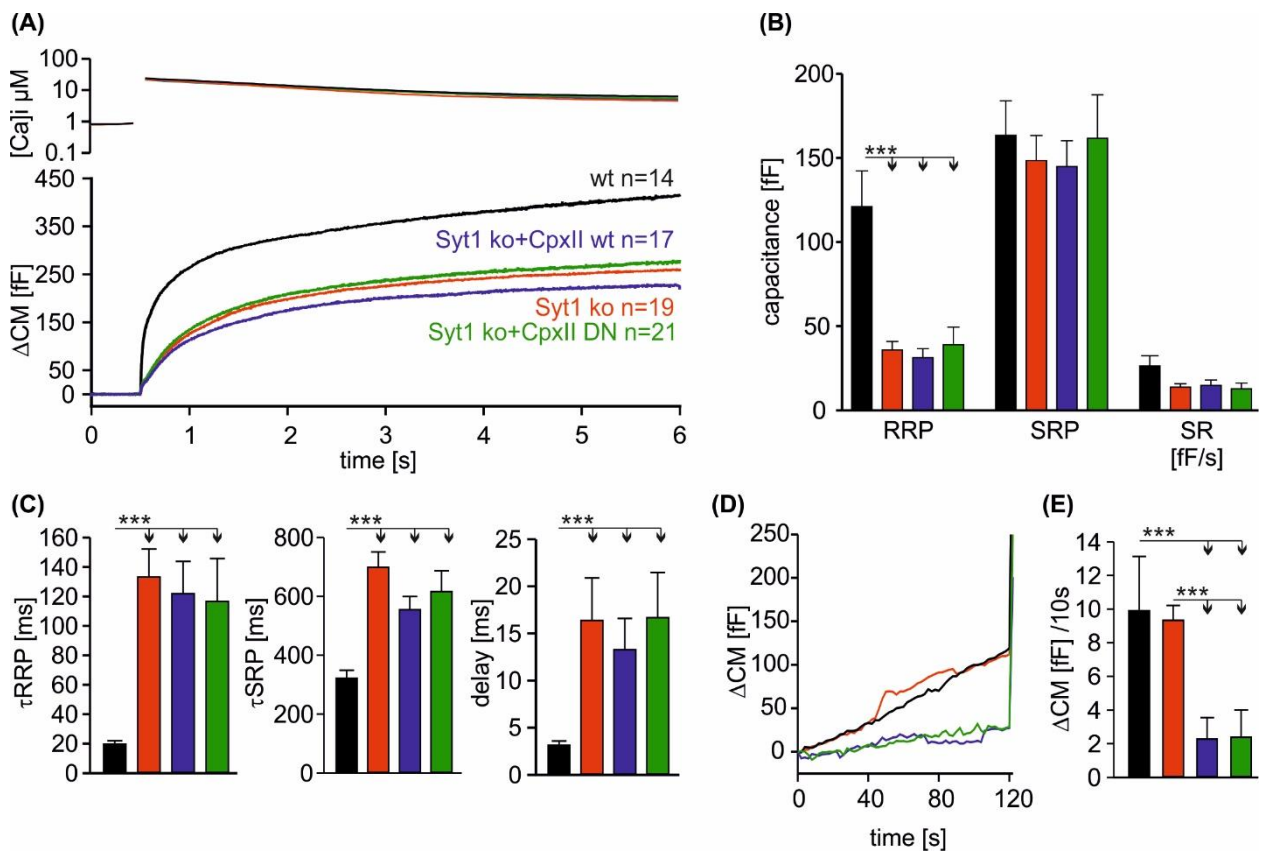


Figure 35. CpxII cooperates with Syt1 to accelerate the synchronized exocytosis. (A) Mean $[Ca^{2+}]_i$ levels (top) and corresponding CM signals (bottom) of Syt1 ko cells ($n = 19$), Syt1 ko + CpxII wt ($n = 17$), and those expressing CpxII DN ($n = 21$), and the wt ($n = 14$). (B) Amplitudes of RRP and SRP, the rate of sustained release (SR; femtofarad/second) determined for Syt1 ko (red), Syt1 ko + CpxII wt (dark blue), Syt1 ko + CpxII Δ N (green), wt (black) with strong reduction of the RRP in the Syt1 ko as well as the Syt1 ko expressing either CpxII or Cpx DN compared to the wt. (C) The time constants for the EB components (τ_{RRP} and τ_{SRP}), and the exocytotic delay showing a clear slowing down by knocking out Syt1. (D) Mean tonic CM traces of the cells shown in (A) before the triggering flash. (E) The rate of tonic exocytosis (determined at similar $[Ca^{2+}]_i$: in nM, Syt1 ko: 756 ± 43 ; Syt1 ko + CpxII wt: 791 ± 80 ; Syt1 ko + CpxII Δ N: 788 ± 108 ; wt: 795 ± 144) is significantly reduced with CpxII Δ N expression. ANOVA followed by Tukey-Kramer post-hoc test. * $p < 0.05$; ** $p < 0.01$; *** $p < 0.001$. Bars indicate mean \pm SEM.

clamps premature vesicle fusion independently of Syt1, but the size of the fast phase of secretion depends on the cooperation of both regulatory proteins CpxII and Syt1.

Overall, the results provide strong evidence that the Syt1 and CpxII cooperate in regulating the timing and the size of the synchronous secretion. They furthermore indicate that CpxII hinders premature vesicle fusion independent of the calcium sensors Syt1 and Syt7.

5.5.3 CpxII modulates Syt1 triggered exocytosis via its NTD

Encouraged by the finding that CpxII and Syt1 act in functionally interdependent fashion to facilitate the synchronous fusion, we aimed to investigate possible, underlying mechanism by

which the CpxII NTD enhances the speed of fusion mediated by Syt1. Based on previous studies, mutations in Syt1 C2A calcium binding domain have changed the behavior of Syt1 interactions with lipid membranes or with the SNAREs, causing alterations in the kinetics of synchronized fusion (Sorensen et al., 2003; Pang et al., 2006). Taking advantage of these mutations in Syt1's C2A domain, we set to investigate if the CpxII NTD determines the kinetics of synchronous fusion by altering the function of the C2A domain. R233Q is a point mutation in the C2A Ca^{2+} binding domain of Syt1 that decreases its affinity for lipid membranes (Li et al., 2006), and causes a twofold decrease in the Ca^{2+} affinity of the synchronous release. Previous recordings in Syt1 R233Q knock in chromaffin cells showed an enlarged EB and slower secretion rates when compared with wt cells (Sorensen et al., 2003). While the latter is consistent with decreased Ca^{2+} -affinity of the

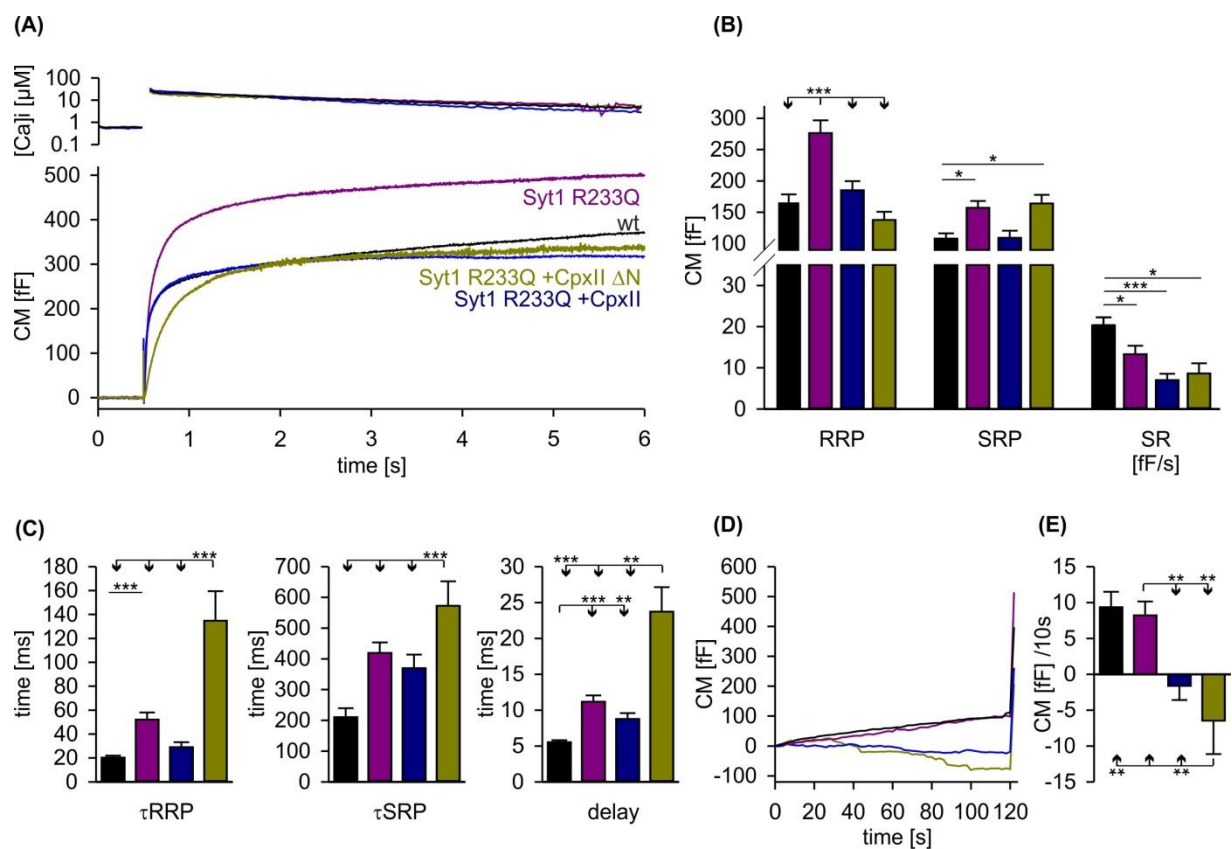


Figure 36. CpxII wt rescues the slow release kinetics of Syt1 R233Q while the CpxII Δ N mutant further aggravates it. (A) Mean $[\text{Ca}^{2+}]_i$ levels (top) and corresponding CM signals (bottom) of Syt1 R233Q cells ($n = 40$) and those expressing CpxII ($n = 25$), the mutant CpxII Δ N ($n = 11$) and the wt ($n = 42$). (B) Amplitudes of RRP and SRP, the rate of sustained release (SR; femtofarad/second) determined for Syt1 R233Q (violet), Syt1 R233Q + CpxII (blue), Syt1 R233Q + CpxII Δ N (dark yellow), wt (black) with a reduced EB with either form of Cpx is expressed in the Syt1 R233Q knock-in cells. (C) The time constants for the EB components (τ_{RRP} and τ_{SRP}), and the exocytotic delay. (D) Mean tonic CM traces of the cells shown in (A) before the triggering flash. (E) The rate of tonic exocytosis (determined at similar $[\text{Ca}^{2+}]_i$: in nM, Syt1 R233Q:623 \pm 31; Syt1 R233Q + CpxII:569 \pm 28; Syt1 R233Q + CpxII Δ N:600 \pm 26; wt: 582 \pm 22) is significantly reduced with CpxII and CpxII Δ N equally. ANOVA followed by Tukey-Kramer post-hoc test. * $p < 0.05$; ** $p < 0.01$; *** $p < 0.001$. Bars indicate mean \pm SEM.

mutant protein, the molecular mechanism for the EB increase remained enigmatic. We also found that Syt1 R233Q knock in chromaffin cells showed an increased EB size and exhibited a prolonged secretory delay as well as slower release kinetics, when compared with wt cells (Figure 36). These phenotypical consequences by the Syt1 R233Q mutation on synchronized fusion are remarkably similar to those by caused by the truncation of CpxII DN mutant in chromaffin cells (Dhara et al., 2014), raising the question of whether the N-terminal truncation of CpxII may affect Syt1 function in a similar way as the R233Q mutation. To test this hypothesis, we expressed CpxII Δ N in Syt1 R233Q knock in chromaffin cells and found that the mutant protein significantly increased the time constants of RRP and SRP fusion as well as the stimulus-secretion delay, as observed previously in wt cells (Figure 36 C, compare Dhara et al., 2014). In contrast, expression of the CpxII wt protein,

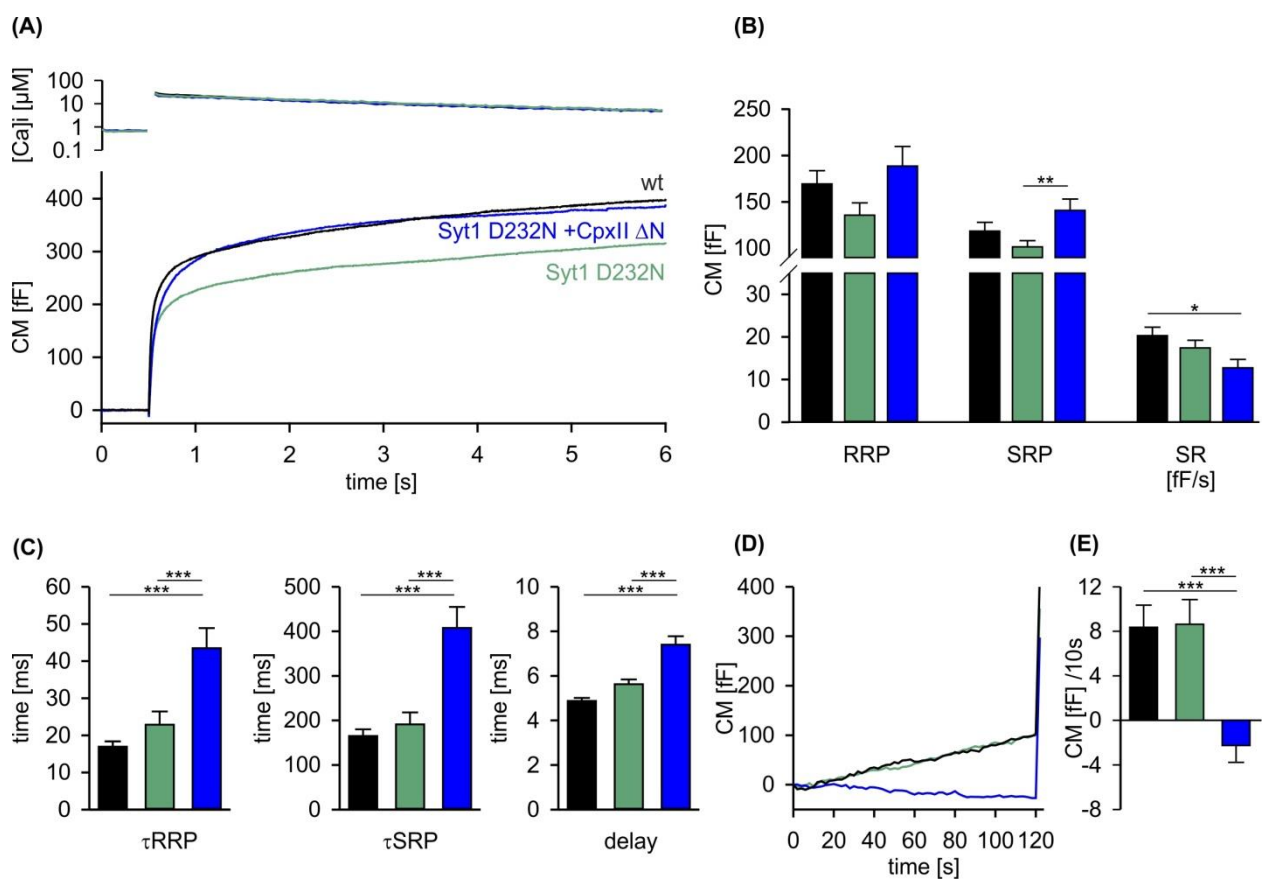


Figure 37. CpxII Δ N decelerates the release kinetics of Syt1 D232N triggered secretion. (A) Mean $[Ca^{2+}]_i$ levels (top) and corresponding CM signals (bottom) of Syt1 D232N cells (n = 22) and those expressing CpxII Δ N (n = 25), and the wt (n = 29). (B) Amplitudes of RRP and SRP, the rate of sustained release (SR; femtofarad/second) determined for Syt1 D232N (light green), Syt1 D232N + CpxII Δ N (blue), and wt (black) with reduced SRP and SR in the Syt1 D232N knock in. (C) The time constants for the EB components (τ_{RRP} and τ_{SRP}), and the exocytotic delay. (D) Mean tonic CM traces of the cells shown in (A) before the triggering flash. (E) The rate of tonic exocytosis (determined at similar $[Ca^{2+}]_i$: in nM, Syt1 D232N: 616 \pm 26; Syt1 D232N + CpxII Δ N: 647 \pm 34; wt: 637 \pm 24). ANOVA followed by Tukey-Kramer post-hoc test. *p<0.05; **p<0.01; ***p<0.001. Bars indicate mean \pm SEM.

at least in part, was able to compensate for the functional deficits seen with the R233Q-mutation (Figure 36 C), confirming the functional interdependence of Syt1 and CpxII in exocytosis timing. Furthermore, Syt1 R233Q cells showed normal asynchronous fusion similar to wt cells and expression of either CpxII wt or CpxII DN efficiently and equally clamped premature release in both cell types (Figure 36 D, E). Taken together, the results show that loss of CpxII NTD in the Syt1 R233Q further aggravates the slow fusion kinetics of the synchronous release whereas a surplus of CpxII wt protein restores the secretion kinetics to the level of wt cells. Particularly the ability of the CpxII to compensate for some of the functional deficits by the Syt1 mutant provides evidence that both proteins cooperate in the regulation of stimulus secretion coupling.

While the Syt1 R233Q mutation has been implicated in altered protein-lipid interactions, another gain-of-function mutation, the Syt1 D232N, was proposed to increase Syt1-SNARE interaction and thus enhances synchronous vesicle fusion in cortical neurons (Pang et al., 2006). In contrast to the observation in neurons, Syt1 D232N cells showed a similar EB size like in wt chromaffin cells (Figure 37 A, B). Additionally, no changes in the secretion kinetics could be observed (Figure 37 C). CpxII Δ N expression boosted the magnitude of the synchronous EB (Figure 37 A, B) and slowed down fusion kinetics to the same degree as observed previously in wt cells (Figure 37 C, compare with Dhara et al., 2014). Furthermore, CpxII Δ N strongly suppressed the asynchronous release from Syt1 D232N cells at sub-micromolar Ca^{2+} concentrations (Figure 37 D, E).

Taken together, changes in the SNARE binding affinity by the Syt1 D232N mutation, as previously observed in biochemical experiments (Pang et al., 2016) do not result in systematic alterations of the stimulus-secretion coupling in chromaffin cells and do not compensate for the slowed fusion kinetics seen with the CpxII DN mutation. Overall, it seems safe to conclude that at least for some Syt1 mutations (i. e. R233Q) a functional crosstalk between CpxII and Syt1 can be demonstrated.

5.5.4 Complexin mutants are expressed to similar levels in chromaffin cells

Variations in gene expression levels can lead to significant phenotypical changes in biological systems, which might be resulting from evolutionary development that is important for the adaptation of the species to its environment (Dekel et al., 2005; Khaitovich et al., 2006; Lopez-Maury et al., 2008). In order to test whether variable expression levels of the studied proteins can be held responsible for their different phenotypes, we expressed CpxII and its mutants in CpxII ko cells and assessed their expression level using immunocytochemistry in comparison to endogenous CpxII wt levels and to signals of CpxII ko cells. CpxII ko cells showed a faint fluorescent

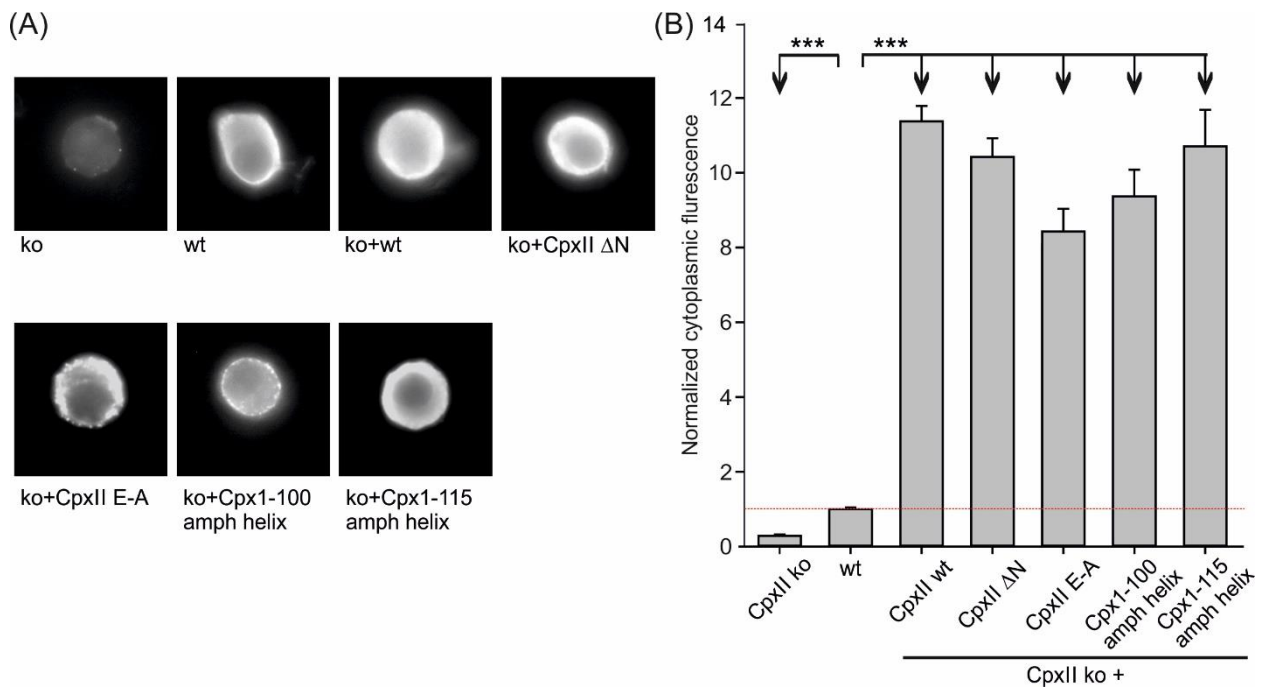


Figure 38. Expression levels of CpxII and its mutants in chromaffin cells. (A) Exemplary images of a wt, CpxII ko and CpxII ko cells overexpressing either CpxII or the CpxII mutants. Immune signals are detected with a polyclonal CpxII antibody (epitope Cpx1-100). Signals are visualized with adjusted exposure times (Cpx ko 2s; wt, 300 ms; CpxII ko +CpxII and mutants 30 ms). **(B)** Mean total fluorescence intensity of wt and CpxII ko cells expressing CpxII or the indicated mutants (determined 5.5 hr after transfection) and normalized to that of wt indicated by the red horizontal line. The mutant variants do not differ from the rescue CpxII wt regarding the level of protein expression (wt, n = 77; CpxII ko, n = 32; CpxII wt n = 35; CpxII DN, n = 52; CpxII E/A, n = 27; Cpx1-100 amph helix, n = 22; Cpx1-115 amph helix, n = 24) Error bars indicate mean \pm SEM. ANOVA followed by Tukey-Kramer post-hoc test. ***p < 0.001.

signal only with very long exposure time (2 s), while the wt cells had a very clear signal already at much lower exposure times (300 ms), which shows the specificity of the primary and the secondary antibodies used for this experiment (Figure 38 A).

In contrast, the cells expressing CpxII and its mutants had to be imaged with an exposure time of 30 ms to avoid pixel saturation of the detector (Figure 38 A). Quantification of fluorescence intensities after correction for the different exposure times showed similar expression levels for the proteins, indicating that structural differences (rather than different expression levels) can be held responsible for the functional properties of the CpxII variants. Furthermore, viral expression of CpxII and its variants produced 8 to 12 times higher protein levels than observed for endogenous CpxII (Figure 38 B). Similar results were obtained for the Cpx1-100; Cpx1-100LC; Cpx1-115; Cpx1-115SC; Cpx1-100helix; Cpx1-115helix; and Cpx1-100 CSP α mutants, which have already been published (Makke et al., 2018).

5.6 Synaptobrevin 2 TMD

The cytosolic domains of SNAREs zipper into a pin generating the force needed for vesicle fusion with the plasma membrane (Sudhof et al., 2009; Jahn et al., 2012). Yet, the importance of the SNARE-lipid interplay for membrane fusion has remained a point of debate. In particular the question the TMD of vesicular SNARE proteins has function that go beyond simple anchoring of the SNARE pin to the membrane has remained unclear (for review see Dhara et al., 2018)). For example, previous studies showed that replacing Syb TMDs with a lipid anchor mediated efficient in-vitro liposome content mixing (Xu et al., 2011), and supported vesicle exocytosis in neurons (Zhou et al., 2013). Nevertheless, the latter studies are difficult to reconcile with previous reports showing that lipid anchored Syb failed to promote liposome-liposome fusion (McNew et al., 2000) or that even slight modifications in the length of Syb2 TMD abolished secretion from PC 12 cells (Fdez et al., 2010). Structural studies indeed suggested that zipping of the SNAREs propagates into the Syb TMDs (Li et al., 2007; Shi et al., 2012). *In vitro* vesicle fusion assays implicated continuous helical assembly of the TMDs as an important step for perturbing lipid membranes to initiate lipid mixing (Bao et al., 2016), and fusion pore expansion (Li et al., 2007; Stein et al., 2009). Interestingly, SNARE TMDs are characterized by an overrepresentation of β branched amino acids (38%), like isoleucine and valine residues (Neumann et al., 2011). The high content of β branched amino acids introduces conformational plasticity and flexibility to the TMDs (Stelzer et al., 2008; Quint et al., 2010; Han et al., 2016) that may be important for catalyzing membrane fusion (Langosch et al., 2001). *In vitro* experiments provided evidence that flexible TMD peptides with similar content of β branched amino acids to that SNARE TMDs enhanced fusion in liposome assays (Langosch et al., 2001; Hofmann et al., 2006). However, these experiments did not track the influence TMDs on synchronized Ca^{2+} -triggered vesicle exocytosis, nor the critical properties of the TMDs essential for the fusion process.

5.6.1 The flexibility of the SybII TMD is essential for efficient membrane fusion

One of the first clues that the vesicular SNARE TMD plays an important role in secretion was the observation that exchange of the TMD with a lipophilic anchor abolished secretion in yeast (Grote et al., 2000). To test whether the flexibility of the SybII TMD is important in Ca^{2+} -triggered exocytosis of chromaffin cells, we substituted its core residues (amino acid positions 97-112) to helix-stabilizing leucines (Dhara et al., 2016). The results showed that such a mutant protein failed to restore exocytosis in v-SNARE deficient chromaffin cells unlike the wt protein. Specifically, the exchange in the N terminal half of the TMD (PolyL-NT) similarly diminished EB like the full exchange

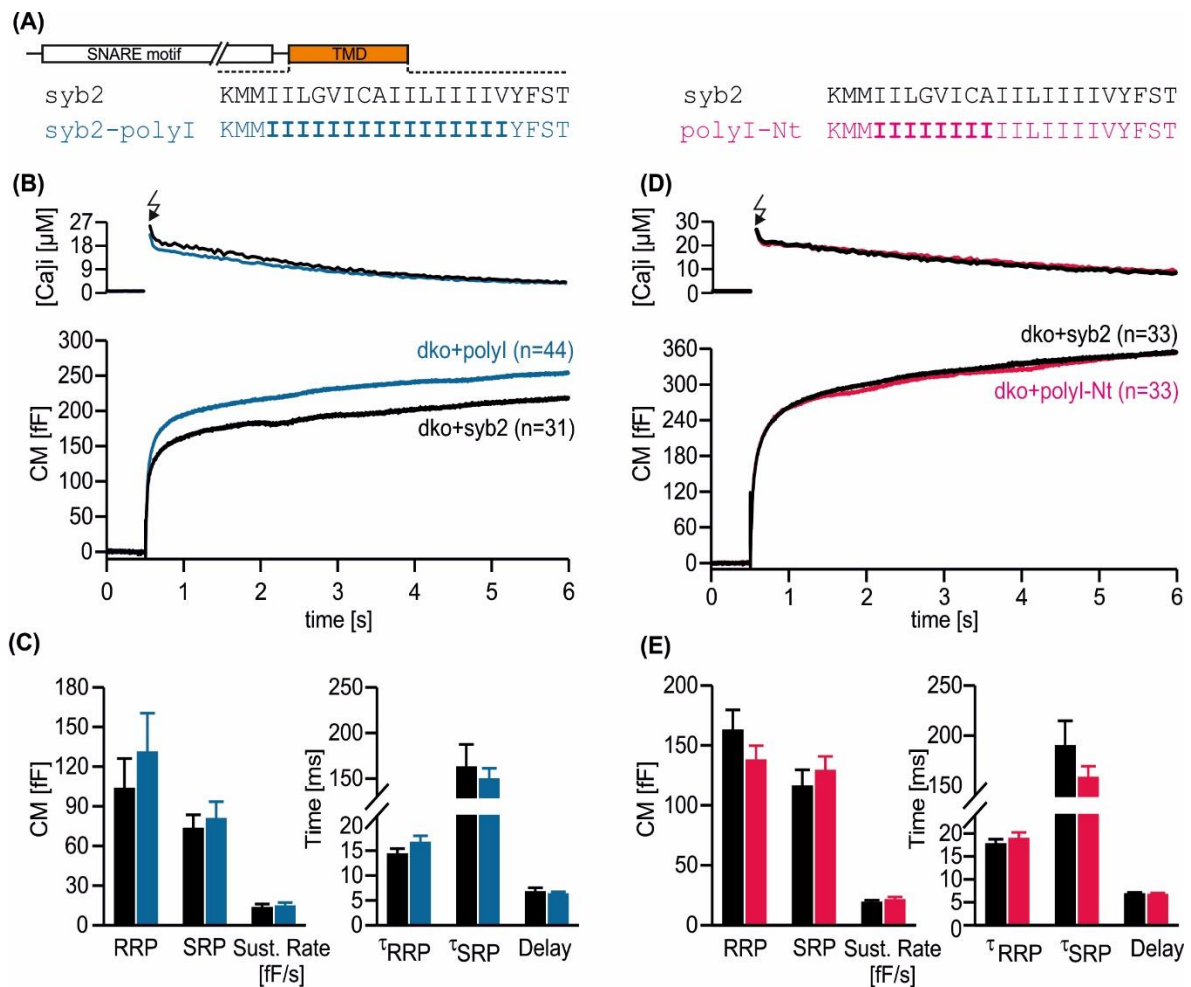


Figure 39. A flexible helix SybII TMD supports undiminished secretion. **(A)** Schematic representation of SybII and corresponding TMD mutants (polyI, polyI-Nt). **(B, D)** Mean flash-induced [Ca²⁺]_i levels (top panels) and corresponding CM responses (middle panels) of dko cells expressing SybII wt, polyL, polyI or polyI-Nt mutants. Substitutions of the TMD core residues or the TMD Nt with isoleucine fully restored exocytosis (bottom panels). **(C, E)** The kinetics of release τ_{RRP} , τ_{SRP} , and the secretory delay are unchanged for all mutants. Arrow indicates flash. Bars represent mean \pm SEM and number of cells is indicated within brackets.

of the TMD with leucine residues (PolyL) (Dhara et al., 2016). To further characterize the importance of flexible TMDs for fusion, we reintroduced flexibility by exchanging either all core residues within the SybII TMD or only its N-terminal half with β branched isoleucine residues, referred to as Syb II polyI and SybII polyINt, respectively (Figure 39 A). SybII polyI fully restored synchronized exocytosis from SybII/Ceb double knockout cells (Figure 39 B). Furthermore, it fully rescued the release kinetics like SybII wt (Figure 39 C). Likewise, exchanging only the TMD region spanning the outer leaflet of the vesicle membrane with isoleucines (SybII polyI-Nt) (Figure 39 A pink) supported full secretion and rescued the kinetics of synchronized fusion to wt levels (Figure 39 D, E). These results allow for several important conclusions: First, they demonstrate that not hydrophobicity but rather structural flexibility of the v-SNARE TMD is crucial for promoting

efficient fusion. In this context, it is important to note that molecular dynamics simulations of the SybII TMD (residues 71-116) and its mutant variants (embedded in an asymmetric membrane containing a physiological lipid composition) confirmed the different TMD backbone dynamics of poly L and the poly V mutant (Dhara et al., 2016). Second, it renders the possibility unlikely that membrane fusion depends on certain key residues at specific positions within the SybII TMD. Overall, these results together with additional experiments, presented in Dhara et al., 2016, favor the view that backbone flexibility of SybII TMD is a crucial characteristic for catalyzing membrane fusion and mediating efficient exocytosis

5.6.2 The highly conserved G100 amino acid in the SybII TMD is not critical for fusion catalysis

Molecular dynamics simulations suggested the presence of a structural pivot at the amino acid G100 in SybII TMD which resides about in the middle of the vesicle membrane (Blanchard et al., 2014). The G100 amino acid is highly conserved in TMDs throughout the animal kingdom. Its

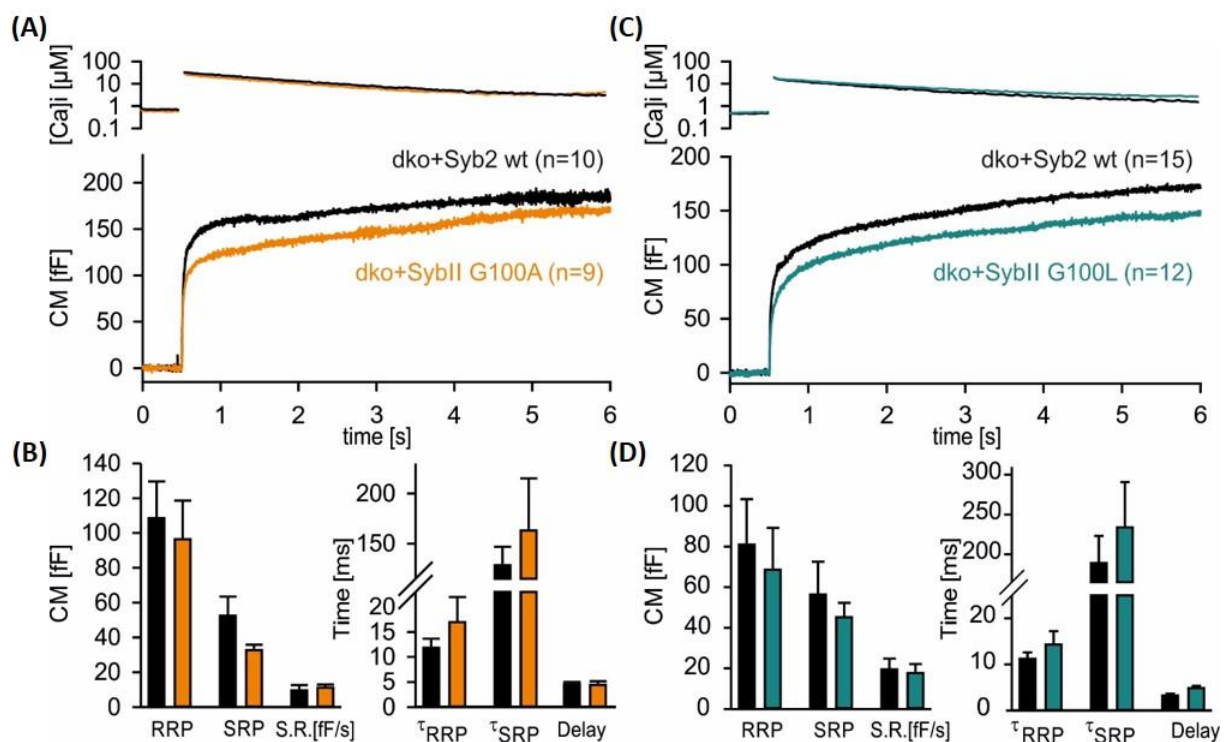


Figure 40. The amino acid G100 is not a crucial amino acid for the function of SybII-TMD in membrane fusion. (A, C) Mean flash-induced $[Ca^{2+}]_i$ levels (top panels) showing similar calcium levels, and the corresponding CM responses (middle panels) of dko cells expressing SybII or G100A (orange) or G100L (dark green) mutants. Mutations in the G100 amino acid does not hinder fusion initiation and facilitation by the SybII TMD in the (bottom panels). Numbers of cells analyzed are indicated within the brackets. (B, D) Magnitudes of RRP and SRP and kinetics of release are unchanged for the mutant proteins compared to SybII wt.

substitution has been reported to reduce secretion from PC12 cells evoked by high potassium depolarization (Hastoy et al., 2017). Furthermore, it may play a role in membrane fusion by mediating the homo and hetero-dimerization of SybII (Margittai et al., 1999; Laage et al., 2000; Fleming et al., 2001; Tong et al., 2009). Conversely, our experiments, exchanging the SybII TMD residues including the G100 with isoleucines, fully restored the fusion capacity from dKO cells similarly to the SybII wt protein (Figure 39). However, it is possible that the overall increase in TMD flexibility by the polyI mutation has masked fusion deficiencies that may result from the exchange of the G100 to an isoleucine. To study the role of the G100 amino acid in synchronized fusion, we substituted it with an alanine (G100A) that is supposed to preserve the dimerization of SybII by the TMD (Citation) but hinders structural kinking of the TMD (Citation). In a second mutant protein, we exchange the G100 with a leucine residue (G100L) to promote enhanced structural rigidity (i. e. helicity) in this TMD region. SybII G100A fully rescued the EB in SybII/Cellubrevin dko chromaffin (Figure 40 A, B). Moreover, no reduction in the kinetics of release was observed compared to the wt rescue (Figure 40 B). Similarly, SybII G100L also supported a full-sized EB (Figure 40 C, D) and reinstated fusion kinetics similar to SybII expressing cells (Figure 40 D).

Taken together this data set shows that neither structural kinking of TMD is not crucial for catalyzing secretion in chromaffin cells. Thus, the contribution of the conserved G100 amino acid to the mechanism of Syb2 TMD in mediating membrane fusion is minuscule.

5.6.3 The rigid SybII PolyL traps secretory vesicles in a non-fusogenic state

To understand how SybII polyL mutant reduced exocytosis of chromaffin granules, we used electron microscopy to resolve possible morphological defects. For this, dKO chromaffin cells were infected with either Syb2 wt or Syb2 polyL. To induce fusion before chemical fixation chromaffin cells were depolarized twice with KCl for 30 seconds each. The high-resolution images obtained from 70 μm thin slices (Figure 41 A) show no changes in the average vesicle diameter between SybII wt and SybII polyL (Figure 41 D). Thereby, the reduced capacitance increase in SybII polyL is not a result of the fusion of smaller sized vesicles (Dhara et al 2016). However, the mutant SybII PolyL showed a significant high accumulation of vesicles in a close proximity to the plasma membrane (Figure 41 B, C) indicating that the vesicle priming is not affected by the SybII Poly L mutation. On the other hand, less frequent vesicle occurrence at the plasma membrane by wt SybII was observed, reflecting that those primed vesicles were able to undergo fusion upon stimulation (Figure 41 B, C). In contrast, SybII/Ceb dKo cells have no accumulation of vesicles proximal to the plasma membrane even though they are devoid of any exocytosis (Borisovska et

al., 2005). This finding is in line with the previous work from our lab reporting that double v-SNARE deficiency (SybII/Ceb) leads to depriming of secretory vesicles (Borisovska et al., 2005).

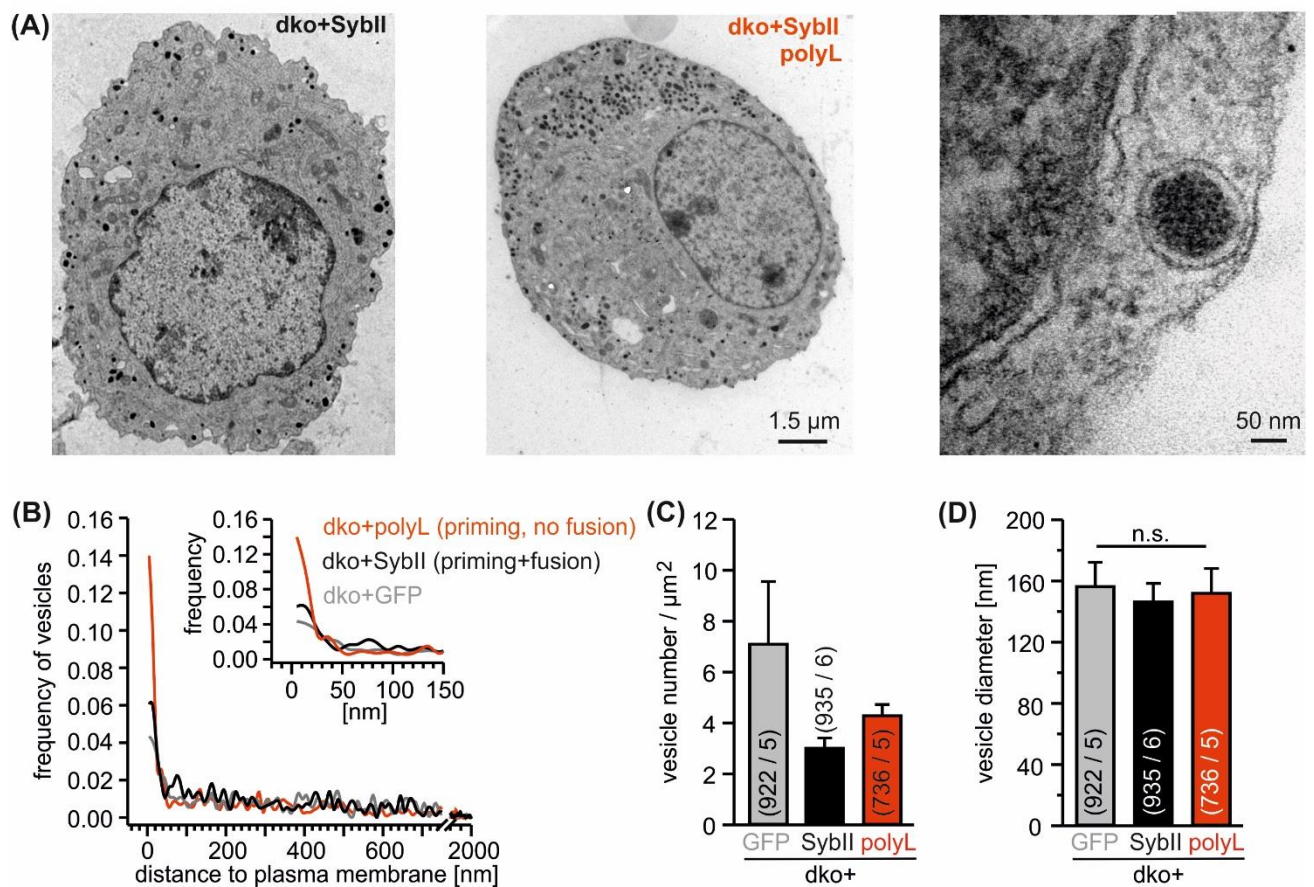


Figure 41. Ultrastructural analysis of stimulated dko chromaffin cells expressing SybII wt vs SybII polyL. (A) Exemplary electron micrographs of SybII/Ceb dKO cells expressing SybII wt or the SybII polyL mutant, and a representation of the vesicle considered to be in contact with the cell membrane. (B) Subcellular distribution (bin width 20 nm) of vesicles with respect to the distance from the plasma membrane of dko cells expressing SybII wt (black) SybII Poly L (red), or GFP (gray) as control for viral infection. The dko cells show reduced vesicle accumulation near the plasma membrane despite their inability to fuse, the SybII shows more vesicles than the dko in the primed state, which is indicative for the balance of vesicle priming and fusion. And the mutant SybII polyL showing double concentration of vesicles in the close proximity than the wt SybII pointing to the possibility that the primed vesicles are unable to fuse. (C) Vesicle diameter and morphology is unchanged in the SybII/Ceb deficient cells, and those expressing either SybII wt or the mutant SybII poly L.

Taken together this data shows that making the SybII TMD more rigid traps the vesicles near the plasma membrane in a non-fusing state, and confirms that structural flexibility of the SybII TMD is a crucial determinant for fusion initiation.

6 Discussion

6.1 Complexin clamps fusion with its CTD

The control of complexin over the exocytosis machinery enables sophisticated and precise timing of vesicular fusion. Cpx plays a dual role in regulating exocytosis, on one hand it inhibits the premature release of vesicles and on the other hand facilitates synchronized fusion upon calcium stimulation (for review see Mohrmann et al., 2015)). Structure-function analysis of CpxII in chromaffin cells by our group showed that Cpx's dual role is carried out by the distinct functional domains at either end of the CpxII protein (Dhara et al., 2014). Specifically, the C terminal domain of CpxII (amino acid 72-134) was found to clamp premature vesicle fusion to increase the size of the primed vesicle pool (Dhara et al., 2014). On the other hand, the N terminal domain of CpxII facilitates the synchronized fusion and reduces the latency of the stimulus-secretion coupling (Dhara et al., 2014).

In contrast, *in vitro* flipped SNARE cell fusion assays have proposed that the accessory α helix together with the central α helix (amino acids 26-83) is the minimal clamping domain for exocytosis in murine complexin (Giraudo et al., 2006; Giraudo et al., 2008). Further mutational analysis showed that making the accessory helix more SybII mimetic enhanced Cpx's clamp efficiency, while a diverging sequence from SybII reduced its efficacy which suggested that CpxII with its accessory helix would compete with SybII for interacting with the cognate t-SNAREs to inhibit fusion (Giraudo et al., 2009). Other knock down of both Cpx isoforms I, and II experiments in cortical neurons also supported the role of the accessory helix in hindering fusion, but provided different mechanisms for clamping fusion by blocking a secondary calcium sensor for fusion (Yang et al., 2010; but see Neher 2010). Alternative NMR an exocytosis analysis of the SybII mimetic mutants in Cpx I, II, III triple knockout neurons suggested an alternative mechanism for fusion clamp by the accessory α by helix increasing the electrostatic and steric hindrance between the opposing membranes (Trimbruch et al., 2014). Furthermore, FRET assays showed that Cpx bound with its central helix to a partially assembled SNARE complex bridges with its accessory helix to a neighboring complex thereby blocking the vacant SybII site in an overall zig-zag arrangement of linked SNARE complexes (Kummel et al., 2011). Yet, the accessory helix could be functionally replaced by an unrelated artificial helix indicating that it contributes to nucleation and stability of the central α helix (Radoff et al., 2014). The mild functional effects of mutating the accessory helix (compare Yang et al., 2010 and Trimbruch et al., 2014) and the opposing interpretations of the

underlying mechanisms in clamping exocytosis gave way to the possibility that other domains in Cpx could contribute to the clamp activity of the protein. Indeed, experiments in various secretory model systems provided evidence that the C-terminal domain of complexin is the relevant domain for unfettered suppression of vesicle fusion (Martin et al., 2011; Kaeser-Woo et al., 2012; Buhl et al., 2013; Dhara et al., 2014).

Previous studies have considered the C terminal domain of Cpx to be functionally inert (Xue et al., 2007) Experiments in *Drosophila*, instead, have assigned this domain an indirect role in clamping fusion, wherein it tethers, by binding with its amphipathic helix to vesicular membranes, other inhibitory domains of the protein to the site of fusion (Wragg et al., 2013; Snead et al., 2014; Gong et al., 2016). Yet, subsequent studies by the same group have shown that membrane association of the Cpx CTD is important but not sufficient to explain Cpx inhibitory effects (Wragg et al., 2017). Our experiments in chromaffin cells provide several lines of evidence that clearly counter the ‘tethering’ hypothesis of being relevant for exocytosis clamping.

First, we show that the truncation of the CTD (Cpx 1-100), upregulates asynchronous release in wt chromaffin cells to the level of CpxII KO (Figure 16, 17), and thereby reduces the magnitude of synchronous exocytotic burst (Dhara et al., 2014). Thus, Cpx1-100 mutant still competes with the endogenous CpxII for the interaction with the SNARE proteins, but is unable to hinder premature vesicle fusion. Evidently, the last 34 amino acids of CpxII are instrumental in clamping secretion.

Second, the infusion of the isolated CTD peptide (10 μ M) into wt chromaffin cells significantly reduces asynchronous fusion and enhances the magnitude of the synchronous pool similar to the expression of CpxII (Figure 18, 19). Thus, the CTD binds directly to the exocytotic machinery and fusion inhibition by the CTD represents a rate-limiting step in exocytosis regulation.

Third, our complementation experiments (CpxII1-100 expressing together with CTD peptide infusion) (Figure 21, 22) demonstrate that the physically separated CTD and NTD of CpxII cooperate and complement each other in regulating exocytosis as a full functional entity. This again opposes the idea of the CTD serving as a targeting sequence and rather suggests that it plays an independent and direct inhibitory role within the fusion machinery.

Forth, exchanging the CTD with the cysteine rich region of CSP- α protein, which efficiently targets Cpx to vesicle membranes, completely fails to restore the inhibitory function of CpxII (Figure 23). The latter observation suggests that membrane binding of the CTD, if needed at all, should rather be reversibly than permanent.

Together, these observations strongly contradict the hypothesis that membrane targeting of CpxII by its CTD represents an essential step in exocytosis clamping. It rather supports the view that the CpxII CTD is instrumental in hindering premature fusion, most likely by arresting partially assembled SNAREs in a prefusion state. Clearly, binding of Cpx to vesicular membranes, as also observed in chromaffin cells, is expected increases its local concentration at the site of fusion.

6.1.1 CpxII CTD hinders zipping by competing with SybII for the interaction with the t-SNAREs to clamp asynchronous exocytosis

As an alternative model, we hypothesize that the CTD with its amphipathic helix hinders SNARE complex assembly. For that, the CTD may fold back and bind with the hydrophobic phase of the amphipathic helix to the membrane proximal region of the partially assembled SNARE complex hindering the zipping progression. Such a scenario is indeed supported by previous biochemical experiments showing that Cpx Cys 105 residue positions near the zero layer of the SNARE motif, placing the downstream region of the Cpx CTD in an optimal location to interact with the membrane proximal parts of the SNARE complex (Bowen et al., 2005).

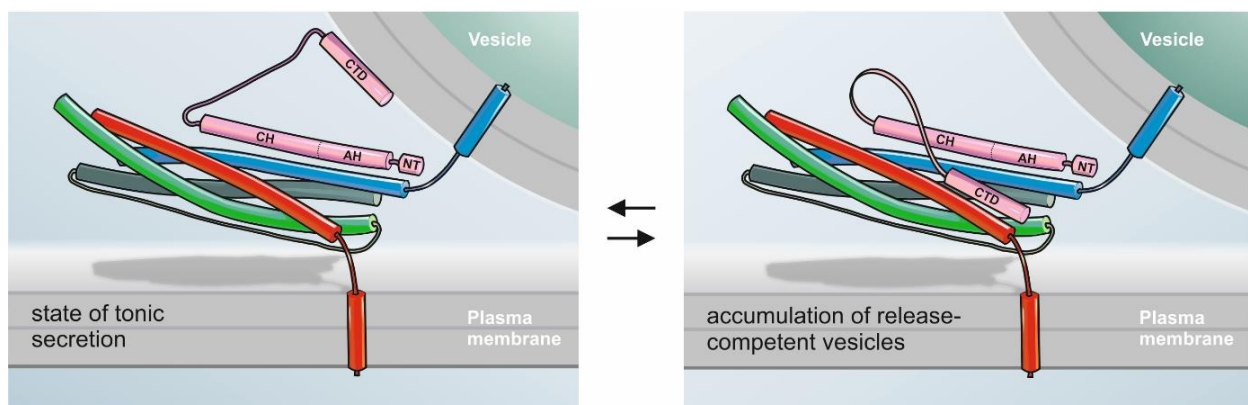


Figure 42. Proposed mechanism for complexin clamping by hindering SNARE complex zipping. Complexin (pink) interacts with high affinity with the partially assembled SNARE proteins SybII (blue), Syx 1a (red), SNAP 25 (green). The CTD interacts with the membranes Cpx does not inhibit tonic secretion, it rather concentrates complexin at the site of membrane fusion. Whereas a switch from membrane binding to the partially assembled SNARE complex, where the CTD folds back and may compete with the SNAP25 SN1 to hinder the further assembly of the SNARE pin permitting the buildup of a ready release vesicles before the Ca^{2+} -stimulus. Hindering the assembly of the SNARE machinery is requires the combined action of the Cpx CTD with the multiple domains of Cpx such as the previously proposed accessory helix, and works in cooperation with Syt1 for the efficient triggering of synchronous release, where the N terminus enhances fusion kinetic and the fusogenicity of vesicles during the Ca^{2+} trigger (Makke et al., 2018).

Furthermore, our co-precipitation assays with brain homogenate demonstrated that immobilized CpxII CTD interacts with the calcium sensor Syt1, and the SNARE proteins Syx1a, SNAP25 and traces

of Syb2 (Figure 25) (Makke et al., 2018). In following up on this, we also compared the protein sequences of the CpxII CTD with those of the SNARE proteins and found that the similarity between the Cpx CTD and the first SNARE motif of the SNAP25 SN1 (50% similarity) is the highest among the other SNARE motifs (Figure 27) (Makke et al., 2018). Therefore, the Cpx CTD with its amphipathic domain might serve as an alternative interaction interface, which competes with the SNAP25-SN1 in binding to the other SNARE motifs. In the same line, we found that the Cpx CTD but not its scrambled variant significantly lowers SNARE complex formation confirming that the Cpx CTD inhibits SNARE assembly to clamp exocytosis (Figure 26) (Makke et al., 2018). Our functional and biochemical results also agree with previous reports showing that full length complexin but not the central domain (aa 26-83) inhibits SNARE-mediated liposome fusion (Schaub et al., 2006; Chicka et al., 2009). To study whether the SNAP-25-SN1 domain and the CpxII CTD are functionally interchangeable, we have generated a chimera mutant, where the entire CTD of CpxII is replaced with the equivalent region of SNAP25-SN1 (amino acid positions 44 to 77). Indeed, expression of the CpxII-SNAP-25-SN1 chimera largely restored secretion in CpxII ko cells like wt CpxII. It almost completely inhibited asynchronous fusion and rescued magnitude as well as exocytosis timing of the synchronous secretion (Figure 28). A shorter chimera mutant, which replaces only the amphipathic region of the CTD with the amino acids 59 to 77 of SNAP25-SN1 fully restored secretion by arresting premature vesicle fusion and recovering the 'primed' vesicle pool (Figure 29). Thus, CpxII CTD competes with SybII for the interaction with the t-SNAREs to prevent the assembly of the SNARE complex and thus inhibit premature vesicle fusion.

To further investigate the structural determinants by which CpxII CTD clamps exocytosis, we exchanged the full CTD (amino acid position 100-134), or the last 19 amino acids within the CpxII CTD with an artificial unrelated helix (referred to as CpxII 1-100 helix and CpxII 1-115 helix). Both CpxII mutants failed to restore exocytosis like their equivalent truncated mutants (Figure 28, 29). Furthermore, replacing CpxII CTD with an unrelated amphipathic helix (CpxII 1-100 amph helix) not only failed to reinstate the clamp function of CpxII CTD, but also deteriorated the fusion facilitation by CpxII (Figure 31). This unexpected effect on fusion facilitation by a mutation in the CTD could result from exchanging non-helical structures within the CTD with helical ones, which might result in structural misfolding of the mutant Cpx. Yet, given the phenotypic similarities between the CpxII 1-100 amph helix mutant and the membrane-anchored Cpx1-100 Csp α expression in CpxII ko chromaffin cells, one could speculate that an overall increase in membrane binding causes the observed loss-of-function phenotype. In stark contrast, exchanging only the last 19 amino acids of the CpxII CTD with an artificial amphipathic helix (Cpx 116-134

amph helix) restored exocytosis like wt CpxII (Figure 32). Thus, the amphipathic character at the end of CpxII CTD is crucial for clamping exocytosis by CpxII. We propose that membrane binding by CpxII CTD is not essential for clamping premature vesicle release; it is rather used by complexin to concentrate at the fusion site. The later equilibrium between membrane bound (unclamped SNAREs) and SNARE bound (clamped SNAREs) Cpx state determines the degree of fusion clamp (Figure 42).

The CTD of CpxII is further characterized by a cluster of acidic amino acids (E¹⁰⁸-E¹¹⁴), which was previously shown to promote an interaction with Syt1, serving as the calcium sensor for fast exocytosis (Tokumaru et al., 2008). Exchanging the glutamate cluster to alanines did not reduce the clamping efficiency of the protein, but caused a substantial reduction in the magnitude and kinetics of synchronous secretion (Figure 33). The reduced efficiency in triggering synchronized release could be a consequence of a weakened interaction with, or an impaired recruitment of Syt1, which may affect Syt1's efficiency to trigger exocytosis. Overall, we show that two distinct domains in the CTD of CpxII act in synergy to drive synchronous secretion in chromaffin cells. While the amphipathic helix arrests assembly of SNARE complex and thereby allows for the build-up of a primed vesicle pool, the poly-glutamate cluster presumably helps in lifting the clamp by Syt1 resulting in faster fusion upon the calcium trigger.

Given that SNAP-25 peptides have previously been reported to inhibit secretion in chromaffin cells, one might question the specificity of CTD effect in hindering fusion (Gutierrez et al., 1995; Gutierrez et al., 1997; Ferrer-Montiel et al., 1998; Aplan et al., 1999). Importantly, infusion of the CTD peptide not only suppresses tonic release but also enhances the fast synchronous release producing a true gain of function phenotype. It is notable that other chimeric forms of Cpx previously failed to recover the protein's functional capabilities. For instance, a chimera of CpxI and CpxIII did not suppress spontaneous release in murine cortical neurons (Kaeser-Woo et al., 2012) which could be due to lack of periodicity of the hydrophobic residues within the CpxIII CTD. Similarly, one might speculate that chimeras of *C. elegans* CpxI and III failed to clamp secretion, because the periodicity of the hydrophobic amino acids is not preserved within the CpxIII CTD (Wragg et al., 2017).

We note that the infusion of CpxII CTD peptide in CpxII ko cells does not inhibit premature vesicle fusion (Figure 18, 20), suggesting that the CTD requires other domains of Cpx to inhibit fusion. In contrast, the CTD peptide enhances fusion clamping in wt chromaffin cells. Yet, the latter result raises the question of how the CTD peptide is able to enhance the fusion clamp despite the

presence of the endogenous CpxII. Taking a maximum of 12 SNAREs in a hemispherical volume around the fusion pore neck (Montecucco et al., 2005), and assuming that each SNARE complex is equipped with 1 Cpx molecule renders an estimate for the local Cpx concentration of about 4.7 μM . Since the concentration of the infused peptide (10 μM) clearly exceeds this estimate, it is conceivable that additional CpxII CTD may boost the proteins clamp activity. In the same line, the CpxII CTD (Cys 105) produced broad FRET peaks with Syx1a (Ser 249) near the central ionic layer of the SNARE complex (Bowen et al., 2005), which are indicative for conformational changes and only transient SNARE-CpxII-CTD interactions. Thus, increasing the local concentration of CpxII CTD by peptide infusion may increase its frequent interactions with the SNAREs, thereby enhancing fusion inhibition.

Collectively, the combined set of data comprising high-resolution electrophysiological recordings together with in-vitro biochemical assays, provide strong evidence for a so far unrecognized mechanism, where the CpxII CTD utilizes the amphipathic helix at its very C terminal end as a wedge to hinder SNARE complex zippering, thus preventing premature release (Figure 42). Due to its similarity with SNAP25, the Cpx CTD may out-compete the SNARE motif SNAP25 SN1 generating an alternative acceptor complex that is expected to hinder fusion.

6.2 CpxII NTD cooperates with Syt1 to facilitate synchronized vesicle fusion

Previous biochemical experiments have suggested that Cpx's inhibitory activity is countered by SytI binding to the SNARE complex leading to Cpx unbinding and exocytosis (Tang et al., 2006). Yet, this 'Syt/Cpx-switch model' was challenged by subsequent observations showing that Cpx and SytI can bind simultaneously to SNARE-complexes (Chicka and Chapman, 2009; Xu et al., 2013). As outlined above, we present in this thesis evidence that CpxII hinders premature secretion with its very CTD and that Syt1 binding to upstream regions of CpxII (i.e. Glutamate cluster) opposes the clamp action of the protein. Evidently, these observations are consistent with the Syt/Cpx-switch model and, in addition, point to the possibility that CpxII and Syt1 can simultaneously interact with the SNAREs to regulate their activity. Still, the absence of CpxII not only unclamped premature exocytosis, but also slowed down stimulus secretion coupling, an observation that was due to the absence of the NTD of CpxII (aa 1-28), (Dhara et al., 2014). The observation that both deficits imposed by the loss of CpxII can be functionally uncoupled is further corroborated by the fact that our C-terminal truncation mutants Cpx 1-100, and Cpx 1-115 showed a significant decrease in the magnitude of the synchronous release without changing the timing and kinetics of secretion.

Furthermore, studies by Dhara et al. (2014) showed that loss of the NTD changes the Ca^{2+} -affinity of the RRP secretion rate but rescued the full clamping activity of the protein. A similarly reduced Ca^{2+} sensitivity for evoked release has been previously observed in autaptic cultures of hippocampal neurons. (Xue et al., 2007; Xu et al., 2009; Dhara et al., 2014). The kinetics of the synchronous release are expected to depend on the stimulus strength and the kinetics of Ca^{2+} binding to the calcium sensors for exocytosis (Voets 2000; Schneggenburger et al., 2005). Since Cpx II has no calcium-binding site, it raises the question of whether it is able to adapt Syt1 and thereby speeds up synchronous release upon calcium elevation via its N terminal domain. Interestingly, the deletion of CpxII NTD (amino acids 1-27) produced a suspiciously similar phenotype as Syt1 ko in chromaffin cells, slowing down the synchronous release with a longer exocytotic delay (Schonn et al., 2007; Dhara et al., 2014). Thus, it is possible that a functional crosstalk between Cpx's NTD and the calcium sensor Syt1 facilitates synchronized vesicle fusion. One conceivable scenario could be that CpxII NTD preferentially promotes Syt1 mediated release, hindering other calcium sensors like the slower acting Syt7 in improperly deputizing in fusion triggering. The loss of CpxII, instead, would result in the more recruitment of Syt7 and may cause the observed slowing of the secretion response. To follow up on this hypothesis, we used neuroendocrine cells deficient of Syt7 leaving Syt1 as the sole calcium sensor to mediate synchronized fusion. The results show that expression of CpxII DN in Syt7 ko cells still slows down stimulus-secretion coupling like in wt cells (Figure 34), rendering the possibility unlikely that CpxII with its NTD shifts the preferred usage of Ca^{2+} -sensors towards Syt1. It rather indicates that CpxII with its NTD somehow cooperates with Syt1.

An intriguing facet to the putative facilitation mechanism came from the observation that synchronized secretion from chromaffin cells was also slowed down by the Syt1 R233Q point mutation showing a prominent delay in the timing of the stimulus secretion coupling (Sorensen et al., 2003). Indeed, the Syt1 R233Q mutation altered the synchronized fusion in chromaffin cells similarly to CpxII NTD expression (Dhara et al., 2014). The similar effects of the two mutations on the synchronous release point to the possibility that CpxII NTD and the Syt1 C2A could mechanistically overlap in tuning the speed of fusion. The Syt1 R233Q point mutation has been shown to cause a twofold reduction in the calcium affinity of Syt1 binding to lipid membranes (Bai et al. 2002; Wang et al., 2003; Herrick et al., 2006) and a 50% decrease in Syt1-SNAP25 interaction (Wang et al., 2003), which diminished the rate of exocytosis in PC12 cells. Further biochemical experiments confirmed that the Syt1 R233Q mutant has a decreased overall Ca^{2+} affinity and makes the C2 domains of Syt1 unable to dive into the lipid membranes, (Fernandez-Chacon et al.,

2001), a phenotype that went hand in hand with smaller EPSCs amplitude as well as a diminished release probability in comparison to wt neurons (Fernandez-Chacon et al., 2001; Li et al., 2006).

Our data shows that expressing full-length CpxII in Syt1 R233Q cells restored release kinetics back to the wt levels (Figure 36), showing that a surplus of CpxII can compensate for the functional deficits of Syt1 caused by the R233Q mutation. Moreover, expressing CpxII with a truncated NTD further aggravated the already slow synchronized exocytosis in the Syt1 R233Q knock in cells (Figure 36). Thus, CpxII cooperates with Syt1 in an NTD dependent fashion, indicating that the very N-terminal domain of Cpx adapts Syt1 to meet the speed requirements of synchronous fusion. To further address the cooperation between Syt1 and CpxII, we made use a second point mutation D232N in the Syt1 C2A that neutralizes one of the calcium binding aspartates and increases the Syt1-SNARE complex interaction, which was found to enhance the synchronous release in cortical neurons (Pang et al., 2006). In chromaffin cells, however, the D232N mutant supported a secretion response that is nearly undistinguishable from wt cells. Furthermore, the expression of CpxII lacking its NTD in Syt1 D232N knock-in chromaffin cells slowed down synchronous fusion as in wt cells (Figure 37). Moreover, expressing CpxII in D232N knock-in chromaffin cells on the other hand did not speed up the synchronized secretion as observed with the R233Q mutation (Figure 37). Taken together, our experimental results show that a surplus CpxII can compensate for functional deficits imposed by specific Syt1 mutations (i.e. R233Q mutation), indicating that both proteins regulate similar molecular steps that govern Ca^{2+} -dependent exocytosis timing.

The recent crystal structure of the primed SNARE–Cpx-Syt1 complex described a tripartite interphase between Syt1, Cpx and the SNAREs (Zhou et al.2017). This study further shows the close positioning between Syt1 C2A and the Cpx N terminal domain, where both of which reside near the C terminal end of the synaptobrevin’s SNARE motif. Due to this proximity, it is possible that CpxII with its N terminal domain can modulate the efficiency of Syt1 in triggering and speeding synchronized exocytosis.

Taken together, we show that the C terminal domain of complexin is essential for clamping premature vesicle release and hindering SNARE complex assembly, thereby, building up a primed pool of vesicles. The N-terminal domain acts mechanistically independent from the CpxII CTD and is critical for effective triggering of Ca^{2+} -dependent secretion, by increasing the apparent calcium affinity of release. Moreover, we find for the first time that CpxII NTD speeds up the Syt1 but not the Syt7 mediated synchronized fusion, showing a mutual interdependence between the Syt1 and CpxII NTD to facilitate exocytosis. Furthermore, N terminal domain of Cpx can rescue the impaired

exocytosis triggering imposed by specific Syt1 mutants, indicating both proteins synergize in mediating fast exocytosis.

6.3 SybII TMD catalyzes membrane fusion

Compared to other single membrane-spanning anchors from other proteins, the SybII TMD is rich in β -branched amino acids (more than 40% of composition Valine and Isoleucine) (Langosch et al., 2001; Neumann et al., 2011). This overabundance of β -branched amino acids is proposed to result in a higher flexibility of the TMD helical structure (Stelzer et al., 2008; Han et al., 2016). In contrast, α helices formed by non β branched amino acids as leucines may form more stable and rigid secondary structures due to the enhanced van der Waals interactions (Quint et al., 2010). Interestingly, the isolated TMDs of SNARE proteins facilitate liposome-liposome fusion suggesting a fusiogenic role of the membrane anchors β -branched amino acids (Langosch et al., 2001; Hofmann et al., 2006). Furthermore, theoretical simulations, in particular Molecular dynamics simulations, have predicted an inherent propensity of SNARE TMDs to disturb lipid packing and promoting lipid splay, which reflects the initial lipid bridge between opposing membranes (Kasson et al., 2010; Markvoort et al., 2011; Risselada et al., 2011)

Force generated by SNARE zippering requires the TMDs to pull the opposing membranes into close proximity (Sudhof et al., 2009). In fact, previous reports have challenged the view of an active role of SNARE TMDs in neuronal exocytosis by showing that they can be replaced with a CSP- α as an anchoring motif without causing any detrimental effects on spontaneous or evoked release in cortical neurons (Zhou et al., 2013). In a comprehensive structure-function we have investigated the functional role of the SybII TMD in Ca^{2+} -triggered exocytosis by substituting its core amino acids (positions 97-112) to either helix-stabilizing leucines or flexibility-promoting β -branched isoleucine/valine residues (Dhara et al., 2016; 2020). The results show that rigidifying mutations (e.g. poly Leucine substitution) reduces the size of the exocytotic burst without changing its kinetics (Dhara et al., 2016). In contrast, flexibility-enhancing amino acid substitutions, like the Poly-Isoleucine mutation rescued secretion to the level of the wt protein (Figure 39). To investigate whether structural flexibility is required throughout the entire TMD region, we substituted either half of the SybII TMD with isoleucine residues. Only substitutions in the N-terminal half of the TMD were effective in regulating the exocytotic burst size (Figure 39). While replacement with Isoleucine residues restored secretion to the level of wt cells (Figure 39), substitution with leucine residues strongly diminished the flash-evoked response (Dhara et al., 2016). These results allowed for several important conclusions: First, not the overall hydrophobicity but rather its structural

flexibility is functionally relevant for the exocytosis competence of the fusing granules. Secondly, flexibility of the N-terminal half of the TMD promotes the observed fusion-catalyzing effect, agreeing with the observation that formation of the initial lipid stalk generally found in the direct vicinity of SNARE TMDs in MD simulations (Risselada et al., 2011). Third, the full rescue of secretion by either poly-Isoleucine or poly valine substitutions indicate that the SybII TMD does not contain key residues that can be held for fusion promotion. To test the last conclusion, we have also substituted highly conserved amino acid G100, which is believed to promote a structural kink in the middle of SybII TMD (Blanchard et al., 2014). We found that mutations neither to alanine nor to leucine interfered with the mutant's capability to restore the secretion response (Figure 40). Taken together, the proposed structural kinking of the SybII TMD by its flexible G100 residue is not critical for catalyzing Ca^{2+} -triggered fusion.

Given these observations it stands to reason how helix-stabilizing mutations interfere with the secretion response in chromaffin cells. Priming and the exocytotic burst in chromaffin cells size is largely determined by the SNARE-SNARE interactions and its regulation by proteins like Synaptotagmin or Munc13 (James et al., 2013; Sudhof 2013a). Since the TMD mutations do not interfere with SNARE complex formation *in vitro* (Dhara et al., 2016), one might speculate that TMD-rigidifying mutations increase the energy barrier for fusion by lowering lipid splay (Dhara et al., 2020). As a consequence, vesicles destined to fuse remain trapped in a fusion incompetent state without changing the kinetics of the remaining response. To test this, we have comparatively analyzed the subcellular distribution of vesicles in v-SNARE dko chromaffin cells expressing the wildtype SybII or the polyL-variant. To unmask a potential fusion deficit, cells were stimulated with high potassium-containing solution immediately before chemical fixation. The results show a clear accumulation of granules close to the plasma membrane (within 5-10 nm) in cells expressing the TMD mutant when compared with the wildtype protein or dko cells (Figure 41). The number of membrane proximal vesicles in stimulated chromaffin cells is expected to reflect both, the efficacy

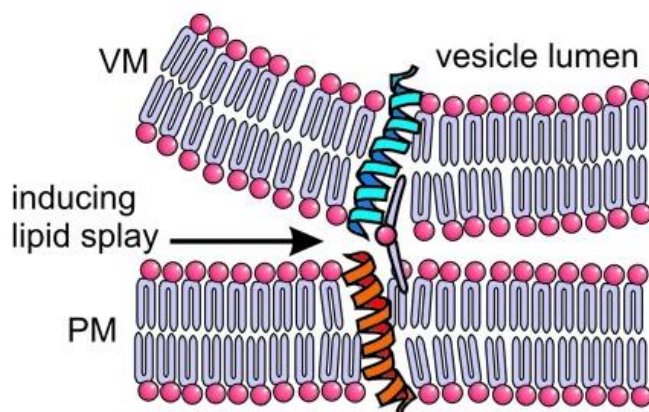


Figure 43. Proposed mechanism for membrane fusion catalysis by SybII TMD. Hypothetical model illustrating how conformational flexibility of the Syb2 TMD (Blue) specifically of the N-terminal region enhances lipid splay to promote intermembrane contact (PM, plasma membrane, VM, vesicle membrane) during fusion initiation. (adapted from Dhara et al., 2016)

of priming and of fusion. In dko cells, which are devoid of any secretion, the number of membrane-proximal vesicles is lowest because these cells are priming deficient (Borisovska et al., 2005), it is intermediate in wt cells (reflecting the balance between priming and fusion) and highest for poly-L expressing cells that enable undiminished priming but hinder fusion. Overall, these results agree with the view that TMD-rigidifying mutations may arrest vesicles in a fusion-incompetent state. These observations have further been corroborated by recent experiments in our lab showing that TMD-stabilizing mutations alter protein-lipid rather than protein-protein interactions (Dhara et al., 2020). It became clear that intracellular application of membrane curvature-promoting phospholipids like lysophosphatidylcholine or oleic acid reduce or increase the exocytotic burst size, respectively. Furthermore, they profoundly alter transmitter discharge kinetics at the level of single fusion events pore expansion and fully rescue the decelerated fusion kinetics of TMD-rigidifying VAMP2 mutants (Dhara et al., 2016). Overall, these results supported the view that v-SNARE TMDs do not only serve as simple membrane anchors, but rather play an active role by modulating crucial protein lipid interactions to lower the energy requirements of membrane fusion (Figure 43).

7 Conclusions

Overall, our experiments provide a new insight into the mechanism of SNARE mediated exocytosis and its regulation by the accessory proteins complexin and the calcium sensors for exocytosis Synaptotagmins. By studying the effects of CpxII mutants on synchronized exocytosis in chromaffin cells together with biochemical evidence and high-resolution imaging, we are able to find evidence for a so far unprecedented mechanism by which CpxII is able to clamp asynchronous vesicle exocytosis. Our experiments indicate that the CpxII CTD, which structurally mimics the C-terminal region of the SNAP25-SN1 domain, is instrumental for clamping SNARE-mediated premature exocytosis. Specifically, the amphipathic character at the very end of CpxII CTD is critical for hindering premature exocytosis which consequently increases the magnitude of synchronized secretion. Upstream of the amphipathic region, the CTD also houses a cluster of glutamates, which may aid the calcium sensor Synaptotagmin to lift the CTD-mediated clamp upon $[Ca^{2+}]_i$ elevation. We hypothesize that the CpxII CTD is present in a dynamic equilibrium between a membrane bound state and a SNARE interacting state. While the former allows for CpxII accumulation at the fusion site, the latter may be instrumental for inhibiting progressive SNARE zipping and the initiation of membrane fusion. In addition, the CpxII NTD specifically accelerates exocytosis most likely by modulating the Syt1 driven synchronized fusion. In the same line, CpxII compensates for mutational functional deficiencies of mutant Syt1. Thus, exocytosis timing appears to rely on a mechanistic cooperation between the SNARE regulators CpxII and Syt1. Evidently, Complexin is not only small but also capable and further experiments are necessary to provide a true understanding of the underlying molecular mechanisms. Further experiments address the role of the proteinaceous TMD of the v-SNARE protein SybII in exocytosis. They provide evidence that the SybII TMD plays an active role that goes beyond simple membrane anchoring. It is likely that the structural flexibility of the TMD may perturb the packing of the surrounding phospholipids to facilitate the first hydrophobic contact between the opposing membranes. Overall, these results are compatible with the view that the most probable route to efficient membrane fusion relies on both protein-protein as well as protein-lipid interactions.

References

- Alberts, B. (2008). Molecular biology of the cell. New York, Garland Science.
- Allen, C. and C. F. Stevens (1994). "An evaluation of causes for unreliability of synaptic transmission." Proc Natl Acad Sci U S A **91**(22): 10380-10383.
- Angleson, J. K., A. J. Cochilla, G. Kilic, I. Nussinovitch and W. J. Betz (1999). "Regulation of dense core release from neuroendocrine cells revealed by imaging single exocytic events." Nat Neurosci **2**(5): 440-446.
- Apland, J. P., J. A. Biser, M. Adler, A. V. Ferrer-Montiel, M. Montal, J. M. Canaves and M. G. Filbert (1999). "Peptides that mimic the carboxy-terminal domain of SNAP-25 block acetylcholine release at an Aplysia synapse." J Appl Toxicol **19 Suppl 1**: S23-26.
- Bacaj, T., D. Wu, J. Burre, R. C. Malenka, X. Liu and T. C. Sudhof (2015). "Synaptotagmin-1 and -7 Are Redundantly Essential for Maintaining the Capacity of the Readily-Releasable Pool of Synaptic Vesicles." PLoS Biol **13**(10): e1002267.
- Bacaj, T., D. Wu, X. Yang, W. Morishita, P. Zhou, W. Xu, R. C. Malenka and T. C. Sudhof (2013). "Synaptotagmin-1 and synaptotagmin-7 trigger synchronous and asynchronous phases of neurotransmitter release." Neuron **80**(4): 947-959.
- Bao, H., M. Goldschen-Ohm, P. Jeggel, B. Chanda, J. M. Edwardson and E. R. Chapman (2016). "Exocytotic fusion pores are composed of both lipids and proteins." Nat Struct Mol Biol **23**(1): 67-73.
- Basso, M., S. Giraud, D. Corpillo, B. Bergamasco, L. Lopiano and M. Fasano (2004). "Proteome analysis of human substantia nigra in Parkinson's disease." Proteomics **4**(12): 3943-3952.
- Becherer, U. and J. Rettig (2006). "Vesicle pools, docking, priming, and release." Cell Tissue Res **326**(2): 393-407.
- Bentz, J. and H. Ellens (1988). "Membrane-Fusion - Kinetics and Mechanisms." Colloids and Surfaces **30**(1-2): 65-112.
- Blanchard, A. E., M. J. Arcario, K. Schulten and E. Tajkhorshid (2014). "A highly tilted membrane configuration for the prefusion state of synaptobrevin." Biophys J **107**(9): 2112-2121.
- Block, M. R., B. S. Glick, C. A. Wilcox, F. T. Wieland and J. E. Rothman (1988). "Purification of an N-ethylmaleimide-sensitive protein catalyzing vesicular transport." Proc Natl Acad Sci U S A **85**(21): 7852-7856.
- Borisovska, M., Y. Zhao, Y. Tsytsyura, N. Glyvuk, S. Takamori, U. Matti, J. Rettig, T. Sudhof and D. Bruns (2005). "v-SNAREs control exocytosis of vesicles from priming to fusion." EMBO J **24**(12): 2114-2126.
- Bowen, M. E., K. Weninger, J. Ernst, S. Chu and A. T. Brunger (2005). "Single-molecule studies of synaptotagmin and complexin binding to the SNARE complex." Biophys J **89**(1): 690-702.
- Bruns, D. (2004). "Detection of transmitter release with carbon fiber electrodes." Methods **33**(4): 312-321.
- Buhl, L. K., R. A. Jorquera, Y. Akbergenova, S. Huntwork-Rodriguez, D. Volfson and J. T. Littleton (2013). "Differential regulation of evoked and spontaneous neurotransmitter release by C-terminal modifications of complexin." Mol Cell Neurosci **52**: 161-172.

- Cai, H., K. Reim, F. Varoqueaux, S. Tapechum, K. Hill, J. B. Sorensen, N. Brose and R. H. Chow (2008). "Complexin II plays a positive role in Ca²⁺-triggered exocytosis by facilitating vesicle priming." Proc Natl Acad Sci U S A **105**(49): 19538-19543.
- Chang, S., T. Trimbuch and C. Rosenmund (2018). "Synaptotagmin-1 drives synchronous Ca²⁺-triggered fusion by C2B-domain-mediated synaptic-vesicle-membrane attachment." Nat Neurosci **21**(1): 33-40.
- Chapman, E. R. (2008). "How does synaptotagmin trigger neurotransmitter release?" Annu Rev Biochem **77**: 615-641.
- Chen, C., R. Satterfield, S. M. Young, Jr. and P. Jonas (2017). "Triple Function of Synaptotagmin 7 Ensures Efficiency of High-Frequency Transmission at Central GABAergic Synapses." Cell Rep **21**(8): 2082-2089.
- Chen, P. and K. D. Gillis (2000). "The noise of membrane capacitance measurements in the whole-cell recording configuration." Biophysical Journal **79**(4): 2162-2170.
- Chen, X., D. R. Tomchick, E. Kovrigin, D. Arac, M. Machius, T. C. Sudhof and J. Rizo (2002). "Three-dimensional structure of the complexin/SNARE complex." Neuron **33**(3): 397-409.
- Chernomordik, L. V., J. Zimmerberg and M. M. Kozlov (2006). "Membranes of the world unite!" J Cell Biol **175**(2): 201-207.
- Chicka, M. C. and E. R. Chapman (2009). "Concurrent binding of complexin and synaptotagmin to liposome-embedded SNARE complexes." Biochemistry **48**(4): 657-659.
- Cho, R. W., Y. Song and J. T. Littleton (2010). "Comparative analysis of Drosophila and mammalian complexins as fusion clamps and facilitators of neurotransmitter release." Mol Cell Neurosci **45**(4): 389-397.
- Cohen, F. S. and G. B. Melikyan (2004). "The energetics of membrane fusion from binding, through hemifusion, pore formation, and pore enlargement." J Membr Biol **199**(1): 1-14.
- Datta, G., M. Chaddha, S. Hama, M. Navab, A. M. Fogelman, D. W. Garber, V. K. Mishra, R. M. Epand, R. F. Epand, S. Lund-Katz, M. C. Phillips, J. P. Segrest and G. M. Anantharamaiah (2001). "Effects of increasing hydrophobicity on the physical-chemical and biological properties of a class A amphipathic helical peptide." J Lipid Res **42**(7): 1096-1104.
- Davis, A. F., J. Bai, D. Fasshauer, M. J. Wolowick, J. L. Lewis and E. R. Chapman (1999). "Kinetics of synaptotagmin responses to Ca²⁺ and assembly with the core SNARE complex onto membranes." Neuron **24**(2): 363-376.
- Dawidowski, D. and D. S. Cafiso (2016). "Munc18-1 and the Syntaxin-1 N Terminus Regulate Open-Closed States in a t-SNARE Complex." Structure **24**(3): 392-400.
- de Wit, H., L. N. Cornelisse, R. F. Toonen and M. Verhage (2006). "Docking of secretory vesicles is syntaxin dependent." PLoS One **1**: e126.
- de Wit, H., A. M. Walter, I. Milosevic, A. Gulyas-Kovacs, D. Riedel, J. B. Sorensen and M. Verhage (2009). "Synaptotagmin-1 docks secretory vesicles to syntaxin-1/SNAP-25 acceptor complexes." Cell **138**(5): 935-946.
- DeFelice, L. J. (1997). Electrical properties of cells : patch clamp for biologists. New York, Plenum Press.
- Dekel, E. and U. Alon (2005). "Optimality and evolutionary tuning of the expression level of a protein." Nature **436**(7050): 588-592.

- Dhara, M., M. Mantero Martinez, M. Makke, Y. Schwarz, R. Mohrmann and D. Bruns (2020). "Synergistic actions of v-SNARE transmembrane domains and membrane-curvature modifying lipids in neurotransmitter release." Elife **9**.
- Dhara, M., R. Mohrmann and D. Bruns (2018). "v-SNARE function in chromaffin cells." Pflugers Arch **470**(1): 169-180.
- Dhara, M., A. Yarzagaray, M. Makke, B. Schindeldecker, Y. Schwarz, A. Shaaban, S. Sharma, R. A. Bockmann, M. Lindau, R. Mohrmann and D. Bruns (2016). "v-SNARE transmembrane domains function as catalysts for vesicle fusion." Elife **5**.
- Dhara, M., A. Yarzagaray, Y. Schwarz, S. Dutta, C. Grabner, P. K. Moghadam, A. Bost, C. Schirra, J. Rettig, K. Reim, N. Brose, R. Mohrmann and D. Bruns (2014). "Complexin synchronizes primed vesicle exocytosis and regulates fusion pore dynamics." J Cell Biol **204**(7): 1123-1140.
- Dolai, S., L. Xie, D. Zhu, T. Liang, T. Qin, H. Xie, Y. Kang, E. R. Chapman and H. Y. Gaisano (2016). "Synaptotagmin-7 Functions to Replenish Insulin Granules for Exocytosis in Human Islet beta-Cells." Diabetes **65**(7): 1962-1976.
- Doupe, A. J., S. C. Landis and P. H. Patterson (1985). "Environmental influences in the development of neural crest derivatives: glucocorticoids, growth factors, and chromaffin cell plasticity." J Neurosci **5**(8): 2119-2142.
- Dulubova, I., S. Sugita, S. Hill, M. Hosaka, I. Fernandez, T. C. Sudhof and J. Rizo (1999). "A conformational switch in syntaxin during exocytosis: role of munc18." EMBO J **18**(16): 4372-4382.
- Eastwood, S. L. and P. J. Harrison (2001). "Synaptic pathology in the anterior cingulate cortex in schizophrenia and mood disorders. A review and a Western blot study of synaptophysin, GAP-43 and the complexins." Brain Res Bull **55**(5): 569-578.
- El-Brolosy, M. A. and D. Y. R. Stainier (2017). "Genetic compensation: A phenomenon in search of mechanisms." PLoS Genet **13**(7): e1006780.
- Ellis-Davies, G. C. and J. H. Kaplan (1994). "Nitrophenyl-EGTA, a photolabile chelator that selectively binds Ca²⁺ with high affinity and releases it rapidly upon photolysis." Proc Natl Acad Sci U S A **91**(1): 187-191.
- Fang, Q. and M. Lindau (2014). "How could SNARE proteins open a fusion pore?" Physiology (Bethesda) **29**(4): 278-285.
- Fasshauer, D., H. Otto, W. K. Eliason, R. Jahn and A. T. Brunger (1997). "Structural changes are associated with soluble N-ethylmaleimide-sensitive fusion protein attachment protein receptor complex formation." J Biol Chem **272**(44): 28036-28041.
- Fasshauer, D., R. B. Sutton, A. T. Brunger and R. Jahn (1998). "Conserved structural features of the synaptic fusion complex: SNARE proteins reclassified as Q- and R-SNAREs." Proc Natl Acad Sci U S A **95**(26): 15781-15786.
- Fdez, E., M. Martinez-Salvador, M. Beard, P. Woodman and S. Hilfiker (2010). "Transmembrane-domain determinants for SNARE-mediated membrane fusion." J Cell Sci **123**(Pt 14): 2473-2480.
- Fernandez-Chacon, R., A. Konigstorfer, S. H. Gerber, J. Garcia, M. F. Matos, C. F. Stevens, N. Brose, J. Rizo, C. Rosenmund and T. C. Sudhof (2001). "Synaptotagmin I functions as a calcium regulator of release probability." Nature **410**(6824): 41-49.

- Fernandez-Chacon, R., O. H. Shin, A. Konigstorfer, M. F. Matos, A. C. Meyer, J. Garcia, S. H. Gerber, J. Rizo, T. C. Sudhof and C. Rosenmund (2002). "Structure/function analysis of Ca²⁺ binding to the C2A domain of synaptotagmin 1." J Neurosci **22**(19): 8438-8446.
- Fernandez, I., J. Ubach, I. Dulubova, X. Zhang, T. C. Sudhof and J. Rizo (1998). "Three-dimensional structure of an evolutionarily conserved N-terminal domain of syntaxin 1A." Cell **94**(6): 841-849.
- Ferrer-Montiel, A. V., L. M. Gutierrez, J. P. Aplan, J. M. Canaves, A. Gil, S. Viniegra, J. A. Biser, M. Adler and M. Montal (1998). "The 26-mer peptide released from SNAP-25 cleavage by botulinum neurotoxin E inhibits vesicle docking." FEBS Lett **435**(1): 84-88.
- Fleming, K. G. and D. M. Engelman (2001). "Computation and mutagenesis suggest a right-handed structure for the synaptobrevin transmembrane dimer." Proteins **45**(4): 313-317.
- Gao, Y., S. Zorman, G. Gundersen, Z. Xi, L. Ma, G. Sirinakis, J. E. Rothman and Y. Zhang (2012). "Single reconstituted neuronal SNARE complexes zipper in three distinct stages." Science **337**(6100): 1340-1343.
- Giraud, C. G., W. S. Eng, T. J. Melia and J. E. Rothman (2006). "A clamping mechanism involved in SNARE-dependent exocytosis." Science **313**(5787): 676-680.
- Giraud, C. G., A. Garcia-Diaz, W. S. Eng, Y. Chen, W. A. Hendrickson, T. J. Melia and J. E. Rothman (2009). "Alternative zippering as an on-off switch for SNARE-mediated fusion." Science **323**(5913): 512-516.
- Giraud, C. G., A. Garcia-Diaz, W. S. Eng, A. Yamamoto, T. J. Melia and J. E. Rothman (2008). "Distinct domains of complexins bind SNARE complexes and clamp fusion *in vitro*." J Biol Chem **283**(30): 21211-21219.
- Gong, J., Y. Lai, X. Li, M. Wang, J. Leitz, Y. Hu, Y. Zhang, U. B. Choi, D. Cipriano, R. A. Pfuetzner, T. C. Sudhof, X. Yang, A. T. Brunger and J. Diao (2016). "C-terminal domain of mammalian complexin-1 localizes to highly curved membranes." Proc Natl Acad Sci U S A **113**(47): E7590-E7599.
- Grote, E., M. Baba, Y. Ohsumi and P. J. Novick (2000). "Geranylgeranylated SNAREs are dominant inhibitors of membrane fusion." J Cell Biol **151**(2): 453-466.
- Grynkiewicz, G., M. Poenie and R. Y. Tsien (1985). "A new generation of Ca²⁺ indicators with greatly improved fluorescence properties." J Biol Chem **260**(6): 3440-3450.
- Gutierrez, L. M., J. M. Canaves, A. V. Ferrer-Montiel, J. A. Reig, M. Montal and S. Viniegra (1995). "A peptide that mimics the carboxy-terminal domain of SNAP-25 blocks Ca²⁺-dependent exocytosis in chromaffin cells." FEBS Lett **372**(1): 39-43.
- Gutierrez, L. M., S. Viniegra, J. Rueda, A. V. Ferrer-Montiel, J. M. Canaves and M. Montal (1997). "A peptide that mimics the C-terminal sequence of SNAP-25 inhibits secretory vesicle docking in chromaffin cells." J Biol Chem **272**(5): 2634-2639.
- Hamill, O. P., A. Marty, E. Neher, B. Sakmann and F. J. Sigworth (1981). "Improved patch-clamp techniques for high-resolution current recording from cells and cell-free membrane patches." Pflugers Arch **391**(2): 85-100.
- Han, J., K. Pluhackova and R. A. Bockmann (2017). "The Multifaceted Role of SNARE Proteins in Membrane Fusion." Front Physiol **8**: 5.
- Han, J., K. Pluhackova, D. Bruns and R. A. Bockmann (2016). "Synaptobrevin transmembrane domain determines the structure and dynamics of the SNARE motif and the linker region." Biochim Biophys Acta **1858**(4): 855-865.

- Hastoy, B., P. A. Scotti, A. Milochau, Z. Fezoua-Boubegtiten, J. Rodas, R. Megret, B. Desbat, M. Laguerre, S. Castano, D. Perrais, P. Rorsman, R. Oda and J. Lang (2017). "A Central Small Amino Acid in the VAMP2 Transmembrane Domain Regulates the Fusion Pore in Exocytosis." Sci Rep **7**(1): 2835.
- Hayashi, T., H. McMahon, S. Yamasaki, T. Binz, Y. Hata, T. C. Sudhof and H. Niemann (1994). "Synaptic vesicle membrane fusion complex: action of clostridial neurotoxins on assembly." EMBO J **13**(21): 5051-5061.
- Heinemann, S., J. Rettig, V. Scott, D. N. Parcej, C. Lorra, J. Dolly and O. Pongs (1994). "The inactivation behaviour of voltage-gated K-channels may be determined by association of alpha- and beta-subunits." J Physiol Paris **88**(3): 173-180.
- Hess, D. T., T. M. Slater, M. C. Wilson and J. H. Skene (1992). "The 25 kDa synaptosomal-associated protein SNAP-25 is the major methionine-rich polypeptide in rapid axonal transport and a major substrate for palmitoylation in adult CNS." J Neurosci **12**(12): 4634-4641.
- Hofmann, M. W., K. Peplowska, J. Rohde, B. C. Poschner, C. Ungermann and D. Langosch (2006). "Self-interaction of a SNARE transmembrane domain promotes the hemifusion-to-fusion transition." J Mol Biol **364**(5): 1048-1060.
- Huang, X., S. Sun, X. Wang, F. Fan, Q. Zhou, S. Lu, Y. Cao, Q. W. Wang, M. Q. Dong, J. Yao and S. F. Sui (2019). "Mechanistic insights into the SNARE complex disassembly." Sci Adv **5**(4): eaau8164.
- Hui, E., J. Bai, P. Wang, M. Sugimori, R. R. Llinas and E. R. Chapman (2005). "Three distinct kinetic groupings of the synaptotagmin family: candidate sensors for rapid and delayed exocytosis." Proc Natl Acad Sci U S A **102**(14): 5210-5214.
- Hyrz, K. L., J. M. Bownik and M. P. Goldberg (2000). "Ionic selectivity of low-affinity ratiometric calcium indicators: mag-Fura-2, Fura-2FF and BTC." Cell Calcium **27**(2): 75-86.
- Imig, C., S. W. Min, S. Krinner, M. Arancillo, C. Rosenmund, T. C. Sudhof, J. Rhee, N. Brose and B. H. Cooper (2014). "The morphological and molecular nature of synaptic vesicle priming at presynaptic active zones." Neuron **84**(2): 416-431.
- Ishizuka, T., H. Saisu, S. Odani and T. Abe (1995). "Synaphin: a protein associated with the docking/fusion complex in presynaptic terminals." Biochem Biophys Res Commun **213**(3): 1107-1114.
- Jahn, R. and D. Fasshauer (2012). "Molecular machines governing exocytosis of synaptic vesicles." Nature **490**(7419): 201-207.
- Jahn, R., T. Lang and T. C. Sudhof (2003). "Membrane fusion." Cell **112**(4): 519-533.
- James, D. J. and T. F. Martin (2013). "CAPS and Munc13: CATCHRs that SNARE Vesicles." Front Endocrinol (Lausanne) **4**: 187.
- Kaesler-Woo, Y. J., X. Yang and T. C. Sudhof (2012). "C-terminal complexin sequence is selectively required for clamping and priming but not for Ca²⁺ triggering of synaptic exocytosis." J Neurosci **32**(8): 2877-2885.
- Kasson, P. M., E. Lindahl and V. S. Pande (2010). "Atomic-resolution simulations predict a transition state for vesicle fusion defined by contact of a few lipid tails." PLoS Comput Biol **6**(6): e1000829.
- Khaitovich, P., W. Enard, M. Lachmann and S. Paabo (2006). "Evolution of primate gene expression." Nat Rev Genet **7**(9): 693-702.

- Klingauf, J. and E. Neher (1997). "Modeling buffered Ca²⁺ diffusion near the membrane: implications for secretion in neuroendocrine cells." Biophys J **72**(2 Pt 1): 674-690.
- Kummel, D., S. S. Krishnakumar, D. T. Radoff, F. Li, C. G. Giraud, F. Pincet, J. E. Rothman and K. M. Reinisch (2011). "Complexin cross-links presynaptic SNAREs into a zigzag array." Nat Struct Mol Biol **18**(8): 927-933.
- Laage, R., J. Rohde, B. Brosig and D. Langosch (2000). "A conserved membrane-spanning amino acid motif drives homomeric and supports heteromeric assembly of presynaptic SNARE proteins." J Biol Chem **275**(23): 17481-17487.
- Lai, Y., U. B. Choi, J. Leitz, H. J. Rhee, C. Lee, B. Altas, M. Zhao, R. A. Pfuetzner, A. L. Wang, N. Brose, J. Rhee and A. T. Brunger (2017). "Molecular Mechanisms of Synaptic Vesicle Priming by Munc13 and Munc18." Neuron **95**(3): 591-607 e510.
- Lai, Y., U. B. Choi, Y. Zhang, M. Zhao, R. A. Pfuetzner, A. L. Wang, J. Diao and A. T. Brunger (2016). "N-terminal domain of complexin independently activates calcium-triggered fusion." Proc Natl Acad Sci U S A **113**(32): E4698-4707.
- Lane, S. R. and Y. Liu (1997). "Characterization of the palmitoylation domain of SNAP-25." J Neurochem **69**(5): 1864-1869.
- Langosch, D., J. M. Crane, B. Brosig, A. Hellwig, L. K. Tamm and J. Reed (2001). "Peptide mimics of SNARE transmembrane segments drive membrane fusion depending on their conformational plasticity." J Mol Biol **311**(4): 709-721.
- Li, F., D. Kummel, J. Coleman, K. M. Reinisch, J. E. Rothman and F. Pincet (2014). "A half-zipped SNARE complex represents a functional intermediate in membrane fusion." J Am Chem Soc **136**(9): 3456-3464.
- Li, F., F. Pincet, E. Perez, W. S. Eng, T. J. Melia, J. E. Rothman and D. Tareste (2007). "Energetics and dynamics of SNAREpin folding across lipid bilayers." Nat Struct Mol Biol **14**(10): 890-896.
- Li, F., N. Tiwari, J. E. Rothman and F. Pincet (2016). "Kinetic barriers to SNAREpin assembly in the regulation of membrane docking/priming and fusion." Proc Natl Acad Sci U S A **113**(38): 10536-10541.
- Li, L., O. H. Shin, J. S. Rhee, D. Arac, J. C. Rah, J. Rizo, T. Sudhof and C. Rosenmund (2006). "Phosphatidylinositol phosphates as co-activators of Ca²⁺ binding to C2 domains of synaptotagmin 1." J Biol Chem **281**(23): 15845-15852.
- Li, Y. C., N. L. Chanaday, W. Xu and E. T. Kavalali (2017). "Synaptotagmin-1- and Synaptotagmin-7-Dependent Fusion Mechanisms Target Synaptic Vesicles to Kinetically Distinct Endocytic Pathways." Neuron **93**(3): 616-631 e613.
- Liu, H., H. Bai, E. Hui, L. Yang, C. S. Evans, Z. Wang, S. E. Kwon and E. R. Chapman (2014). "Synaptotagmin 7 functions as a Ca²⁺-sensor for synaptic vesicle replenishment." Elife **3**: e01524.
- Lodish, H. F., A. Berk, P. Matsudaira, C. A. Kaiser, M. Krieger, M. P. Scott, S. L. Zipursky and J. E. Darnell (2003). Molecular cell biology. New York, N.Y., W.H. Freeman and Company.
- Lopez-Maury, L., S. Marguerat and J. Bahler (2008). "Tuning gene expression to changing environments: from rapid responses to evolutionary adaptation." Nat Rev Genet **9**(8): 583-593.
- Lu, B., S. Song and Y. K. Shin (2010). "Accessory alpha-helix of complexin I can displace VAMP2 locally in the complexin-SNARE quaternary complex." J Mol Biol **396**(3): 602-609.

- Luo, F. and T. C. Sudhof (2017). "Synaptotagmin-7-Mediated Asynchronous Release Boosts High-Fidelity Synchronous Transmission at a Central Synapse." Neuron **94**(4): 826-839 e823.
- Ma, C., W. Li, Y. Xu and J. Rizo (2011). "Munc13 mediates the transition from the closed syntaxin-Munc18 complex to the SNARE complex." Nat Struct Mol Biol **18**(5): 542-549.
- MacDougall, D. D., Z. Lin, N. L. Chon, S. L. Jackman, H. Lin, J. D. Knight and A. Anantharam (2018). "The high-affinity calcium sensor synaptotagmin-7 serves multiple roles in regulated exocytosis." J Gen Physiol **150**(6): 783-807.
- Makke, M., M. Mantero Martinez, S. Gaya, Y. Schwarz, W. Frisch, L. Silva-Bermudez, M. Jung, R. Mohrmann, M. Dhara and D. Bruns (2018). "A mechanism for exocytotic arrest by the Complexin C-terminus." Elife **7**.
- Margittai, M., H. Otto and R. Jahn (1999). "A stable interaction between syntaxin 1a and synaptobrevin 2 mediated by their transmembrane domains." FEBS Lett **446**(1): 40-44.
- Markvoort, A. J. and S. J. Marrink (2011). "Lipid acrobatics in the membrane fusion arena." Curr Top Membr **68**: 259-294.
- Martin, J. A., Z. Hu, K. M. Fenz, J. Fernandez and J. S. Dittman (2011). "Complexin has opposite effects on two modes of synaptic vesicle fusion." Curr Biol **21**(2): 97-105.
- Maximov, A., J. Tang, X. Yang, Z. P. Pang and T. C. Sudhof (2009). "Complexin controls the force transfer from SNARE complexes to membranes in fusion." Science **323**(5913): 516-521.
- McMahon, H. T., M. Missler, C. Li and T. C. Sudhof (1995a). "Complexins: cytosolic proteins that regulate SNAP receptor function." Cell **83**(1): 111-119.
- McMahon, H. T. and T. C. Sudhof (1995b). "Synaptic core complex of synaptobrevin, syntaxin, and SNAP25 forms high affinity alpha-SNAP binding site." J Biol Chem **270**(5): 2213-2217.
- McNew, J. A., T. Weber, F. Parlati, R. J. Johnston, T. J. Melia, T. H. Sollner and J. E. Rothman (2000). "Close is not enough: SNARE-dependent membrane fusion requires an active mechanism that transduces force to membrane anchors." J Cell Biol **150**(1): 105-117.
- Moghadam, P. K. and M. B. Jackson (2013). "The functional significance of synaptotagmin diversity in neuroendocrine secretion." Front Endocrinol (Lausanne) **4**: 124.
- Mohrmann, R., H. de Wit, E. Connell, P. S. Pinheiro, C. Leese, D. Bruns, B. Davletov, M. Verhage and J. B. Sorensen (2013). "Synaptotagmin interaction with SNAP-25 governs vesicle docking, priming, and fusion triggering." J Neurosci **33**(36): 14417-14430.
- Mohrmann, R., H. de Wit, M. Verhage, E. Neher and J. B. Sorensen (2010). "Fast vesicle fusion in living cells requires at least three SNARE complexes." Science **330**(6003): 502-505.
- Mohrmann, R., M. Dhara and D. Bruns (2015). "Complexins: small but capable." Cell Mol Life Sci **72**(22): 4221-4235.
- Montecucco, C., G. Schiavo and S. Pantano (2005). "SNARE complexes and neuroexocytosis: how many, how close?" Trends Biochem Sci **30**(7): 367-372.
- Morton, A. J., R. L. Faull and J. M. Edwardson (2001). "Abnormalities in the synaptic vesicle fusion machinery in Huntington's disease." Brain Res Bull **56**(2): 111-117.
- Moser, T. and E. Neher (1997). "Estimation of mean exocytic vesicle capacitance in mouse adrenal chromaffin cells." Proc Natl Acad Sci U S A **94**(13): 6735-6740.
- Neher, E. (2010). "What is Rate-Limiting during Sustained Synaptic Activity: Vesicle Supply or the Availability of Release Sites." Front Synaptic Neurosci **2**: 144.

- Neher, E. and B. Sakmann (1976). "Single-channel currents recorded from membrane of denervated frog muscle fibres." Nature **260**(5554): 799-802.
- Neher, E. and R. S. Zucker (1993). "Multiple calcium-dependent processes related to secretion in bovine chromaffin cells." Neuron **10**(1): 21-30.
- Neumann, S. and D. Langosch (2011). "Conserved conformational dynamics of membrane fusion protein transmembrane domains and flanking regions indicated by sequence statistics." Proteins **79**(8): 2418-2427.
- Nichols, B. J. and H. R. Pelham (1998). "SNAREs and membrane fusion in the Golgi apparatus." Biochim Biophys Acta **1404**(1-2): 9-31.
- Nicholson, K. L., M. Munson, R. B. Miller, T. J. Filip, R. Fairman and F. M. Hughson (1998). "Regulation of SNARE complex assembly by an N-terminal domain of the t-SNARE Sso1p." Nat Struct Biol **5**(9): 793-802.
- Nofal, S., U. Becherer, D. Hof, U. Matti and J. Rettig (2007). "Primed vesicles can be distinguished from docked vesicles by analyzing their mobility." J Neurosci **27**(6): 1386-1395.
- Pabst, S., J. W. Hazzard, W. Antonin, T. C. Sudhof, R. Jahn, J. Rizo and D. Fasshauer (2000). "Selective interaction of complexin with the neuronal SNARE complex. Determination of the binding regions." J Biol Chem **275**(26): 19808-19818.
- Pang, Z. P., O. H. Shin, A. C. Meyer, C. Rosenmund and T. C. Sudhof (2006). "A gain-of-function mutation in synaptotagmin-1 reveals a critical role of Ca²⁺-dependent soluble N-ethylmaleimide-sensitive factor attachment protein receptor complex binding in synaptic exocytosis." J Neurosci **26**(48): 12556-12565.
- Parsegian, R. P. R. V. A. (1989). "Hydration forces between phospholipid bilayers." Biochimica et Biophysica Acta (BBA) - Reviews on Biomembranes **988**(3): 351-376.
- Pusch, M. and E. Neher (1988). "Rates of diffusional exchange between small cells and a measuring patch pipette." Pflugers Arch **411**(2): 204-211.
- Quint, S., S. Widmaier, D. Minde, D. Hornburg, D. Langosch and C. Scharnagl (2010). "Residue-specific side-chain packing determines the backbone dynamics of transmembrane model helices." Biophys J **99**(8): 2541-2549.
- Radoff, D. T., Y. Dong, D. Snead, J. Bai, D. Eliezer and J. S. Dittman (2014). "The accessory helix of complexin functions by stabilizing central helix secondary structure." Elife **3**.
- Rao, T. C., D. R. Passmore, A. R. Peleman, M. Das, E. R. Chapman and A. Anantharam (2014). "Distinct fusion properties of synaptotagmin-1 and synaptotagmin-7 bearing dense core granules." Mol Biol Cell **25**(16): 2416-2427.
- Rao, T. C., Z. Santana Rodriguez, M. M. Bradberry, A. H. Ranski, P. J. Dahl, M. W. Schmidtke, P. M. Jenkins, D. Axelrod, E. R. Chapman, D. R. Giovannucci and A. Anantharam (2017). "Synaptotagmin isoforms confer distinct activation kinetics and dynamics to chromaffin cell granules." J Gen Physiol **149**(8): 763-780.
- Reim, K., M. Mansour, F. Varoqueaux, H. T. McMahon, T. C. Sudhof, N. Brose and C. Rosenmund (2001). "Complexins regulate a late step in Ca²⁺-dependent neurotransmitter release." Cell **104**(1): 71-81.
- Reim, K., H. Wegmeyer, J. H. Brandstatter, M. Xue, C. Rosenmund, T. Dresbach, K. Hofmann and N. Brose (2005). "Structurally and functionally unique complexins at retinal ribbon synapses." J Cell Biol **169**(4): 669-680.

- Rettig, J. and E. Neher (2002). "Emerging roles of presynaptic proteins in Ca⁺⁺-triggered exocytosis." Science **298**(5594): 781-785.
- Risselada, H. J., C. Kutzner and H. Grubmuller (2011). "Caught in the act: visualization of SNARE-mediated fusion events in molecular detail." Chembiochem **12**(7): 1049-1055.
- Roggero, C. M., G. A. De Blas, H. Dai, C. N. Tomes, J. Rizo and L. S. Mayorga (2007). "Complexin/synaptotagmin interplay controls acrosomal exocytosis." J Biol Chem **282**(36): 26335-26343.
- Sakmann, B. N., E (2009). Single-Channel Recording, Springer.
- Schaub, J. R., X. Lu, B. Doneske, Y. K. Shin and J. A. McNew (2006). "Hemifusion arrest by complexin is relieved by Ca²⁺-synaptotagmin I." Nat Struct Mol Biol **13**(8): 748-750.
- Schneggenburger, R. and E. Neher (2005). "Presynaptic calcium and control of vesicle fusion." Curr Opin Neurobiol **15**(3): 266-274.
- Schneggenburger, R. and C. Rosenmund (2015). "Molecular mechanisms governing Ca(2+) regulation of evoked and spontaneous release." Nat Neurosci **18**(7): 935-941.
- Schonn, J. S., A. Maximov, Y. Lao, T. C. Sudhof and J. B. Sorensen (2008). "Synaptotagmin-1 and -7 are functionally overlapping Ca²⁺ sensors for exocytosis in adrenal chromaffin cells." Proc Natl Acad Sci U S A **105**(10): 3998-4003.
- Seven, A. B., K. D. Brewer, L. Shi, Q. X. Jiang and J. Rizo (2013). "Prevalent mechanism of membrane bridging by synaptotagmin-1." Proc Natl Acad Sci U S A **110**(34): E3243-3252.
- Shi, L., Q. T. Shen, A. Kiel, J. Wang, H. W. Wang, T. J. Melia, J. E. Rothman and F. Pincet (2012). "SNARE proteins: one to fuse and three to keep the nascent fusion pore open." Science **335**(6074): 1355-1359.
- Snead, D., A. L. Lai, R. T. Wragg, D. A. Parisotto, T. F. Ramlall, J. S. Dittman, J. H. Freed and D. Eliezer (2017). "Unique Structural Features of Membrane-Bound C-Terminal Domain Motifs Modulate Complexin Inhibitory Function." Front Mol Neurosci **10**: 154.
- Snead, D., R. T. Wragg, J. S. Dittman and D. Eliezer (2014). "Membrane curvature sensing by the C-terminal domain of complexin." Nat Commun **5**: 4955.
- Sollner, T., S. W. Whiteheart, M. Brunner, H. Erdjument-Bromage, S. Geromanos, P. Tempst and J. E. Rothman (1993). "SNAP receptors implicated in vesicle targeting and fusion." Nature **362**(6418): 318-324.
- Sorensen, J. B., R. Fernandez-Chacon, T. C. Sudhof and E. Neher (2003). "Examining synaptotagmin 1 function in dense core vesicle exocytosis under direct control of Ca²⁺." J Gen Physiol **122**(3): 265-276.
- Sorensen, J. B., K. Wiederhold, E. M. Muller, I. Milosevic, G. Nagy, B. L. de Groot, H. Grubmuller and D. Fasshauer (2006). "Sequential N- to C-terminal SNARE complex assembly drives priming and fusion of secretory vesicles." EMBO J **25**(5): 955-966.
- Stein, A., G. Weber, M. C. Wahl and R. Jahn (2009). "Helical extension of the neuronal SNARE complex into the membrane." Nature **460**(7254): 525-528.
- Stelzer, W., B. C. Poschner, H. Stalz, A. J. Heck and D. Langosch (2008). "Sequence-specific conformational flexibility of SNARE transmembrane helices probed by hydrogen/deuterium exchange." Biophys J **95**(3): 1326-1335.
- Stevens, D. R., C. Schirra, U. Becherer and J. Rettig (2011). "Vesicle pools: lessons from adrenal chromaffin cells." Front Synaptic Neurosci **3**: 2.

- Sudhof, T. C. (2012). "Calcium control of neurotransmitter release." Cold Spring Harb Perspect Biol **4**(1): a011353.
- Sudhof, T. C. (2013a). "A molecular machine for neurotransmitter release: synaptotagmin and beyond." Nat Med **19**(10): 1227-1231.
- Sudhof, T. C. (2013b). "Neurotransmitter release: the last millisecond in the life of a synaptic vesicle." Neuron **80**(3): 675-690.
- Sudhof, T. C. and J. E. Rothman (2009). "Membrane fusion: grappling with SNARE and SM proteins." Science **323**(5913): 474-477.
- Sugita, S., O. H. Shin, W. Han, Y. Lao and T. C. Sudhof (2002). "Synaptotagmins form a hierarchy of exocytotic Ca(2+) sensors with distinct Ca(2+) affinities." EMBO J **21**(3): 270-280.
- Sutton, R. B., D. Fasshauer, R. Jahn and A. T. Brunger (1998). "Crystal structure of a SNARE complex involved in synaptic exocytosis at 2.4 Å resolution." Nature **395**(6700): 347-353.
- Tadokoro, S., M. Nakanishi and N. Hirashima (2005). "Complexin II facilitates exocytotic release in mast cells by enhancing Ca²⁺ sensitivity of the fusion process." J Cell Sci **118**(Pt 10): 2239-2246.
- Takahashi, S., H. Yamamoto, Z. Matsuda, M. Ogawa, K. Yagyu, T. Taniguchi, T. Miyata, H. Kaba, T. Higuchi, F. Okutani and et al. (1995). "Identification of two highly homologous presynaptic proteins distinctly localized at the dendritic and somatic synapses." FEBS Lett **368**(3): 455-460.
- Tang, J., A. Maximov, O. H. Shin, H. Dai, J. Rizo and T. C. Sudhof (2006). "A complexin/synaptotagmin 1 switch controls fast synaptic vesicle exocytosis." Cell **126**(6): 1175-1187.
- Tannenberg, R. K., H. L. Scott, A. E. Tannenberg and P. R. Dodd (2006). "Selective loss of synaptic proteins in Alzheimer's disease: evidence for an increased severity with APOE varepsilon4." Neurochem Int **49**(7): 631-639.
- Tokumaru, H., C. Shimizu-Okabe and T. Abe (2008). "Direct interaction of SNARE complex binding protein synaphin/complexin with calcium sensor synaptotagmin 1." Brain Cell Biol **36**(5-6): 173-189.
- Tong, J., P. P. Borbat, J. H. Freed and Y. K. Shin (2009). "A scissors mechanism for stimulation of SNARE-mediated lipid mixing by cholesterol." Proc Natl Acad Sci U S A **106**(13): 5141-5146.
- Trimbuch, T., J. Xu, D. Flaherty, D. R. Tomchick, J. Rizo and C. Rosenmund (2014). "Re-examining how complexin inhibits neurotransmitter release." Elife **3**: e02391.
- Tsui, M. M. and D. K. Banfield (2000). "Yeast Golgi SNARE interactions are promiscuous." J Cell Sci **113** (Pt 1): 145-152.
- Verhage, M. and J. B. Sorensen (2008). "Vesicle docking in regulated exocytosis." Traffic **9**(9): 1414-1424.
- Voets, T. (2000). "Dissection of three Ca²⁺-dependent steps leading to secretion in chromaffin cells from mouse adrenal slices." Neuron **28**(2): 537-545.
- Voets, T., E. Neher and T. Moser (1999). "Mechanisms underlying phasic and sustained secretion in chromaffin cells from mouse adrenal slices." Neuron **23**(3): 607-615.
- Volynski, K. E. and S. S. Krishnakumar (2018). "Synergistic control of neurotransmitter release by different members of the synaptotagmin family." Curr Opin Neurobiol **51**: 154-162.

- von Ruden, L. and E. Neher (1993). "A Ca-dependent early step in the release of catecholamines from adrenal chromaffin cells." Science **262**(5136): 1061-1065.
- Wang, S., Y. Li, J. Gong, S. Ye, X. Yang, R. Zhang and C. Ma (2019). "Munc18 and Munc13 serve as a functional template to orchestrate neuronal SNARE complex assembly." Nat Commun **10**(1): 69.
- Wang, S., Y. Li and C. Ma (2016). "Synaptotagmin-1 C2B domain interacts simultaneously with SNAREs and membranes to promote membrane fusion." Elife **5**.
- Weber, T., B. V. Zemelman, J. A. McNew, B. Westermann, M. Gmachl, F. Parlati, T. H. Sollner and J. E. Rothman (1998). "SNAREpins: minimal machinery for membrane fusion." Cell **92**(6): 759-772.
- Weidman, P. J., P. Melancon, M. R. Block and J. E. Rothman (1989). "Binding of an N-ethylmaleimide-sensitive fusion protein to Golgi membranes requires both a soluble protein(s) and an integral membrane receptor." J Cell Biol **108**(5): 1589-1596.
- Weninger, K., M. E. Bowen, U. B. Choi, S. Chu and A. T. Brunger (2008). "Accessory proteins stabilize the acceptor complex for synaptobrevin, the 1:1 syntaxin/SNAP-25 complex." Structure **16**(2): 308-320.
- Wightman, R. M., J. A. Jankowski, R. T. Kennedy, K. T. Kawagoe, T. J. Schroeder, D. J. Leszczyszyn, J. A. Near, E. J. Diliberto, Jr. and O. H. Viveros (1991). "Temporally resolved catecholamine spikes correspond to single vesicle release from individual chromaffin cells." Proc Natl Acad Sci U S A **88**(23): 10754-10758.
- Wragg, R. T., D. A. Parisotto, Z. Li, M. S. Terakawa, D. Snead, I. Basu, H. Weinstein, D. Eliezer and J. S. Dittman (2017). "Evolutionary Divergence of the C-terminal Domain of Complexin Accounts for Functional Disparities between Vertebrate and Invertebrate Complexins." Front Mol Neurosci **10**: 146.
- Wragg, R. T., D. Snead, Y. Dong, T. F. Ramlall, I. Menon, J. Bai, D. Eliezer and J. S. Dittman (2013). "Synaptic vesicles position complexin to block spontaneous fusion." Neuron **77**(2): 323-334.
- Xu, H., M. Zick, W. T. Wickner and Y. Jun (2011). "A lipid-anchored SNARE supports membrane fusion." Proc Natl Acad Sci U S A **108**(42): 17325-17330.
- Xu, J., Z. P. Pang, O. H. Shin and T. C. Sudhof (2009). "Synaptotagmin-1 functions as a Ca²⁺ sensor for spontaneous release." Nat Neurosci **12**(6): 759-766.
- Xue, M., T. K. Craig, J. Xu, H. T. Chao, J. Rizo and C. Rosenmund (2010). "Binding of the complexin N terminus to the SNARE complex potentiates synaptic-vesicle fusogenicity." Nat Struct Mol Biol **17**(5): 568-575.
- Xue, M., K. Reim, X. Chen, H. T. Chao, H. Deng, J. Rizo, N. Brose and C. Rosenmund (2007). "Distinct domains of complexin I differentially regulate neurotransmitter release." Nat Struct Mol Biol **14**(10): 949-958.
- Yang, B., L. Gonzalez, Jr., R. Prekeris, M. Steegmaier, R. J. Advani and R. H. Scheller (1999). "SNARE interactions are not selective. Implications for membrane fusion specificity." J Biol Chem **274**(9): 5649-5653.
- Yang, X., P. Cao and T. C. Sudhof (2013). "Deconstructing complexin function in activating and clamping Ca²⁺-triggered exocytosis by comparing knockout and knockdown phenotypes." Proc Natl Acad Sci U S A **110**(51): 20777-20782.

- Yang, X., Y. J. Kaeser-Woo, Z. P. Pang, W. Xu and T. C. Sudhof (2010). "Complexin clamps asynchronous release by blocking a secondary Ca(2+) sensor via its accessory alpha helix." Neuron **68**(5): 907-920.
- Yoon, T. Y. and M. Munson (2018). "SNARE complex assembly and disassembly." Curr Biol **28**(8): R397-R401.
- Zdanowicz, R., A. Kreutzberger, B. Liang, V. Kiessling, L. K. Tamm and D. S. Cafiso (2017). "Complexin Binding to Membranes and Acceptor t-SNAREs Explains Its Clamping Effect on Fusion." Biophys J **113**(6): 1235-1250.
- Zhang, Z., Y. Wu, Z. Wang, F. M. Dunning, J. Rehfuss, D. Ramanan, E. R. Chapman and M. B. Jackson (2011). "Release mode of large and small dense-core vesicles specified by different synaptotagmin isoforms in PC12 cells." Mol Biol Cell **22**(13): 2324-2336.
- Zhou, P., T. Bacaj, X. Yang, Z. P. Pang and T. C. Sudhof (2013). "Lipid-anchored SNAREs lacking transmembrane regions fully support membrane fusion during neurotransmitter release." Neuron **80**(2): 470-483.
- Zhou, Q., P. Zhou, A. L. Wang, D. Wu, M. Zhao, T. C. Sudhof and A. T. Brunger (2017). "The primed SNARE-complexin-synaptotagmin complex for neuronal exocytosis." Nature **548**(7668): 420-425.

List of Publications

Dhara, M., M. Mantero Martinez, **M. Makke**, Y. Schwarz, R. Mohrmann and D. Bruns (2020). "Synergistic actions of v-SNARE transmembrane domains and membrane-curvature modifying lipids in neurotransmitter release." Elife **9**.

Makke, M., M. Mantero Martinez, S. Gaya, Y. Schwarz, W. Frisch, L. Silva-Bermudez, M. Jung, R. Mohrmann, M. Dhara and D. Bruns (2018). "A mechanism for exocytotic arrest by the Complexin C-terminus." Elife **7**.

Dhara, M., A. Yarzagaray, **M. Makke**, B. Schindeldecker, Y. Schwarz, A. Shaaban, S. Sharma, R. A. Bockmann, M. Lindau, R. Mohrmann and D. Bruns (2016). "v-SNARE transmembrane domains function as catalysts for vesicle fusion." Elife **5**.

Conferences

Cell Physics, June 2019 (Saarbrücken, Germany)

poster presentation titled "The functional pas de deux of the SybII transmembrane domain and lipids in membrane fusion".

Cell Physics PI meeting, June 2019 (Saarbrücken, Germany)

Oral presentation titled "The functional pas de deux of the SybII transmembrane domain and lipids in membrane fusion".

Biophysical Society (BPS) 63rd Annual Meeting, March 2019 (Baltimore, USA)

Poster presentation "A mechanism for exocytotic arrest by complexin C-terminus"

BioBeirut 8th international meeting, October 2018 (Beirut, Lebanon)

Oral presentation titled "A mechanism for hindering exocytosis by the Complexin C-terminus."

Cell Physics, June 2016 (Saarbrücken, Germany)

Poster presentation titled " v-SNARE transmembrane domains function as catalysts for vesicle fusion"

Acknowledgements

I would like to extend my thanks and appreciation to all the people who had a role in making my PhD work successful and fruitful.

First of all, I thank my doctoral supervisor Prof. Dr. Dieter Bruns for allowing me to perform my work towards my doctoral thesis in his laboratory. I am deeply grateful for his support and guidance throughout the time I was working at his lab. His teachings built the base of my scientific thinking and helped me as well to develop a set of skills that are important for my future career. Also I would like to thank Prof. Dr. Ralf Mohrmann for his discussions and suggestions throughout my work time at the lab. I would like to thank also my colleagues at the department of Molecular Neurophysiology without whom this work would not have been possible. Marina Roter our lab manager for all her efforts in organizing our paperwork, our mice breeding, and acquiring our resources. Also I thank Walentina Frisch, Vanessa Schmidt, Patrick Schmidt, and Jana Foderer for their excellent technical support. As well I extend my appreciation for our animal caretakers specially Birgit Bimperling and Martina Didion, in the animal facility whose work is essential for the continuity of our research.

To my colleagues, Yvonne Schwarz, Antonio Yarzagaray, Madhurima Dhara, Katharina Oleinikov, Maria Mantero Martinez, Jose Rego Terol, Alejandro Pastor Ruiz, Praneeth Chitirala, and our latest PhD student Michelle Zimmer I thank you for the exchange of information and for all the good times at the bench as well as outside the laboratory and wish you all the best in your future work.

During my time in the Center of integrative Physiology and Molecular Medicine I had the privilege to get in contact with experts in the domain of physiology, who were never reluctant in giving me advice and help when needed. I deeply appreciate those people who were a positive influence throughout my PhD. Of those people several have left their mark, Prof. Dr. Jens Rettig with whom I had my first contact in Lebanon, and who initiated the contact between me and my supervisor Prof. Bruns. As well I would like to thank my second supervisor Prof. Dr. Frank Schmitz for his valuable discussions. From the Department of Medicinal Biochemistry and Microbiology I thank Prof. Dr. Martin Jung for the successful collaboration and for his advice which gave a valuable support for my first author paper. I want to extend my gratitude also to Dr. David Stevens for all the scientific discussions that we had which enriched my scientific background and developed my thinking, and for the time he invested in helping me establish new techniques in our laboratory.

I like to thank my friends Ali Shaib, Hawraa Bzeih, Ali Harb, Ahmad Shaaban, and Marwa Sleiman, for all the fun times here in Homburg.

Last but not least I want to thank my family for their support, and whose care and love throughout my life brought me to where I am today, and I hope that I made them proud.

Curriculum vitae

The curriculum vitae was removed from the electronic version of the doctoral thesis for reasons of data protection

Tag der Promotion: Montag 01.03.2021

Dekan: Univ.-Prof. Dr. med. Michael D. Menger

Berichterstatter: Univ.-Prof. Dr. Dieter Bruns

Univ.-Prof. Dr. med. Frank Schmitz